Generalized Terminal Modeling of
Electro-Magnetic Interference

Andrew Carson Baisden

Dissertation submitted to the Faculty of the Virginia Polytechnic Institute and State University in partial fulfillment of the requirements for the degree of

Doctor of Philosophy

in

Electrical Engineering

Dushan Boroyevich, Chairman

Fei Wang

Shuo Wang

Sedki M. Riad

Traian Iliescu

November 6, 2009

Blacksburg, Virginia

Generalized Terminal Modeling of
Electro-Magnetic Interference

by

Andrew C. Baisden

Dushan Boroyevich, Chairman

Electrical Engineering

ABSTRACT

Terminal models have been used for various power electronic applications. In this work a two- and three-terminal black box model is proposed for electro-magnetic interference (EMI) characterization. The modeling procedure starts with a time-variant system at a particular operating condition, which can be a converter, set of converters, sub-system or collection of components. A unique, linear equivalent circuit is created for applications in the frequency domain. Impedances and current / voltage sources define the noise throughout the entire EMI frequency spectrum. All parameters needed to create the model are clearly defined to ensure convergence and maximize accuracy.

The model is then used to predict the attenuation caused by a filter with increased accuracy over small signal insertion gain measurements performed with network analyzers. Knowledge of EMI filters interactions with the converter allows for advanced techniques and design constraints to optimize the filter for size, weight, and cost. Additionally, the model is also demonstrated when the operating point of the system does not remain constant, as with AC power systems. Modeling of a varying operating point requires information of all the operating conditions for a complete and accurate model. However, the data collection and processing quickly become unmanageable due to the large amounts of data needed. Therefore, simplification techniques are used to reduce the complexity of the model while maintaining accuracy throughout the frequency spectrum.

The modeling approach is verified for linear and power electronic networks including: a dc-dc boost converter, phase-leg module, and a simulated dc-ac inverter. The accuracy of the model is confirmed up to 100 MHz in simulation and at least 50 MHz for experimental validation.

ACKNOWLEDGEMENTS

I would like to extend my greatest thanks to my advisor Dr. Dushan Boroyevich. He has continually guided and pushed me to excel past any barrier through his perpetual questioning. His support, knowledge, confidence, and mentorship are unprecedented and I strive to incessantly learn from him day in and day out. His creative approach has kept my interest and drive at its peak throughout my graduate degrees. I would also like to thank the rest of my committee members, Dr. Fred Wang and his vast knowledge of the subject matter assisted me to always find something to improve upon. Dr. Shuo Wang's EMI and experimental experience furthered my understanding and expanded my capabilities to struggle through this phenomenon. Dr. Sedki Riad and Dr. Traian Iliescu have been a pleasure to work with. They are very kind and generous with their time and efforts in assisting me during this task.

I would also like to thank all of the staff at CPES for their assistance for the ever so important day to day matters. Bob Martin, Dan Huff, Doug Sterk, and David Gilham kept the labs in working order and provided insight to many problems along the way. Marianne Hawthorne, Trish Rose, Teresa Shaw, Linda Gallagher, Linda Long, Elizabeth Tranter, and Michelle Czamanske for their administrative ingenious to get me from one day to the next. Additionally, the assistance and guidance of my industrial sponsor including Nicolas Gazel, Regis Meuret, and Remi Robutel is greatly appreciated.

None of this could have been possible without the network within CPES; working at CPES has provided the knowledge and experience of nearly a hundred people at my fingertips. I want to express my thanks to all of the CPES students who have helped me along the way, especially, Bryan Charboneau, Tim Thacker, Jerry Francis, Anish Prasai, Fang Luo, Igor Cvetkovic, Rixin Lai, Hemant Bishnoi, Yoann Maillet, Daniel Ghizoni, Qian Liu, Bing Lu, and Arman Roshan for their suggestions and friendship whether it be related to this work or not. I would also like to thank Vassilis Siomos, Rory Cantu, Brandon Hoeft, and Chad Hudson for their support and friendship throughout our lives.

My family has provided me the strength to continue on through their love and support. First and foremost my beautiful and loving wife, Kristie Baisden, has had infinite patience during my studies. Her love and support never wavered through the arduous times caused by our distance apart while I finished my degree. I am forever grateful and honored to have her by my side for

all the new journeys we will encounter together. I want to thank my mother, Theresa Baisden, and father, John Baisden for an endless amount of love, support, and belief in their youngest son. Finally, I would like to send a thank you to all my brothers, Jeff and Steve, my sister, Jennifer, and all their families, as well as my entire extended family.

To my beautiful and devoted wife

Kristie Wolfe Baisden

And

My loving and supportive parents

John and Theresa Baisden

TABLE OF CONTENTS

LIST OF FIGURES

LIST OF TABLES

1 INTRODUCTION

1.1 BACKGROUND

Existing trends within power electronics focus on driving the switching frequency higher and enhancing power management. As a result, the power density of converters increases. However, converters with higher switching frequencies and closer proximities of the power stage components are more vulnerable to electro-magnetic interference (EMI). Electro-magnetic noise, or EMI, that propagates through a system can potentially harm the components or deteriorate the systems operation [1]. The integrity of the system – including the supply, conversion, and load – is highly dependent on the EMI generated and propagating through the system. As seen in Fig. 1.1 any noise produced from the converter can reduce the quality of both the input and output lines.
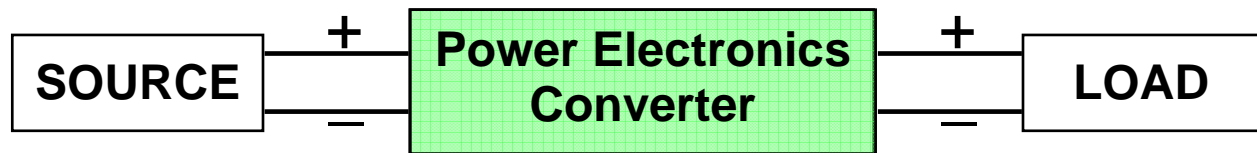
Fig. 1.1: Typical matching of the characteristics of a source to the load using power electronics conversion.

The noise susceptibility of the load determines if the system will function as designed. When EMI propagates back into the system with other power conversion systems and loads, they too can be damaged or malfunction due to the noise. With the growing number of electronic loads and power supplies using active switching devices at increased switching frequencies degradation of the utility system is of concern. This is the primary reason many standards have been set for EMI noise generated [2]. The standards help protect the utility grid and the components connected to it from any disturbances produced by EMI. Standards range in severity depending on application and location. An example of an EMI noise frequency spectrum and a common standard is shown in Fig. 1.2. The solid (red) line is the International Special Committee on Radio Interference, (CISPR, from its French title, Comite International Special des Perturbations Radioelectriques) Publication 22 standard for residential applications under their testing guidelines [3-4]. The (black) noise plot is an example of the total EMI noise

generated by a typical power supply used in a household. The noise is measured in decibels (dB) with a base unit of a micro-volt (dBμV) over a frequency spectrum specified by the application.
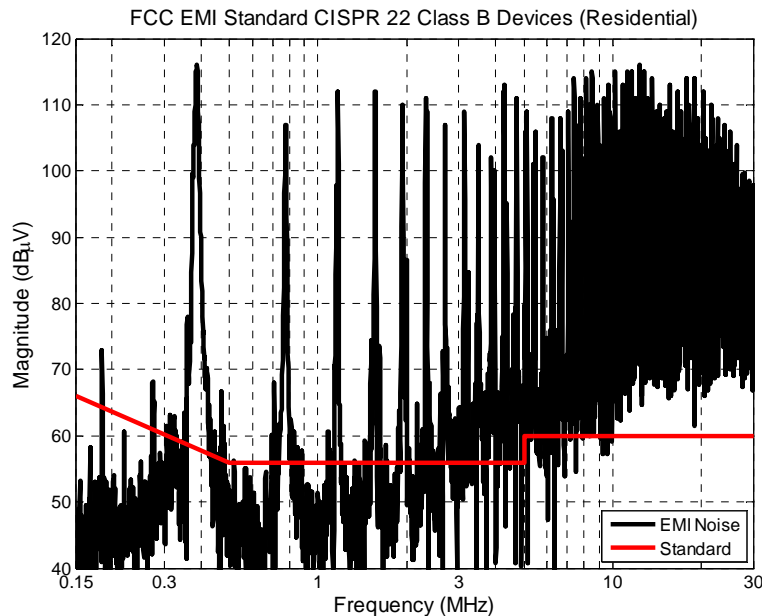
Fig. 1.2: CISPR 22 EMI Standard for Class 2 devices (residential).

The total EMI produced in a system can be categorized into conducted and radiated EMI. The range of conducted EMI is determined by the application of the product. Most residential and commercial applications regulate the conducted region between 150 kHz and 30 MHz as seen in Fig. 1.2. Some military or sensitive applications go as far down at 10 kHz while above 10-30 MHz is usually considered radiated noise [5]. Radiated EMI is typically for the frequencies above the conducted region; it will not be considered here since it has fundamental differences from the focus of this study. Emissions and susceptibility define the two directions EMI noise effects. Emissions are regulated through the standards mentioned, where the susceptibility to outside noise is self-regulating by the device's operation. If the unit in question is susceptible to EMI then it will not function properly and likewise income will not be produced from the product. Some military standards, however, will regulate the susceptibility of a device. A picture to represent some EMI phenomena is shown in Fig. 1.3. The dashed (blue) line represents the conducted EMI propagating from and to all sources, conversions, and loads. Furthermore, the radiated EMI is emitted by every piece of equipment, and can cause susceptibility issues as well. In the end, everything affects each other in some form or another and all components must be able to work in all operating conditions without emitting too much noise.
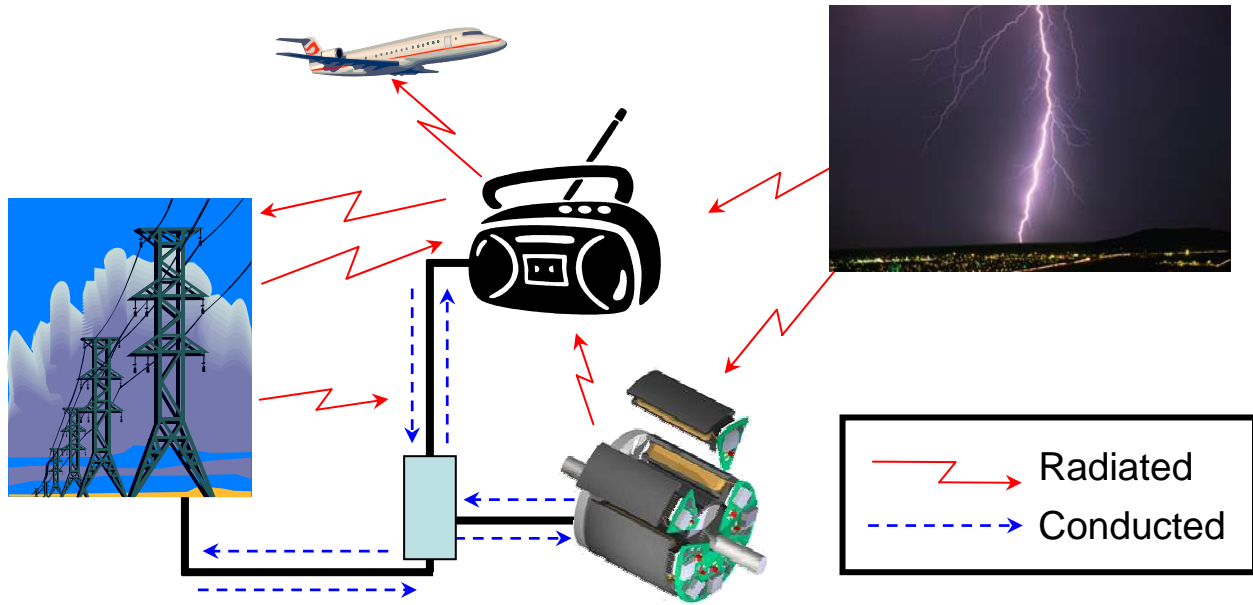
Fig. 1.3: Conducted and radiated EMI examples, showing emissions and susceptibility from potential sources and loads.

Conducted emissions can be further categorized into common-mode (CM) and differential-mode (DM) EMI. CM EMI is noise that is conducted through a common path: often a heatsink or a ground path. The common path is coupled to the system via parasitic impedances, such as the capacitance between a device and the heatsink. An example of this is illustrated with a classical boost converter in Fig. 1.4a. The current through the capacitance (which contributes to the overall CM current) is found by $i_C = C \cdot \frac{dv_C}{dt}$. Similarly, the DM noise conducted throughout the system circulates through the power paths via coupled impedances such as self and mutual inductances as shown in Fig. 1.4b. Considering the closer proximities and higher switching frequencies both the coupling impedances and rate of change of the voltage and current increase respectively, therefore increasing the CM and DM noise.

In order to measure EMI and provide reproducible results a line impedance stabilization network (LISN) is used, which is in compliance with the standards. Also shown in Fig. 1.4, the LISN is composed of passive components and designed to filter out any outside noise and only measure noise emitted and propagated related to the device under test (DUT). A LISN provides a nearly pure resistive component – 100 Ω and 25 Ω for DM and CM, respectively – at the input of the DUT over the frequencies in question for conducted EMI. Likewise at frequencies below the conducted range – system operating frequency, such as DC or 60 Hz – the LISN passes the

power. The voltage is measured across the two resistors R_1 and R_2, each 50 Ω, where the CM

and DM EMI are calculated using equations (1-1) and (1-2), respectively.

$$V_{CM} = \frac{V_{R1} + V_{R2}}{2} \qquad (1\text{-}1)$$

$$V_{DM} = \frac{V_{R1} - V_{R2}}{2} \qquad (1\text{-}2)$$

Voltages V_{R1} and V_{R2} are the total noise voltages measured across the LISN resistors, R_1 and R_2

respectively, as shown in Fig. 1.4.

(a)

(b)
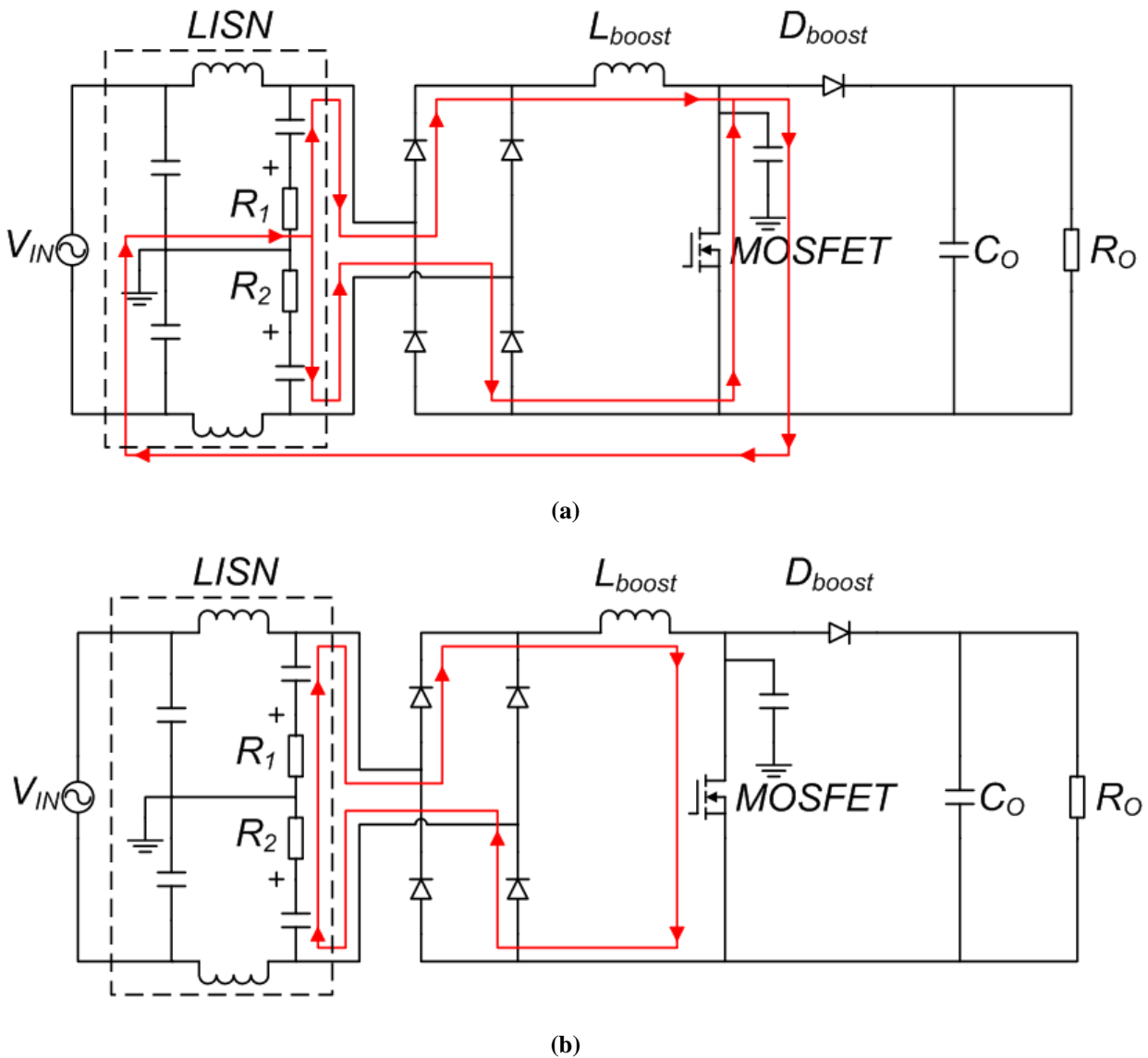
Fig. 1.4: A path for (a) CM and (b) DM noise in a power factor correction (PFC) boost converter.

1.2 LITERATURE REVIEW

There are many techniques to reduce the EMI emissions of a converter; some methods include, for example: numerous variations of passive and active filters [4, 6-10], shielding and grounding [1, 4, 11], noise balancing or canceling [8, 12-14], converter's controls [8, 15-16], and packaging design [8, 17-20]. EMI still posses many challenges to power electronic engineers albeit there are many known ways of reducing the noise in the system [4]. The later the engineer attempts to reduce the noise the more costly the task becomes. If the filtering or containment of the noise is achieved earlier in the design stage more techniques are available to the engineer. Layout, device selection, or filtering are only a few of the options that can reduce the noise and can easily be changed earlier in the design process. If the EMI is still a problem in the production phase of the product the only option an engineer has is to increase the size of the EMI filter with the consequence of increased cost, longer design cycle time, and decreased power density [1]. A quantitative graph of this is given in Fig. 1.5.
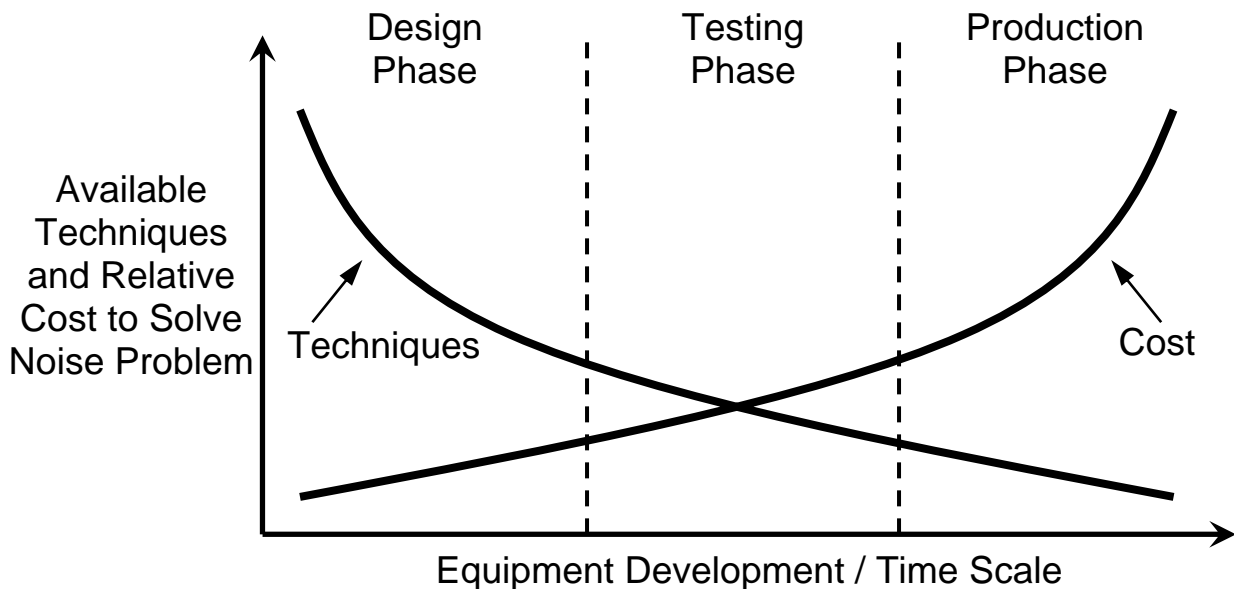
Fig. 1.5: Trade-off of available EMI reduction techniques and design cost versus time [1].

With a good model that accurately predicts the EMI in a system the reduction of noise may be optimized for size, weight, reliability, and cost. With this in mind many efforts have been made to model and characterize (EMI) noise emissions of a particular device or system in power electronics [1, 21-49]. However, there is still no definitive way for a unified approach of

modeling EMI. The accuracy, speed, generality, applications and information required to provide a model vary greatly in each approach.

The modeling of EMI can generally be broken down into two categories: detailed, physics based modeling [21-30] and behavioral modeling [31-49]. Either method can be used to model the EMI propagation path or the noise source. The propagation path is typically a purely passive network that encompasses all connections and components between the LISN and the noise source. EMI noise is generated via the noise source which usually consists of the active switching device(s) through their fast transients and high $\frac{dv}{dt}$ and $\frac{di}{dt}$.

1.2.1 Detailed, Physics Based Modeling Approach

Detailed modeling can incorporate many aspects of the system model, such as active switching or driving devices, discrete or integrated passives, interconnections and control circuitry. Typically these detailed models are created for an end application in time-domain circuit simulations. The models vary widely in their complexity, and likewise accuracy. The ultimate goal is to reduce the complexity without sacrificing the accuracy. In this context, research is ongoing to continually improve the device model. A device model can range from an ideal switch, to an ideal switch with some parasitic passives, all the way to a complete physics based analytical model that fully describes the electron transfer process in the silicon. A complete model of an active device includes non-linear and higher order switching and static characteristics. One of the more complex devices to model is the insulated gate bipolar transistor (IGBT); an accurate physics based model is presented in [21]. This model allows for examination of the switching behavior under certain loading conditions. A very similar device model was used in conjunction with lumped parasitic impedances and a bus bar with transmission line effects for a motor drive application in [22]. This method was found to be fairly accurate – within 10 dB – throughout the EMI frequency spectrum. However, these device models can be quite complex and when many devices are included in a system, in addition to other components, there may be issues with convergence errors and it can take a long time to simulate. Other switching models include device models which may be created by the manufacture and provided to the end user [23-24]. These models can also vary in complexity and accuracy; unfortunately they are often encrypted, therefore the details of the model are not fully known and cannot be modified.

The next major factor in an EMI model is the propagation path, primarily composed of passive components, coupling paths and parasitics. Similar to the device model, there exists a wide range of complexity in modeling the propagation path. Complete models can be described by the physics and electromagnetic laws [25-28]. In order to properly characterize all the EMI propagation phenomena for the full frequency range the material properties, proximity and skin effects as well as the structures geometry need to be included. These analytical electromagnetic models do not have a lumped parameter equivalent, but rather tend to provide insight to how the passives will operate. Full electromagnetic models, however, contain too much information to be efficiently used in a time-domain simulation. Another step is usually required to reduce the model into a simpler form for use in simulations, which generally results in a lumped passive model that attempts to capture the characteristics within the frequency range of interest.

Since the full electromagnetic model does not suite well for a complete EMI simulation model, reduction techniques are attempted. One example is to use time-domain reflectometry which uses the reflected signals from a system or component to determine the impedance [22-23]. Reference [23] then used the impedance vs. frequency information to create a lumped circuit model to represent a transmission line. This procedure attempts to capture the major components of the propagation path. One downfall of this approach is that it is up to the intuition of the engineer to determine what is major and what is insignificant which results in a long modeling time and often something is overlooked. Another approach uses computer simulations such as finite element methods (FEM) to calculate the impedances [24, 29]. This requires intimate knowledge of the geometry and materials, which leads to increased time to create the FEM simulation. Similarly to reducing the full electromagnetic models, the FEM simulation produce too many variables that often do not influence the system in the desired frequency ranges, and a reduction needs to be completed. Again, the experience of the engineer is usually how the reduction is decided. One final method to characterize passives is to measure the impedance with an impedance analyzer and fit a lumped model to the bode plot curves [24, 30]. This, again, will limit the frequency range of accuracy, but is often adequate for many discrete components. The accuracy, however, suffers as the component resembles transmission line effects at increased frequencies.

In order to create an accurate representation of the EMI, a full system model is required. This includes all devices, passives, gate drives, control, and interconnects [24]. The full system

model for a power factor correction boost converter (that uses many components and their respective models) is illustrated in Fig. 1.6. One MOSFET device model is created from datasheet parameters to match the nominal voltage and current ratings, output characteristics, non-linear capacitors and switching speeds. Meanwhile another device model, the diode, is provided by the manufacture. The gate driver was found to be a critical component and was likewise modeled to fit measured characteristics under nominal operating conditions. Interconnections between each discrete device on the PCB were modeled using FEM simulation, while the discrete passive components used a lumped parameter model that was fit to impedance measurements. A reduction, as described above, of the interconnection model was done to limit the number of simulated system equations needed. The results of the complete system's EMI are provided in Fig. 1.7.

As seen in this example the detailed time-domain circuit model can produce very accurate results throughout the frequency spectrum if care is taken for each and every component in the system. These models can theoretically help troubleshoot an EMI problem in a system and even provide the means for early and accurate prediction and likewise optimal filtering techniques can be incorporated. However, it is not without cost. The time to create such a detailed model for every part of the system is very time consuming and complete working knowledge of all the components is required. Also, the time to simulate the model can be extremely long. For example, the system time constant was on the order of 10 ms while the time step required for accurate EMI results is 1-2 ns. With this system the total simulation time can take a full day or longer; this will only get worse as the complexity of the system increases or when multiple systems are investigated. This causes a great burden on the design engineer and any savings from early detection of EMI issues could be lost.
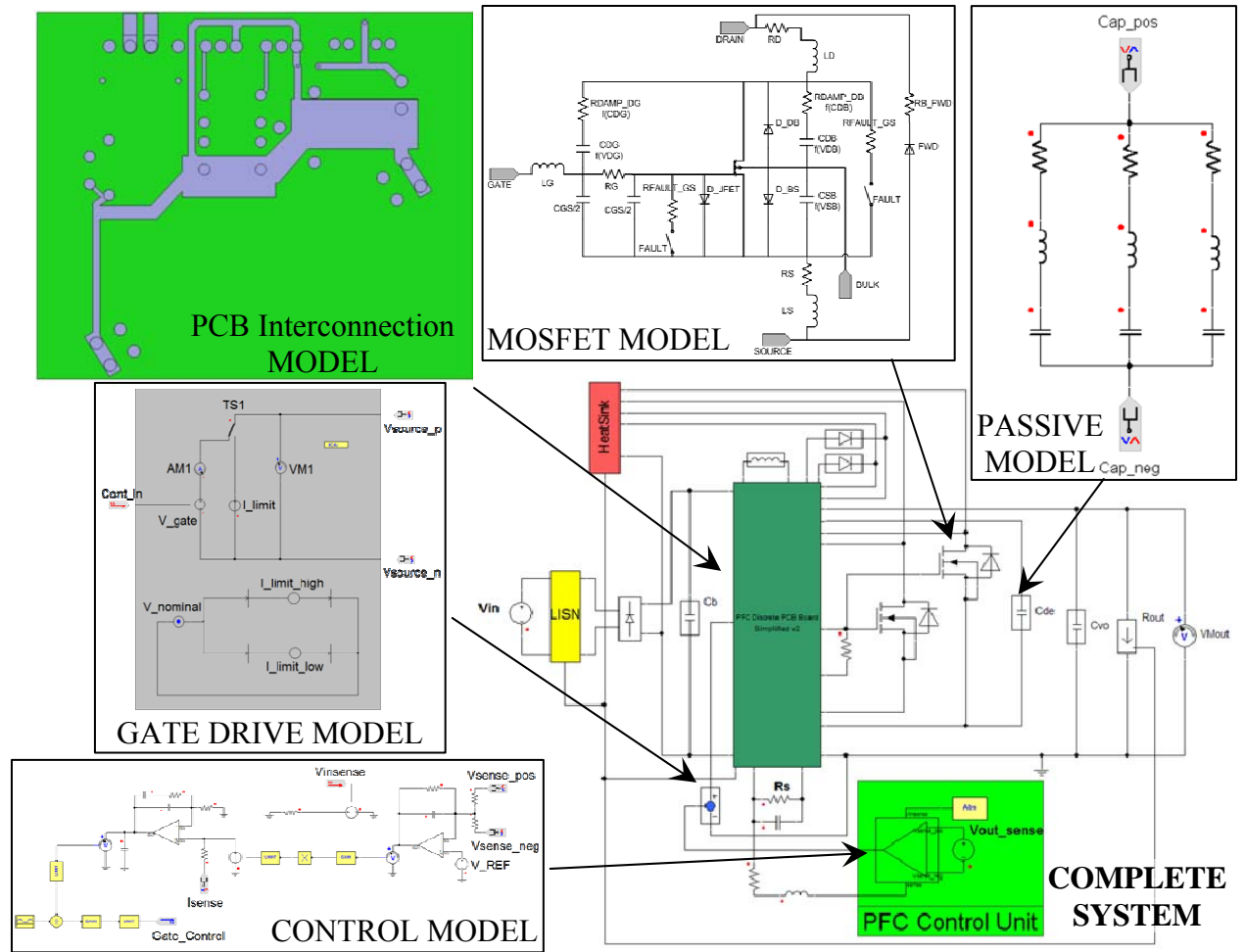
Fig. 1.6: **Time-domain system model of a power factor correction boost converter created from many detailed component model [24].**
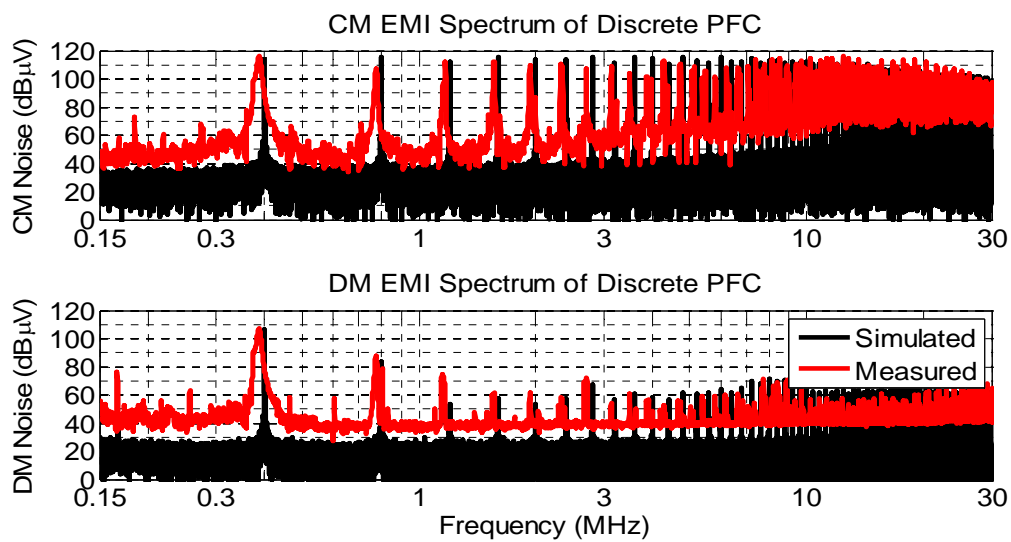
Fig. 1.7: **Simulated vs. measured EMI results for the power factor correction boost converter at 120 V$_{RMS}$ input voltage, 1 kW output power, and 400 kHz switching frequency [24].**

1.2.2 Behavioral (Terminal) Modeling Approach

Similar to detailed modeling, behavioral modeling also incorporates many aspects of the system model, such as active devices, passives, etc. The goal with the behavioral models is to capture the characteristics of the system (or components) without intimate knowledge of the inner workings. EMI behavioral models are often created to be used in the frequency-domain for faster computations since the detailed time-domain circuit information is not necessarily required to witness the EMI noise seen at the LISN. This is where the phrase terminal modeling is also used and discussed in this study along with behavioral modeling; terminal models define the properties of only the system's external ports where the system is seen as a black box.

Typically, behavioral and terminal models represent the system as an equivalent simplified model that incorporates all circuit characteristics in a few elements. For example, the input impedance of a converter can be represented a single impedance as a function of frequency. In the design of an input filter the impedance matching/mismatching is critical and defines the attenuation seen at the input of the filter [31]. Rules along these lines were placed on the EMI filter design; however, an accurate representation of the input impedance of a converter was difficult to achieve throughout the EMI frequencies of interest. Much research followed to predict and characterize the impedance that interacts with an EMI filter. Stability issues can be avoided when an EMI filter's impedance does not harmfully interact with a converter's impedance [32]. This, however, is valid for frequencies below the switching frequency and does not deal much with the actual attenuation at higher EMI frequencies since the converter's impedance was not easily attainable.

The noise source and noise impedance of a converter was used to predict the EMI noise and design a filter in [33]. The results were limited to a specific converter and the method was not easily implemented. It did, however, show promise in the ability to model the converter's EMI with a Norton-Mayer or, its dual, the Thevenin-Helmholtz equivalent circuit. To reduce the computation time and complexity of these equivalent models [34-35] solved the models in the frequency domain directly. Analytical derivations that defined the system's equivalent parameters in the frequency domain were derived and thus a very simple electrical model was left to be solved. One downfall of the analytical models was that some EMI phenomena that are not easily depicted through the lower order equations may not be observed.

Many efforts have since been attempted to improve the accuracy of the impedance and source models. Instead of finding the solution to the system through analytical equations a measurement based approach was adopted in [36]. Through a few sets of measurements and equations the impedance can be determined for much of the frequency spectrum. This however, required separate models for the CM and DM impedances. Although this provided good insight to the filter design parameters it did not take into account any mixed mode noise or interactions between CM and DM. This measurement approach was later improved in [37], where the active devices in the system are modeled with the impedance as noise source equivalents. The propagation paths were left to be solved independently through other measurement methods. The accuracy of this method was improved; however, it was still limited to less than 5-10 MHz.

Many people have used the equivalent models to characterize their system, but no model appears to be complete. That is, they do not contain all EMI phenomena, maybe only CM or DM, or the frequency range of interest does not encompass the entire EMI range. Reference [38] did not include all stray inductance and resistance in the impedance model and it only investigated the CM with an accuracy only up to a couple MHz (due to the fact it did not include all impedances). Some papers that only investigated CM are [39-40], where others only DM [41] and if they investigate both phenomena they are usually separate models for CM and DM [36, 42-44]. Often the focus is only on the equivalent noise impedance or the noise source. When the noise impedance is the focus of a particular work an idealized noise source is used [39, 45-48]. This is usually of the form of a pulsed voltage source that mimics the switched voltage across a switch. As models advanced the ideal pulsed voltage was improved to a trapezoidal voltage source that incorporated the rise and fall times of the switch, but no other transient characteristics. The most complete model for the noise sources is [37], where most use the trapezoidal equivalent of the source [40] solved for the other non-idealities; however, only the magnitude of the source was found so the full model still did not exist.

As mentioned, no model covers all the EMI phenomena. Most models only partially characterize the impedance: [41] only included first order stray inductances and the junction capacitor, [42] used a unique approach with some success, however, limits are placed on the magnitude/form of the unknown impedance and the overall power rating of the converter, [44] only measured the CM impedance while the converter was not operating in order to only find the capacitive coupling to ground, so information could be lost since no other impedances are found,

[47] only has a pure capacitance for the CM impedance, [48] has a simplified model for all passive components and it still requires knowledge of all parasitic components. When the model is not fully complete the accuracy is reduced as the frequency increases, typically beyond 1-10 MHz.

Although the models may not create an all encompassing EMI prediction, they are not without purpose. They can be used to show general trends or provide the engineer some basic trade-offs in the system, even with simplified sources and impedances [49]. However, a full model will provide an accurate representation of the EMI with and without a filter. It will also allow for an optimal design of the filter and potentially save cost from overdesign, redesign, and costly standard measurements.

1.3 MOTIVATION AND OBJECTIVES

An accurate EMI model throughout the entire EMI frequency range is needed to predict a system's EMI performance earlier in the design stage. This provides the engineer much more flexibility to characterize, mitigate, or attenuate the EMI. The ability to witness interactions – whether between multiple converters or between a converter and filter (another passive network) – can lead to better system design, stability, and cheaper, more efficient, smaller/lighter EMI filtering. However, after an evaluation of existing literature there are still shortfalls in the much needed EMI model. Detailed models necessitate 100s or 1000s of parameters to be known and implemented requiring extensive knowledge of the system and a great deal of time from the engineer. Due to the large size and complexity, even after the investment is made to create the model the simulation time is often unmanageable for use. With that said, the model often cannot be created since some parameters may be unknown. This validates the importance of a simplified modeling procedure, the behavioral model.

The behavioral models, however, are also lacking in many areas. For example, a complete model that does not separate the CM and DM noise, but rather considers the entire converter without specific predefined noise characteristics is important especially at higher frequencies. Often the behavioral models are over simplified and only provide a general idea of what EMI may be, but miss some important interactions. The generality of the model is also a needed key feature; that is, many models only consider a particular type of system, AC drives, boost converter, etc. The modular-terminal-behavioral (MTB) concept first introduced in [50] and

built upon in [37, 51-53] tackles these important factors in the model. Although this concept covers many of these needed features it is still lacking in some areas. That is, an error analysis is needed to optimize the accuracy of the model. Furthermore, the accuracy at the upper end of the EMI frequency spectrum is reduced. The model does not consider a black box approach but rather more of a gray box. It requires knowledge of the topology and access to various components within the system. Finally, the MTB model is specifically for a two-terminal switching module with a separate method for characterizing the impedance around the module.

The goal of this work is to expand upon this MTB concept to include the points mentioned above, specifically focusing on the following:

1) Identify specific parameters needed to minimize the error during the model acquisition up to and beyond the EMI frequencies.

2) Allow any system to be characterized: two-, three-, or an n-terminal system. For example, a phase-leg, a group of switching devices, an entire converter, or even a set of converters.

3) Removing the need for any a priori knowledge of the inner workings of the system, black box modeling.

4) Combine with other (converter or passive / filter) models to examine interactions and noise characteristics at the system-level.

5) Demonstrate the model for AC operations.

6) Establish boundaries / limits of the modeling approach.

Similar to previous methods, the model is to be used in the frequency domain. The model will improve upon the previous MTB method as outlined in TABLE I.

In order to achieve these improvements, investigating some of the fundamental principles required in a two-terminal model will be conducted. This then provides the means to increase the order of the model to develop to a complete three-terminal model. This includes the parameters needed for the model manipulated using the fast Fourier transform (FFT) and the limitations of such a model. A proper equivalent circuit and accompanying equations that uniquely define any three-terminal system are derived. Various methods to solve the system of non-linear equations are discussed and the convergence and accuracy of the solutions are delineated. Furthermore, a simplification process in the calculations drastically reducing the number of operations is used. This simplicity of the modeling process allows very large systems to be modeled and simulated simultaneously. Another key factor involved with the modeling of

a power converter is the linearization of the system. This model produces an equivalent linear circuit to characterize the EMI; therefore care needs to be taken when producing the model in the frequency domain from an inherent time-variant system. In addition, the uniqueness of the model is also under investigation.

TABLE I.
COMPARISON BETWEEN TWO MODELING METHODS.

	MTB Method [37]	Proposed
Model	1 switching device	Entire system
	"Gray Box"	"Black Box"
	2-Terminal	2, 3, … , n-Terminals
Model Information	Noise source(s)	Noise source(s) & noise impedance(s)
Frequency range of accuracy	~5 MHz	100 MHz
Measurements	Current & Voltage	Voltage only
Measurement condition	Double pulse	Nominal operation
Error Analysis	N/A	Defines conditions to maximize accuracy

2 MODELING DEFINITION AND THEORY

2.1 TWO-TERMINAL

A two-terminal model, by definition, is only differential mode noise. The two-terminal model is not necessarily new or novel; however, it is identified and evaluated first since the concepts are easier to comprehend and visualize. Although it is not a novel concept, the error analysis and limitation on the parameters to minimize the errors has not been investigated. Understanding the two-terminal model in detail will provide the means to evaluate a three (or higher) terminal model more efficiently.

2.1.1 Equivalent Circuit

The model was designed to be as simple as possible. The most concise two-terminal equivalent circuit is either the Norton-Mayer or, its dual, the Thevenin-Helmholtz circuit [54]. The Norton equivalent circuit is initially chosen since it closely resembles the physical representation of a DM system; that is, it consists of a noise current source and noise impedance. There has been some work in creating a linear Norton equivalent circuit from non-linear systems. Some have applied this circuit to power system and load flow analysis [55-57] and common non-linear loads in power electronics [58-59]. Others have looked into simulation and simplified solving of non-linear systems [60-61] and many applications outside of power electronics or electrical engineering [62-63]. Although many of these models may be adequate for the given application, many issues remain. One of the most prominent problems is the uniqueness of the models. Often the models are accurate; however, a complete unique model does not exist, instead there are an infinite number of possible models. Furthermore, the previous methods require many assumptions and are not generalized for any given system; they may assume linearity, but time-variance of the system is still of concern and a unified approach is not used.

Given a source impedance, Z_{Source}, the equivalent circuit is illustrated in Fig. 2.1a. The source impedance is shown as a typical line impedance stabilization network (LISN), which is dominated by its resistive element, R_{LISN}, at the EMI frequencies. The model is created by using the nominal case, Fig. 2.1a, and an attenuated case, Fig. 2.1b. Typically, the Norton equivalent parameters are defined by short and open circuit conditions; however, this cannot be done for an operating converter or active system. For this reason a second measurement is needed that is

different enough (as explained later in this section) from the nominal case. An attenuated case is created by choosing an appropriate Z_{Shunt}, as shown in Fig. 2.1b.

With the knowledge of Z_{Shunt} and the difference between the terminal voltages, V_{PN} and V_{PN}', the unknown equivalent circuit can be solved. The two equations used to solve the two unknowns, I_{PN} and Z_{PN}, are found by inspection of the equivalent circuits in Fig. 2.1(a, b) and provided in (2-1)(a, b), respectively. Through solving the system of equations the definitions for Z_{PN} and I_{PN} are defined in (2-2).

$$V_{PN} = I_{PN} \cdot Z_{PN}||Z_{Source} \qquad \text{(a)}$$
$$V_{PN}' = I_{PN} \cdot Z_{PN}||Z_{Source}||Z_{Shunt} \qquad \text{(b)}$$

$$\text{(2-1)}$$

$$Z_{PN} = \frac{Z_{Source} \cdot Z_{Shunt} \cdot (V_{PN} - V_{PN}')}{Z_{Source} \cdot V_{PN}' + Z_{Shunt} \cdot (V_{PN}' - V_{PN})} \qquad \text{(a)}$$
$$I_{PN} = \frac{V_{PN} \cdot V_{PN}'}{Z_{Shunt} \cdot (V_{PN} - V_{PN}')} \qquad \text{(b)}$$

$$\text{(2-2)}$$

(a) Nominal condition

(b) Attenuated condition
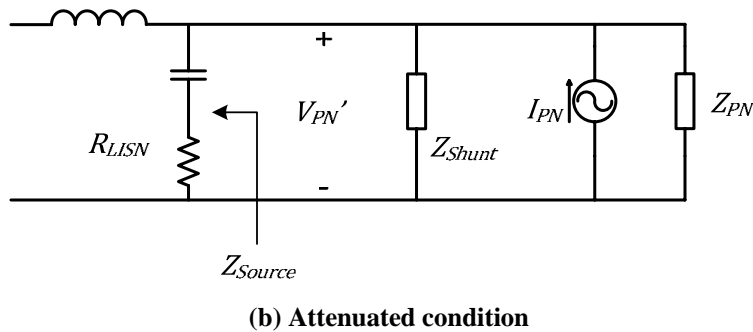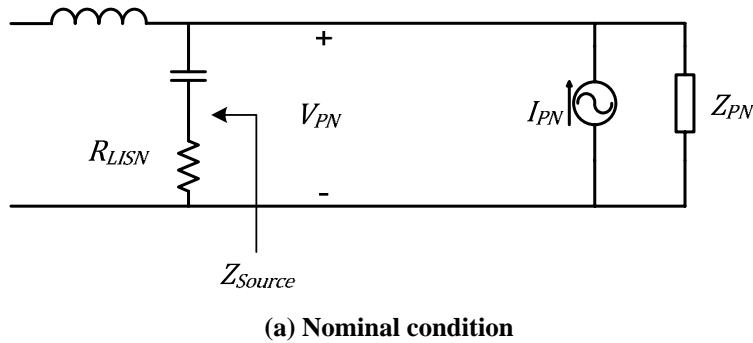
Fig. 2.1: Equivalent Norton circuit, showing both measurement situations needed to create the model.

2.1.2 Error Analysis & Required Parameters

Assuming, for now, that the measurement error is negligible, the following section will evaluate the errors through the inherent physics of the electronics and mathematical manipulations. Since all the calculations are performed in the frequency domain, and most measurements are acquired in the time domain the fast Fourier transform (FFT) is used. The FFT is a critical step in the modeling process, which enables the necessary conversion of time domain data into the frequency domain. There are some inherent errors in the FFT algorithm which can causes errors up to 100% if the proper parameters are not implemented, which include: the sampling frequency, total time of the data captured, bit resolution of the acquisition equipment, and leakage. The details for using the FFT accurately are provided in APPENDIX A.

An important metric in determining the error is the magnitude of difference between the two cases. The attenuation, A, that Z_{Shunt} provides to the terminal voltage is defined as (2-3). Additionally, (2-1) can be rewritten as (2-4) to observe Z_{PN} and I_{PN} as a function of A.

$$A = \frac{V_{PN}}{V_{PN}'} \tag{2-3}$$

$$Z_{PN} = \frac{(A-1) \cdot Z_{Source} \cdot Z_{Shunt}}{Z_{Source} - (A-1) \cdot Z_{Shunt}} \tag{a}$$

$$(2\text{-}4)$$

$$I_{PN} = \frac{V_{PN}}{Z_{Shunt} \cdot (A-1)} \tag{b}$$

The larger A is, the closer the model will be to the traditional open and short conditions for a Norton equivalent circuit. Clearly if A is too small then the difference between the two cases is not adequate which results in an ill-conditioned model; this accounts for part of the error in the previous modeling techniques [37]. This is also seen in (2-4); as A approaches unity large errors occur, as observed in (2-5). Therefore, A needs to be chosen to be adequately large.

$$\lim_{A \to 1} Z_{PN} = 0 \tag{a}$$

$$(2\text{-}5)$$

$$\lim_{A \to 1} I_{PN} = \infty \tag{b}$$

Additionally, when (2-1) is inserted into (2-3) the relation shown in (2-6) occurs. If $Z_{PN} \gg Z_{Source}$, then when (2-6) is substituted into (2-4)a the denominator is nearly zero, thereby creating a large error, (2-7). This can also be intuitively explained; if $Z_{PN} \gg Z_{Source}$, then most of the noise current source, I_{PN}, will flow through Z_{Source} not providing any information about Z_{PN}.

Through analyzing the propagation error in the calculation of Z_{PN}, (2-1)a, the error caused when $Z_{PN} \gg Z_{Source}$ is increased by the order of *A*, as defined by (2-8). This becomes increasingly significant as the frequency approaches the Nyquist frequency due to inherent errors from the FFT. Therefore, *A* also needs to be chosen so that it is not too large where it will affect the error of *Z_PN*. However, as discussed, this error in *Z_PN* can better be controlled by choosing a *Z_Source* that more closely matches *Z_PN* in the desired frequency ranges. The analysis of the error of *Z_PN* (when *Z_PN* is ideally a 100 μH inductor) is illustrated in Fig. 2.2 where the attenuation is varied. In Fig. 2.2, $Z_{Source} = 50\ \Omega\ \&\ 1\ k\Omega$ and A=50, 500, 5000, clearly showing that the error increases as $Z_{PN} \gg Z_{Source}$ and as the attenuation increases. The parameters that should be implemented for accurate modeling results are summarized in (2-9).

One issue that may arise from using two different conditions for a particular system is the similarity of the operating points. In order for this model to be valid the operating point must be the same for each condition. For a power electronics converter that is voltage-fed, the shunt attenuation impedance ensures the converter operates under the same conditions. If, for example, a converter were current-fed, then using a series impedance to attenuate may better apply to that application.

$$A = \frac{V_{PN}}{V_{PN}'} = \frac{I_{PN} \cdot Z_{PN}||Z_{Source}}{I_{PN} \cdot Z_{PN}||Z_{Source}||Z_{Shunt}}$$
$$\vdots$$
$$(A - 1) \cdot Z_{shunt} = Z_{PN}||Z_{Source}$$

(2-6)

$$\text{if } Z_{PN} \gg Z_{Source} \text{ then } (A - 1) \cdot Z_{shunt} = Z_{Source}$$

$$Z_{PN} = \frac{(A - 1) \cdot Z_{Source} \cdot Z_{Shunt}}{Z_{Source} - (A - 1) \cdot Z_{Shunt}} \Rightarrow Z_{PN}|_{Z_{PN} \gg Z_{Source}} \to \infty$$

(2-7)

$$Z^*_{Source} = Z_{Source}\left(1 + \varepsilon_{Z_{Source}}\right)$$

$$Z^*_{Shunt} = Z_{Shunt}\left(1 + \varepsilon_{Z_{Shunt}}\right)$$

$$V^*_{PN} = V_{PN}(1 + \varepsilon_V)$$

$$V'^*_{PN} = V'_{PN}(1 + \varepsilon_{V'})$$

(a)

Assuming $A \gg 1$

(2-8)

$$Z^*_{PN} = Z_{PN}\left(1 + \varepsilon_{Z_{pn}}\right)$$

$$= \frac{(A^* - 1) \cdot Z^*_{Source} \cdot Z^*_{Shunt}}{Z^*_{Source} - (A^* - 1) \cdot Z^*_{Shunt}}$$

$$\vdots$$

$$Z^*_{PN}|_{Z_{PN} \gg Z_{Source}} \approx Z_{PN}\left(1 - \varepsilon_{Z_{Source}} + (A - 2) \cdot \varepsilon_{Z_{Shunt}}\right)$$

$$\approx Z_{PN}\left(1 + A \cdot \varepsilon_{Z_{Shunt}}\right)$$

(b)

$$|Z_{Source}| > \frac{|Z_{PN}|}{10}$$ (a)

(2-9)

$$10 < A < 1000$$ (b)

(a) $Z_{Source} \approx 50\ \Omega, A \approx 5,000$

(b) $Z_{Source} \approx 1\ k\Omega, A \approx 5,000$

(c) $Z_{Source} \approx 50\ \Omega, A \approx 500$

(d) $Z_{Source} \approx 1\ k\Omega, A \approx 500$

(e) $Z_{Source} \approx 50\ \Omega, A \approx 50$
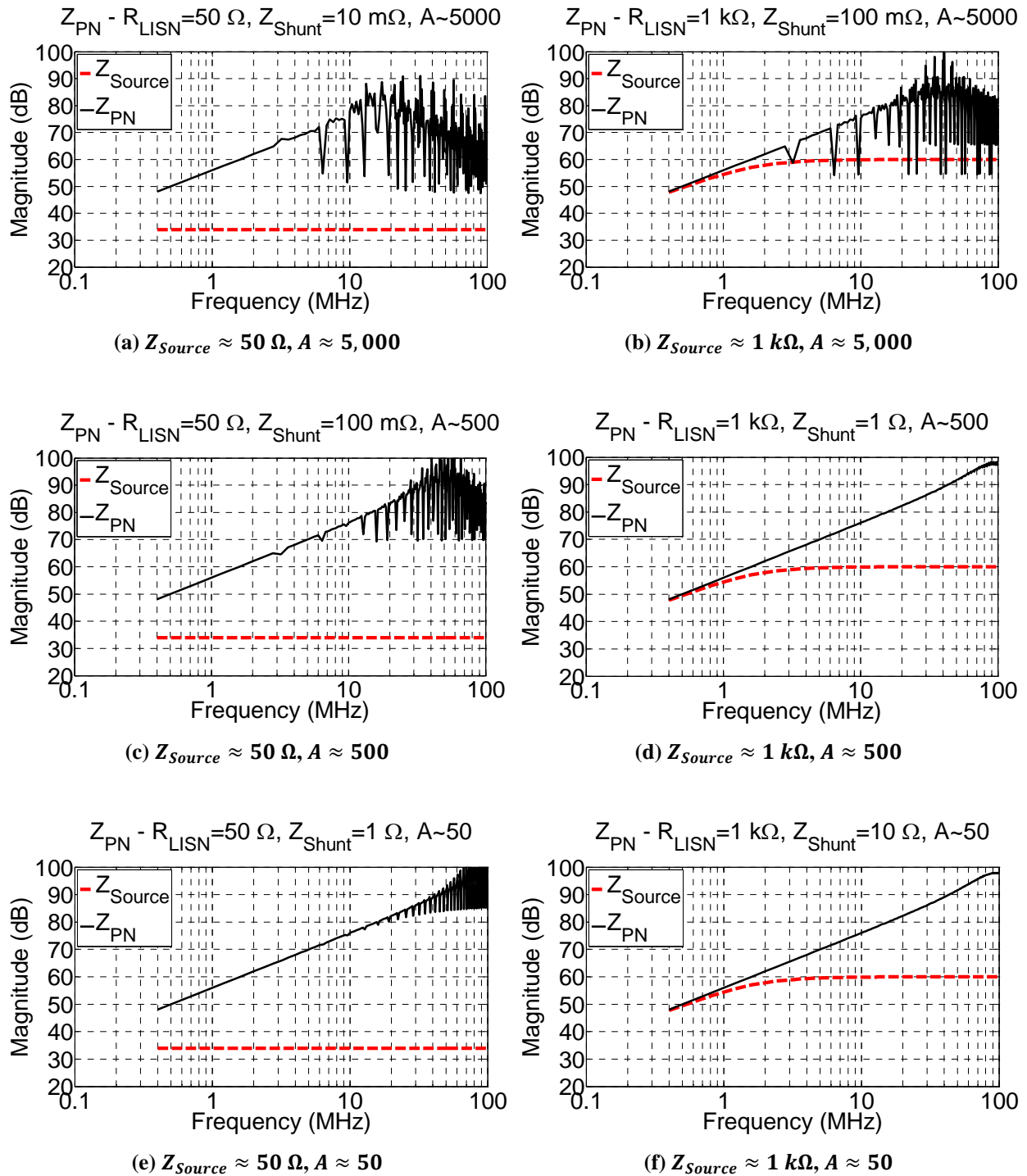
(f) $Z_{Source} \approx 1\ k\Omega, A \approx 50$

**Fig. 2.2: Calculated Z_{PN} (100 μH) for an ideal boost converter as Z_{Source}
(a, c, e – $Z_{Source} \approx 50\,\Omega$ & b, d, f – $Z_{Source} \approx 1\,k\Omega$) and the attenuation
(a, b – $A \approx$ 5,000 & c, d – $A \approx$ 500 & e, f – $A \approx$ 50) vary.**

2.2 MODEL LIMITATIONS

The previous section established the definitions and theory for the modeling process, as well as adding insight to reducing errors. The limitations of this modeling method are still uncertain. Other works, [53], claim that the concept of simplifying a circuit to an equivalent Norton / Thevenin is valid for any system. An issue not discussed in previous works includes modeling switched impedances in this fashion. A simplified illustration of a switched resistance is shown in Fig. 2.3.
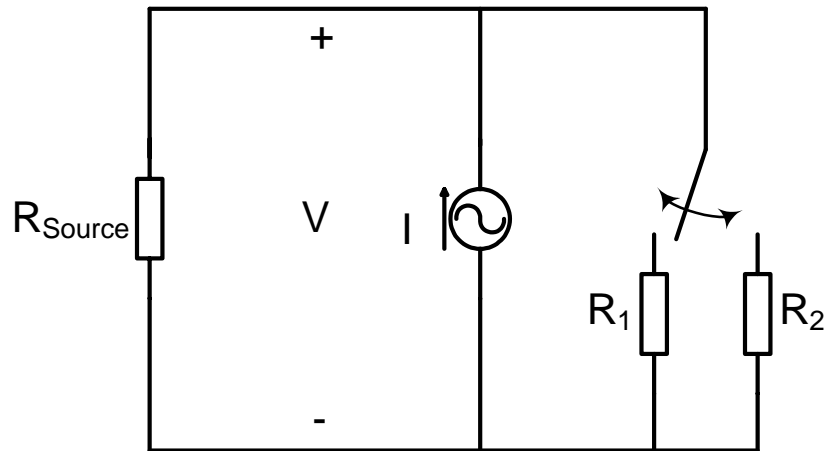

Fig. 2.3: System of switched impedances; includes a source resistance, a constant (DC) Norton current source and switched resistance as the Norton impedance.

The nature of power electronic systems brings attention to this circuit. For example, a classical DC-DC converter has a constant input excitation and uses an electronic switch to toggle between different impedances. Although the switching in a power electronics converter is used to transfer energy stored in passive components, resistors are initially discussed for simplicity. An extension from resistances to power electronic systems will be discussed later.

First, the definition of the voltages produces at the terminal in Fig. 2.3 is defined in (2-10), likewise the equation for the attenuated case can be determine, shown in (2-11).

$$V(t) = V^0 + \sum_{n=1}^{\infty} V^n$$

$$V^0 = I \cdot \frac{R_1 || R_{Source} + R_2 || R_{Source}}{2}$$

$$V^n = \frac{2 \cdot A}{n \cdot \pi} \cdot \sin(n \cdot \pi \cdot d) \cdot \cos(2\pi f \cdot n \cdot t)$$

$$= (R_1 || R_{Source}) \cdot I \cdot c_n$$

$$= R_{eq} \cdot I \cdot c_n \qquad \qquad \text{(2-10)}$$

$$\text{where, } A = \frac{I \cdot R_1 || R_{Source} - I \cdot R_2 || R_{Source}}{2},$$

$$f := \text{fundamental frequency,}$$

$$d := \text{duty cycle of the switch, and}$$

$$c_n = \frac{1}{n \cdot \pi} \sin(n \cdot \pi \cdot d) \cdot \cos(2\pi f \cdot n \cdot t)$$

$$V'^n = (R_1 || R_{Source} || R_{Shunt} - R_2 || R_{Source} || R_{Shunt}) \cdot I \cdot c_n$$

$$= R'_{eq} \cdot I \cdot c_n \qquad \qquad \text{(2-11)}$$

Using the two voltages described above in the switched resistance example, the modeling method is attempted. When the modeling equations, (2-2), are used to solve for an equivalent Norton the results are as follows in (2-12), where R_{Norton} and I_{Norton} are the equivalent values as depicted in Fig. 2.4.

$$R_{Norton}^n = \frac{R_{Source} \cdot X}{R_{Shunt} \cdot R_{Source}^2 - R_1 \cdot R_2 \cdot (R_{Shunt} + R_{Source})} \qquad \text{(a)}$$

$$I_{Norton}^n = \frac{I \cdot R_{Shunt} \cdot R_{Source} \cdot (R_1 - R_2)}{X} \cdot c_n \qquad \text{(b)} \qquad \text{(2-12)}$$

$$\text{where,}$$

$$X = (R_1 \cdot (R_2 \cdot (2 \cdot R_{Shunt} + R_{Source}) + R_{Shunt} \cdot R_{Source}) + R_2 \cdot R_{Shunt} \cdot R_{Source})$$
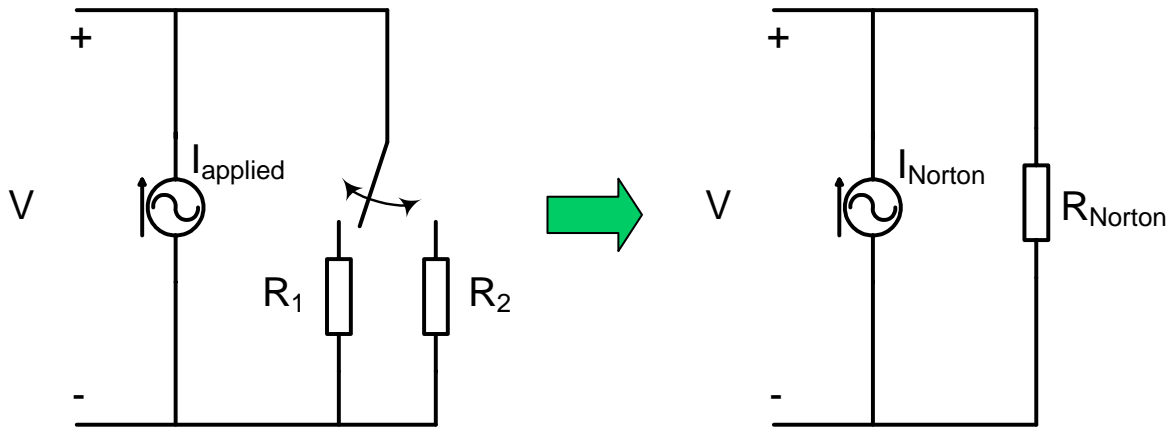
Fig. 2.4: Proposed modeled equivalency of switched impedance.

A couple of points to notice in the solution for the switched impedance using the proposed modeling approach are below. First, the equivalent Norton impedance is constant for all frequency, which depicts a time-invariant resistance. Second, the Norton current source varies as a function of frequency. In the original switched impedance circuit the current source was constant. Since, by definition, impedance is a frequency dependant parameter there is no equivalence between time-varying impedances to the frequency-domain. The impedance is then forced to be a pure resistance. Another anomaly of using this modeling procedure on systems with switched impedances is the equivalent Norton impedance determined is usually negative. This implies the Norton impedance is creating energy and physically does not have any correlation to the actual system. An example of Norton impedances that the model predicts as a function of the source and shunt impedances is shown in Fig. 2.5. This example uses the same circuit shown in Fig. 2.3 with R_1=100 Ω and R_2=10 Ω. The equivalent Norton impedance is displayed on the vertical or Z-axis as it varies with the source and shunt impedances. Solutions of the Norton equivalents should not depend on the source or shunt impedances; clearly Fig. 2.5 shows that there is not a unique solution to the switched impedance model. The impedance exponentially changes and approaches ±∞ under certain conditions. The current source takes on the switched resistance phenomena in order to make the terminal voltage consistent between the actual solution and the modeled approach. However, this is not a suitable justification since the modeled combination of the impedance and current source are only valid for the specific case of Z_{Source}. If the model is used with a different Z_{Source} from the one it was created with it is no longer accurate, which renders the model worthless.
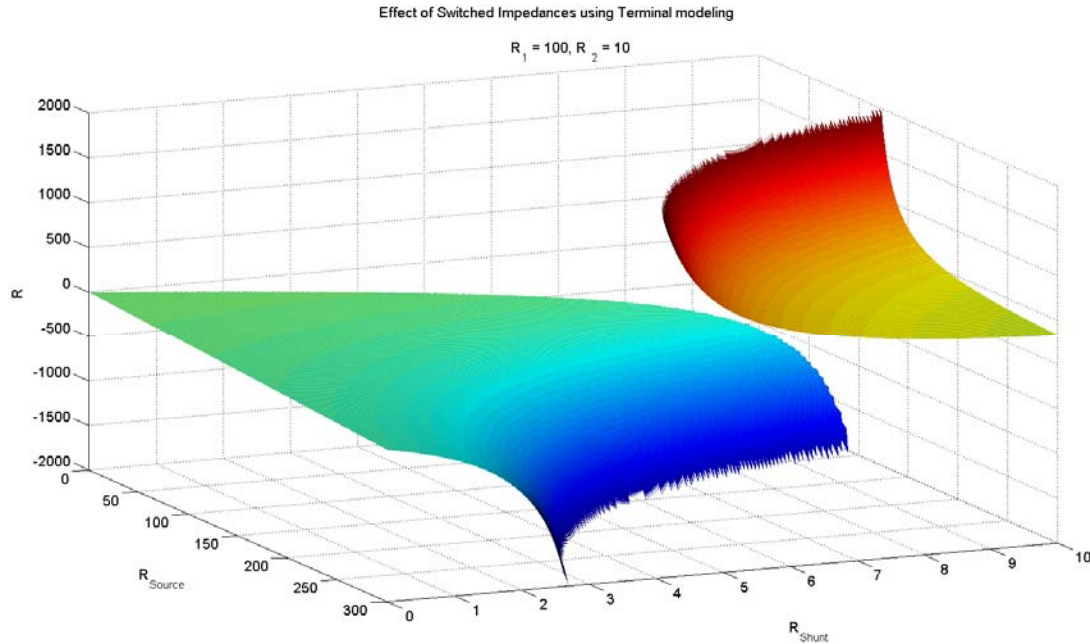
Fig. 2.5: Effects of switched impedances using the terminal modeling approach.

Ohm's law implies that the impedance is a parameter while the current and voltage are variables, which give the linear relation between the two. When the impedance is time-varying, Ohm's law becomes a non-linear relation and therefore it no longer resembles the physical meaning of the electrical parameters modeled. In fact, the Norton equivalent of the switched impedance system is not defined in the frequency-domain and it can only be represented exactly as a switched time-domain circuit.

The importance of this limitation is critical in the validity of the modeling method. Since it is shown that switched impedances cannot be modeled as a linear time-invariant Norton equivalent, how can this approach be valid for power electronic converters? As mentioned power electronic converter circuits can be simplified down to switched impedances at a particular operating point. An ideal switch has the impedance of $0\,\Omega$ or $\infty\,\Omega$. This clearly will not have a linear time-invariant model, but a model may exist if the impedances switched are not far apart. In the example from Fig. 2.5 the switched impedances are an order of magnitude apart. If a much larger impedance is in series with time-invariant impedance then the time-invariance in the systems may not be dominant; Fig. 2.6 illustrates this. However, when this was used and the series impedance was many orders of magnitude larger than either of the switched impedances inconsistencies and uniqueness issues may still arise. Therefore, generality cannot be assumed.
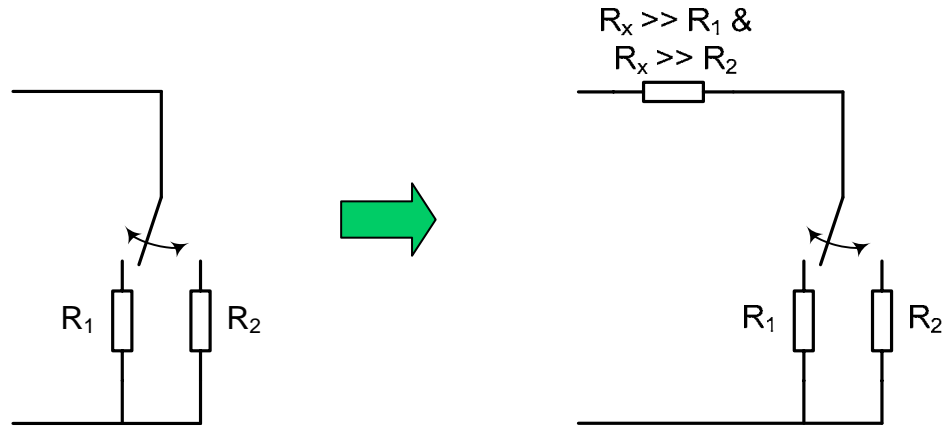
Fig. 2.6: Possible solution to the trouble of modeling switching impedances. This impedance configuration will often occur in a power electronics system.

The theory that is required by the proposed terminal modeling procedure is the traditional time-invariant impedance with a time-varying excitation. Thankfully, this can also be assumed the case in most pulse width modulation (PWM) power electronic converters. The circuit in Fig. 2.7a is not a valid system for modeling with this approach; however, Fig. 2.7b can be confidently modeled.   The issues of switched impedances are not seen in Fig. 2.7b.   Although the impedances are switching the capacitor in Fig. 2.7b eliminates much of the fundamental issues of modeling the time-invariant impedances. The structure is very similar to a boost converter, and the first order approximation of output capacitor's voltage is constant. The other impedance that is switched is the on-resistance of the switch, and can be approximated as 0 V. This system then appears as one time-invariant impedance (the boost inductor in this converter example) and a switched voltage source (switching between V_{OUT} and 0). A similar approximation can also be explained for a buck converter; switching current source (switching between I_{OUT} and 0) and a time-invariant parallel impedance. As long as the power electronic system commutates with a PWM scheme and the 1st order approximation of the energy storage components is satisfied then the modeling procedure proposed is adequately valid. Any other non-idealities of the output capacitor, switching commutation, or interconnections are also included in this approximation of a switched voltage source. This includes all of the necessary information to fully characterize power electronic systems in question. The modeling approach is validated for linear systems with time-invariant impedances and power electronic systems in the next chapter.

a) switched resistors   **b) switched impedances appearing to be a switched voltage source**
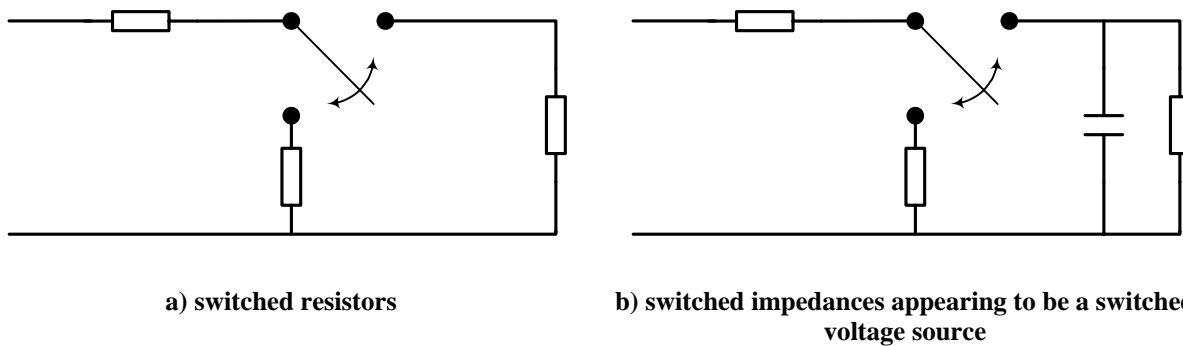
Fig. 2.7: Example circuit (boost converter) that illustrates how the modeling procedure is still valid for power electronic converters.

An issue with non-unique results for time-invariant impedances is still in question for the modeling of a switch in power electronic systems. The claim that converter systems can accurately be modeled will be confirmed, however, the ability to model any subsystem of a converter may not be possible. That is, it may be desired to only model the switches of a converter then later include the passive elements. As stated earlier, a switch is essentially a time-variant impedance; a very low impedance and very large impedance. Therefore, this modeling approach cannot be used unless energy storage elements are included that mimic the switched impedances as a switched voltage source as described above. This is different from an ideal switched source in that it includes other parasitics and ringing in the switched voltage source. Ideal or even trapezoidal pulses do not include ringing and other non-idealities that are caused by parameters within the switched voltage circuit; for example, parasitics of the output capacitor, parasitics of the switch/diode, etc.

2.3 THREE-TERMINAL

As stated earlier, the most concise two-terminal equivalent circuit is either the Norton-Mayer or Thévenin-Helmholtz circuit. The simplest network that fully and uniquely defines a three-terminal system is composed of three impedances and two sources [64]. There must always be an impedance between every terminal, therefore in a three-terminal system the impedances are in a delta configuration. The two sources (current or voltage) can be placed in conjunction with any two of the impedances (to complete a Norton or Thévenin, respectively) in the equivalent circuit model; moreover, a combination of current and voltage sources can also be implemented. A simple algebraic conversion would allow a Thévenin equivalent instead of the Norton, and vice versa. Similar to the two-terminal case, given source impedances from ground to each

power path, $Z_{Sourcep}$ and $Z_{Sourcen}$, the equivalent circuit used is illustrated in Fig. 2.8. Any system can be represented by the network in the dashed box to produce identical voltages and currents at the terminals. The source impedance is shown as one complex impedance. A typical approach to ensure a well known source impendence is to use a LISN as illustrated in the two-terminal schematic.

The model is created by using the nominal case and at least two attenuated cases. Fig. 2.8 shows the nominal case of the system when the grayed impedances, Z_{Shuntp} and Z_{Shuntn}, are not used. An attenuated case is when one or more shunt impedance(s) are inserted into the system that significantly affects the voltage seen at the terminals. An example of this is shown with the two grayed impedances, Z_{Shuntp} and Z_{Shuntn}, in Fig. 2.8. There are seven different attenuation schemes that can be implemented: one impedance between any two-terminals (three possibilities), two impedances as illustrated (three possibilities), or three impedances in a delta configuration (one possibility). Any two of these possibilities along with the nominal system will provide enough information to solve all the unknowns. The next section will discuss which attenuation schemes are the best to use. It should be noted that at least three *different* circuits should be used. Using one attenuation scheme twice, with two different shunt impedance values, may appear to be adequate, however, once the system is attenuated in a particular manner providing more attenuation in the same way will not provide much more information of the unknowns. That is, once a shunt impedance is used most of the current will already flow through that shunt. Intuitively, this is what allows information to be gathered about the unknowns assuming the shunt impedance and the voltage change across the terminals is known. When an additional shunt is added in the same manner the only information that can be gathered is a comparison between the two shunts used and not on the unknowns.
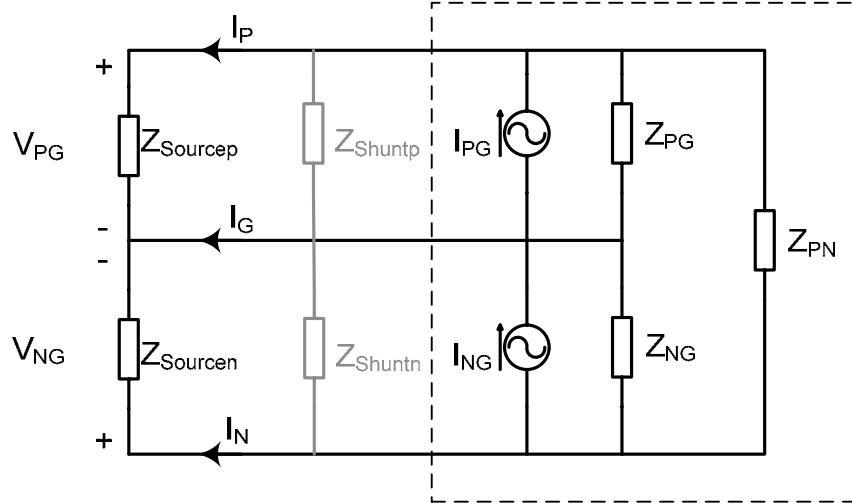
Fig. 2.8: Equivalent circuit with the minimum components. The grayed impedances, Z_{Shuntp} and Z_{Shuntn}, are one example of an attenuated case.

In a two-terminal Norton/Thévenin network there are only two unknowns, however in a three-terminal system there exist five unknowns. From each circuit two independent parameters are found, therefore three cases are needed in order to solve for all the unknowns. The system of equations that define the nominal case are determined by inspection and provided in (2-13). The example of the attenuated case shown in Fig. 2.8 is defined by (2-14) and similarly all equations can be found for any attenuation scheme used.

$$V_{PG} = \left(I_{PG} - \frac{V_{PG} - V_{NG}}{Z_{PN}} \right) \cdot Z_{PG} || Z_{Sourcep}$$
$$V_{NG} = \left(-I_{NG} + \frac{V_{PG} - V_{NG}}{Z_{PN}} \right) \cdot Z_{NG} || Z_{Sourcen}$$

$$(2\text{-}13)$$

$$V_{PG}{}' = \left(I_{PG} - \frac{V_{PG}{}' - V_{NG}{}'}{Z_{PN}} \right) \cdot Z_{PG} || Z_{Sourcep} || Z_{Shuntp}$$
$$V_{NG}{}' = \left(-I_{NG} + \frac{V_{PG}{}' - V_{NG}{}'}{Z_{PN}} \right) \cdot Z_{NG} || Z_{Sourcen} || Z_{Shuntn}$$

$$(2\text{-}14)$$

With the knowledge of all Z_{Shunts}, $Z_{Sources}$ and the terminal voltages, V_{PG}, V_{NG} and $V_{PG}{}'$, $V_{NG}{}'$ and $V_{PG}{}''$, $V_{NG}{}''$ the unknown equivalent circuit can be solved. However, a difference between the three-terminal and two-terminal model is the method of solving for the unknowns. It is trivial with the two-terminal model since there are 2 equations and 2 unknowns with an explicit solution easily attainable. As stated earlier, the three-terminal model has 8 different sets of (two) equations that are possible. Depending on which leg of the system is more dominant with various coupling situations, different sets of equations may produce less error. Therefore, a

method to solve an over determined system of non-linear equations is advantageous to minimize the error. The system of equations – five unknowns – is solved in Matlab, by Mathworks [65], using *lsqnonlin*. The details of using this function are outlined in APPENDIX A.

Section 2.1.2 defines the parameters needed to find an accurate solution to a two-terminal system. In general, the same principles hold for the three-terminal model, summarized in (2-15), where A is the attenuation provided by a shunt impedance.

$$\frac{|Z_{PG}|}{10} < |Z_{Sourcep}| < 10 \cdot |Z_{PG}|$$

$$\frac{|Z_{NG}|}{10} < |Z_{Sourcen}| < 10 \cdot |Z_{NG}|$$
(a)   (2-15)

$$10 < A < 1000$$
(b)

Another difference for the three-terminal model compared to the two-terminal model is the existence of coupling between the two legs: positive-ground and negative-ground. The coupling is determined by the value of Z_{PN} compared to Z_{PG} and Z_{NG}. The equations account for this coupling, however, the errors in solving the system of equations may increase if certain conditions are not met. That is, equation (2-9)a should be maintained but if the source impedance is much larger than the equivalent impedance then a similar error may also occur. Therefore, an upper and lower bound should be placed on the source impedances, shown in (2-15)a.

2.4 N-TERMINAL

The implementation of a three-terminal system allows for the investigation of EMI in single phase or DC systems with a ground or common point. However, it may also be of some interest to explore EMI and terminal characteristics of three-phase systems (also with a fourth ground or common terminal). The principles set forth in this chapter lead directly to defining a four-terminal model. A four-terminal equivalent circuit would consist of six impedances (one between every terminal combination) and three sources (current or voltage). An example of a four-terminal equivalent circuit is drawn in Fig. 2.9. The configuration shown is derived from the one used in the three-terminal examples. Terminals P-O-N use the three-terminal equivalent circuit. The four-terminal is shown as a ground terminal where an additional impedance is included from each P, O, and N terminal to ground. One more source is needed to uniquely define the entire system so a voltage source is added in one of the ground legs. Many equivalent

circuits can be created for a four-terminal system; 20 possible combinations of the sources and each source can be either a voltage or current source giving 120 possibilities. There is no variation in the impedance configuration within the model. This circuit is used for discussion purposes since it closely resembles an actual circuit's performance.
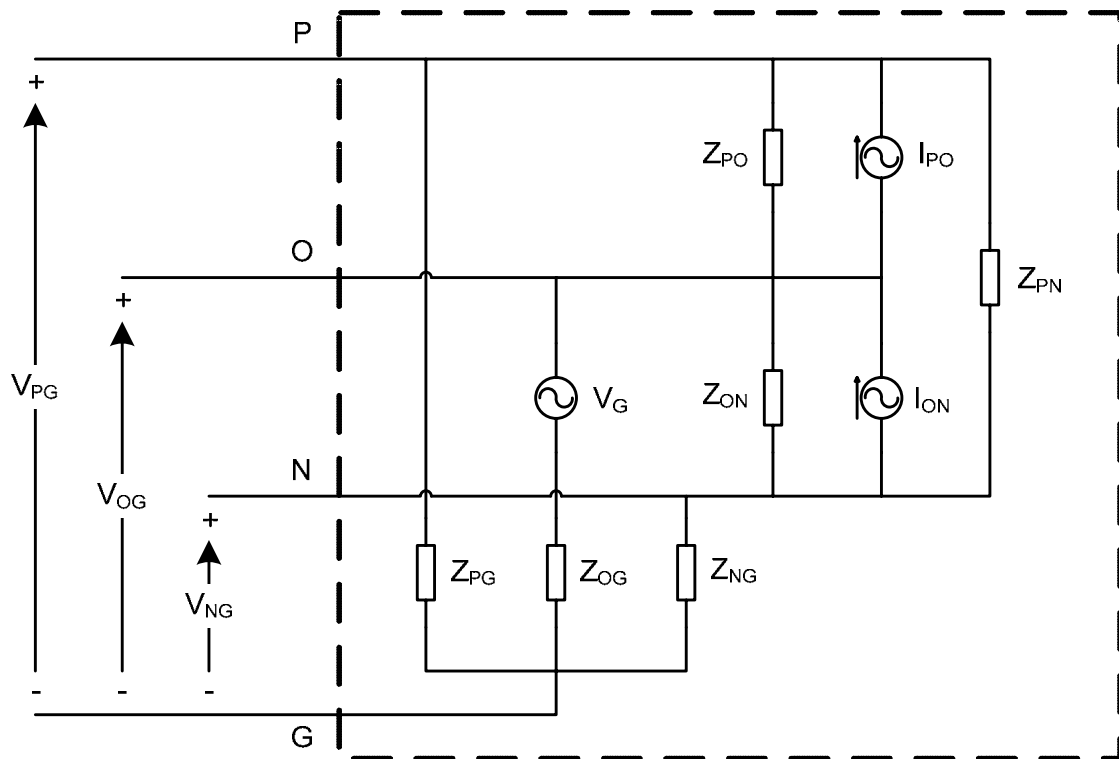
Fig. 2.9: Example four-terminal equivalent circuit with 6 impedances and three sources. This shows the same configuration as the three-terminal example for P-O-N, with additional impedances from each terminal to a ground. One more source is needed so a voltage source is added in one of the ground legs.

In a four-terminal system there are three independent measurements available for every condition; therefore, the minimum number of attenuation schemes needed would remain at two. Similarly, if the need arises, this modeling approach can be adapted to an n-terminal system. Likewise the number of impedances and sources required for a unique equivalent circuit for a given number of terminals is provided in TABLE II, and illustrated in Fig. 2.10. The number of independent measurements that can be acquired from one n-terminal circuit is also shown which leads to the minimum number of different configurations (nominal case and all attenuation schemes) that are required to solve for all the unknowns. Finally, the number of possible attenuation schemes that can be implemented for the number of terminals is also provided. With exception to the two-terminal case, every system can be over determined.

<div align="center">

TABLE II.

REQUIRED NUMBER OF COMPONENTS AND MEASUREMENTS NEEDED TO CHARACTERIZE A SYSTEM VERSUS THE NUMBER OF TERMINALS.

</div>

Terminals	2	3	4	5	6	7	n
Impedances	1	3	6	10	15	21	$\dfrac{n \cdot (n-1)}{2}$
Sources (Current or Voltage)	1	2	3	4	5	6	$n-1$
# of independent measurements per attenuation scheme	1	2	3	4	5	6	$n-1$
Minimum # of different measurement sets required	2	3	3	4	4	5	$\left\lceil \dfrac{n+2}{2} \right\rceil$
# of possible attenuation schemes	1	7	63	1,023	32,767	2,097,151	$\displaystyle\sum_{r=1}^{x} \dfrac{x!}{(x-r)! \cdot r!}$ $x = \dfrac{n \cdot (n-1)}{2}$
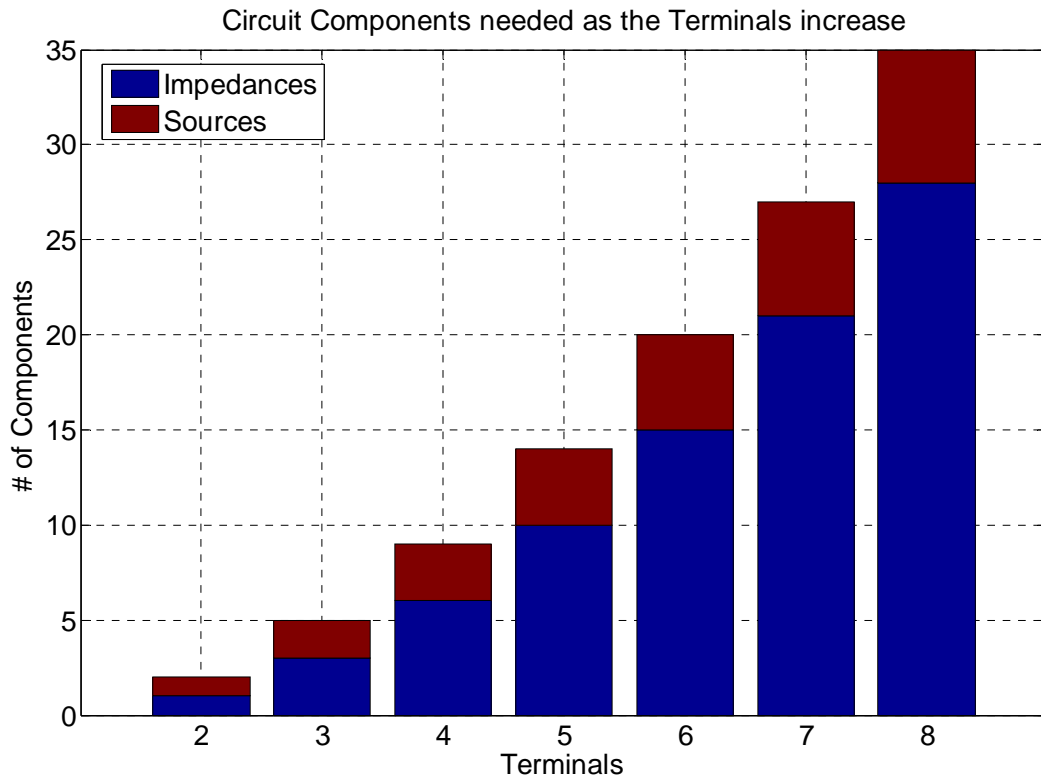
Fig. 2.10: Illustration how the model complexity increases with each terminal in the system.

With only four-terminals, solving the system of equations becomes increasingly complex; nine equations are required from three different conditions. Although it can be done for the four-terminal system, it shows potential issues of even finding a closed form solution to all the variables in the system for higher order models.

A four-terminal system is considered in the Future Work Section of this dissertation, 5.2, but a brief overview and some potential issues were examined. For example, a problem can be the values of impedances in the system. With an increasing number of components needed in the model, the variation between all impedances can vary greatly. Very small and very large impedances can make it difficult to attenuate all conditions in every case. This, therefore, makes it difficult to achieve three or more different sets of measurements which may lead to an ill-conditioned model. The parameters needed to create an accurate model have not been defined as they were with the two- and three-terminal model, (2-9) and (2-15), respectively. Furthermore, the values of noise sources may have a large range. In many cases, not all three sources are significant in producing voltage across the terminals. If these noise sources are not significant and do not contribute to the system then the inclusion of them in the model may not be needed. However, in a general sense this procedure will attempt to create a complete model of any noise source, regardless of its significance, and large errors may occur in these situations. Issues seen in the four-terminal model are discussed in the next chapter, Section 3.1.3.

With that said, modeling a three-phase system implies an AC system where the operating point is constantly changing. Therefore, to fully utilize this model a method must be adapted to account for the non-linearities of a varying operating point, see Chapter 4 for approximations in using this model under AC operation.

3   MODELING VALIDATION AND APPLICATION

3.1   MODEL VERIFICATION THROUGH SIMULATIONS

3.1.1 Two-Terminal

3.1.1.1 Linear example

In order to verify the model, a completely linear example with time-invariant impedances is demonstrated first. This eliminates any errors due to non-linearities or switched impedances and allows a simple comparison of the well-known equivalent circuit solution to the model.   The linear system used is shown in Fig. 3.1, where the schematic of the nominal and attenuated conditions are shown in Fig. 3.1(a, b), respectively.   The dashed box encloses the system that is modeled.   The two impedances are a simple resistive-inductive (R-L) combination arbitrarily chosen, where $Z_1 = 10\Omega + 7\mu H$ and $Z_2 = 1.5\Omega + 1\mu H$. Similarly, the current sources are also arbitrarily chosen with various rise and fall times and magnitudes to provide a rich and complex frequency spectrum. Both of the current sources are periodic with a period of 2.5 μs (400 kHz). All impedances are labeled in the schematics and the two current waveforms are provided in Fig. 3.1(c, d).

A source impedance of 50 Ω is used initially since it is a well-known standard LISN impedance at EMI frequencies. Furthermore, the shunt impedance for the attenuated condition is chosen to be 100 mΩ; this was shown to provide a proper amount of attenuation defined by (2-9)b. The simulation was performed in Ansoft's simulation package, Simplorer [66], and ran for total simulation time of 3 ms at a time step of 1 ns. The captured data had a length of 1 ms (2-3 ms) that is subsequently transformed into its frequency spectrum using the FFT; therefore the time-domain data set consisted of 1,000,000 data points.

(a) Nominal system

(b) Attenuated system

(c) Current waveform for I_{PN1}

(d) Current waveform for I_{PN2}
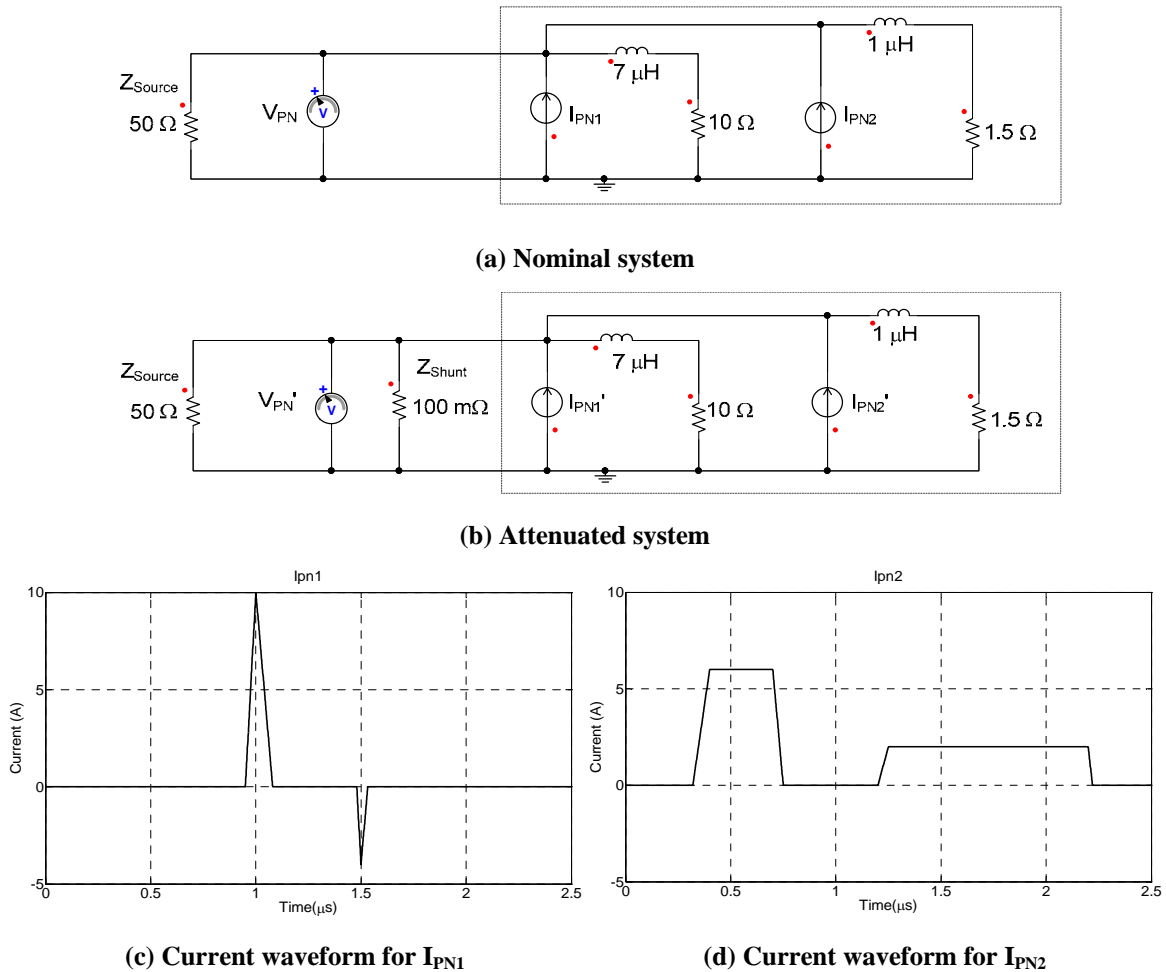
Fig. 3.1: Linear two-terminal system used for verification: composed of two periodic (400 kHz) linear current sources and two resistive-inductive impedances.

Through simulating the simple circuit in Fig. 3.1, a great deal of information is seen and the modeling methodology is verified for this elementary case. The two measurements needed to create the model are the voltages at the terminals of the system, V_{PN} and V_{PN}'. Both voltages are plotted in Fig. 3.2. The plot shows the frequency content of the terminal voltages after the FFT has been performed. The thicker lines are the respective envelopes of their complete FFT data (complete FFT information is shown as the thinner black line for V_{PN} only). Since only the peaks are needed (the rest is considered zero, or background noise) the envelope is the key data set required for the calculations. This also allows for very fast and efficient use of computer resources, since the envelope in the frequency range of interest is composed of 250 data points as opposed to the 1,000,000 points for the raw FFT data. A comparison of the terminal voltages shows the attenuation between the two conditions is between 20 and 50 dB.

Through the use of (2-4) and the measurements in Fig. 3.2, the Norton equivalent terminal impedance and current source are calculated. The impedance is plotted in Fig. 3.3. The plot has both the ideal equivalent impedance found by the parallel combination of the two R-L networks, $Z_1 \| Z_2$, from Fig. 3.1 and the modeled terminal impedance. The two impedance curves overlap each other up to 50 MHz, where a small error (<2 dB) becomes visible. This is because the condition stated in (2-9)a is not maintained, that is $Z_{PN} > 50\ dB$ and $Z_{Source} \approx 34\ dB$ so there is more than an order of magnitude difference between the two curves. It was observed that using $Z_{Source} > 50\ \Omega$ would help reduce this error, as illustrated in Fig. 2.2.
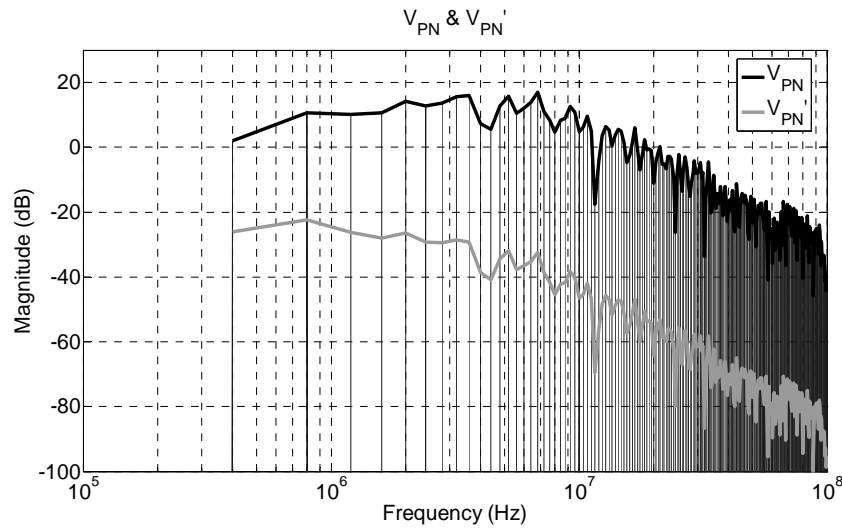
Fig. 3.2: **Plot of the two-terminal linear network voltage measurements. The bold lines are the envelopes of the frequency data; provided from the complete FFT data (shown for V$_{PN}$).**
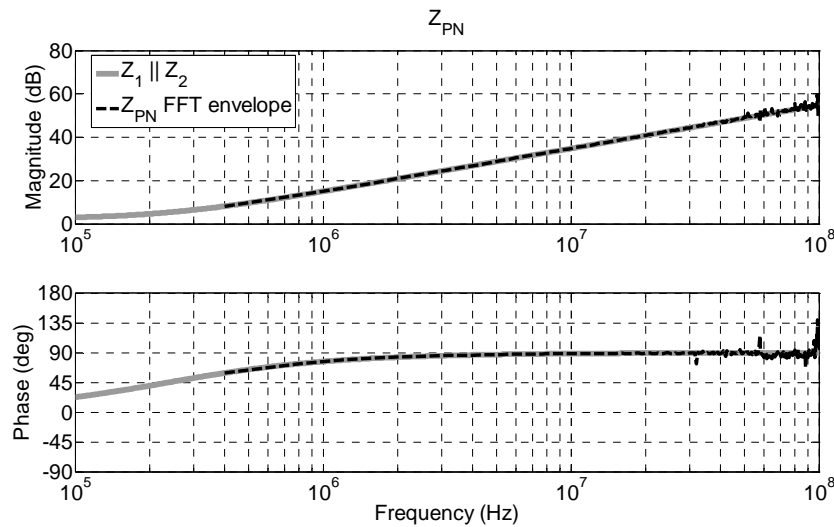
Fig. 3.3: **Comparison of the calculated (modeled equivalent terminal) impedance and the actual equivalent impedance in the system of the two-terminal linear network.**

35

The current source as a function of frequency is shown in Fig. 3.4a. This frequency data for the current source can be transformed back into the time domain for comparison using the inverse FFT (IFFT). The IFFT of the equivalent terminal current source is plotted against the summation of the two original current sources, I_{PN1} and I_{PN2}, shown in Fig. 3.4b. The solid gray line is the original current sources, and the dashed black line is the modeled terminal current source transformed (IFFT) from Fig. 3.4a. It is clear that the two current waveforms overlap completely, verifying the accuracy of the model.

Additionally, it would be worthwhile to compare the total noise seen at the terminals. Using standard EMI measurement and plotting practices, the noise at the 50 Ω source impedance is measured and plotted in dBμV. The comparison between the noise from the original time-domain (nominal) simulation, Fig. 3.1a, and the terminal model's prediction is plotted in Fig. 3.5. For clarity in visualizing the comparison, the entire frequency spectrum (gray) is provided for the original system's noise, while only the envelope (black line) is plotted for the terminal model. A nearly perfect agreement is seen throughout the spectrum up to 100 MHz.

It should be noted that the terminal modeling process also showed similar agreements for different combinations of impedances and current sources, not simply a summation of currents and parallel combination of impedances.
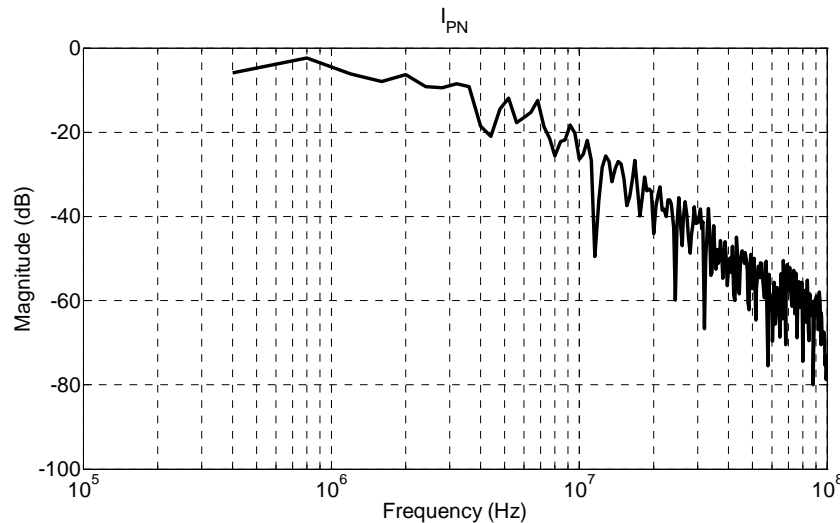
(a) Frequency spectrum calculated for the equivalent terminal current source.
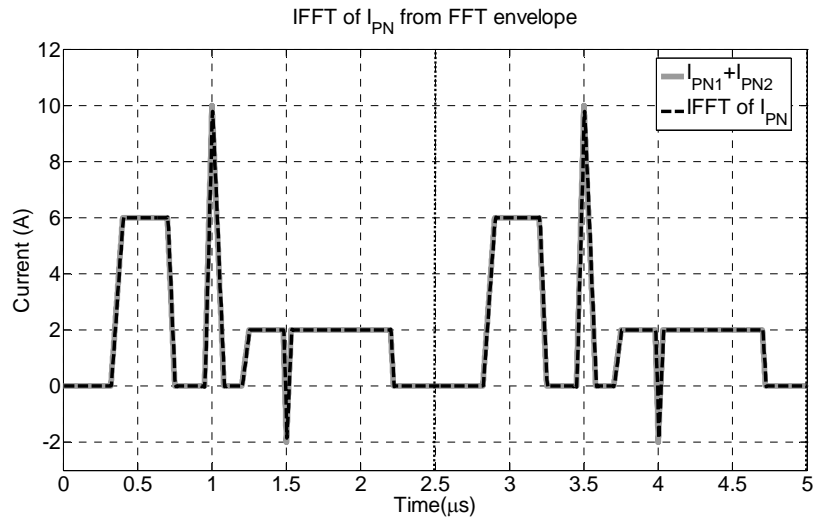
(b) Time-domain current plot over two periods. The solid line is the summation of the two current sources in Fig. 3.1 and the black dashed line is the inverse FFT (IFFT) of the calculated terminal current source, (a).

Fig. 3.4: Equivalent terminal current source of the two-terminal linear network.
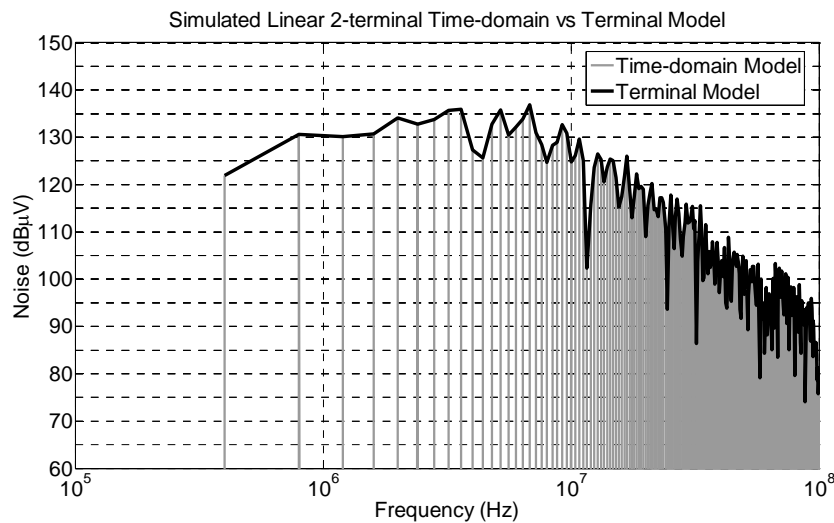
Fig. 3.5: Comparison of EMI for the original two-terminal linear network defined in the time-domain (gray) and the terminal model (black envelope).

3.1.1.2 Converter example

The model is simple and well-defined for linear systems; however, power electronic systems can cause many issues when modeled as a linear network. Although this method should work for nearly any system described in Chapter 2, it is demonstrated for use with a power electronics application. A boost converter's schematic is shown in Fig. 3.6. The nominal condition has an input voltage of 50 V and an output voltage of 400 V. The converter switches at 400 kHz with open loop control. The active (MOSFET and diode) and passive (boost inductor and output

capacitors) components shown in Fig. 3.6 are modeled from the components of an actual boost converter [24].

(a) Nominal system

(b) Attenuated system
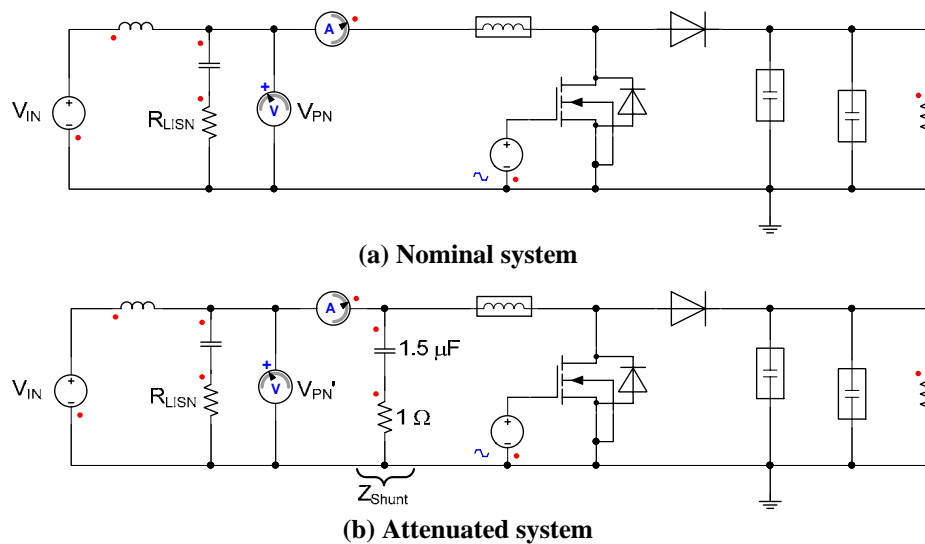
Fig. 3.6: Power electronic system used for verification: boost converter working in open loop with 50 V input and 400 V output, switching at 400 kHz. The active and passive models represent an actual converter.

There is an ideal voltage source with a LISN to provide a well-known and realistic source impedance. The LISN resistor, however, is 1 kΩ in order to comply with the condition set forth in (2-9)a. The converter operates in continuous conduction mode at roughly 50 W. The attenuated case has a shunt impedance comprised of a 1.5 µF capacitor to block the DC component and a 1 Ω resistor to attenuate at the desired frequencies. Similar to the linear example, the simulation was performed in Simplorer at a time step of 1 ns.

The measured terminal voltages in Fig. 3.7 are again displayed in the same fashion as the linear example. The bold lines are the respective envelopes of the complete FFT data. The attenuation between the two conditions is roughly 60 dB, which again is on the order desired.

The modeled impedance is plotted in Fig. 3.8. The equivalent Norton impedance for the converter starts out to be inductive, then resonates and is mostly capacitive with exception of a resonance at about 20 MHz. This physically makes sense since at lower frequencies the terminal impedance will be dominated by the 400 µH boost inductor, which is the impedance of Z_{PN} from 400 kHz to 1 MHz. At higher frequencies, the parasitic capacitances of the inductor and the junction capacitance of the MOSFET will be seen at the terminals, through the resonances at 2 MHz and ~20 MHz, respectively. It should be noted that this model calculates an equivalent impedance only and will not necessarily map directly to a specific parameter in the circuit.
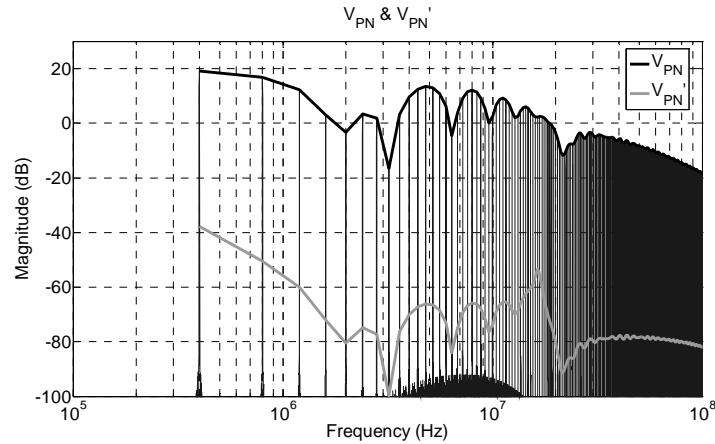
Fig. 3.7: Plot of the two-terminal boost converter voltage measurements. The bold lines are the envelopes of the frequency data; provided from the complete FFT data (shown for V_{PN}).
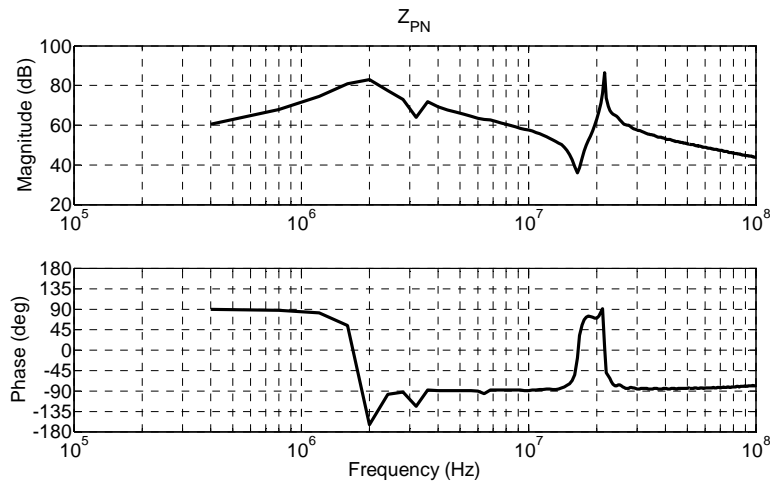
Fig. 3.8: Equivalent Norton impedance of the two-terminal boost converter determined from the model.

The current source, as a function of frequency, is shown in Fig. 3.9a. The IFFT of the equivalent current source is plotted in Fig. 3.9b for visual inspection of the waveform in the time-domain. The time-domain plot clearly shows two different switching instances, roughly 1.25 μs and 1.56 μs, providing for the proper duty cycle. Furthermore, the overall shape of the current source is very similar to the terminal current's characteristics. For example, turn-off of the MOSFET shows the dominant ringing, which is consistent with measurements.

Finally, the modeled terminal EMI is compared to the EMI seen at the LISN resistor of Fig. 3.6. The noise of the nominal condition using the detailed time-domain simulation from Fig. 3.6a, is compared with the terminal model's prediction and plotted in Fig. 3.10. Again, the entire frequency spectrum (gray) is provided for the original system's noise, while only the envelope (black line) is plotted for the terminal model. A nearly perfect agreement is seen throughout the spectrum up to 100 MHz.
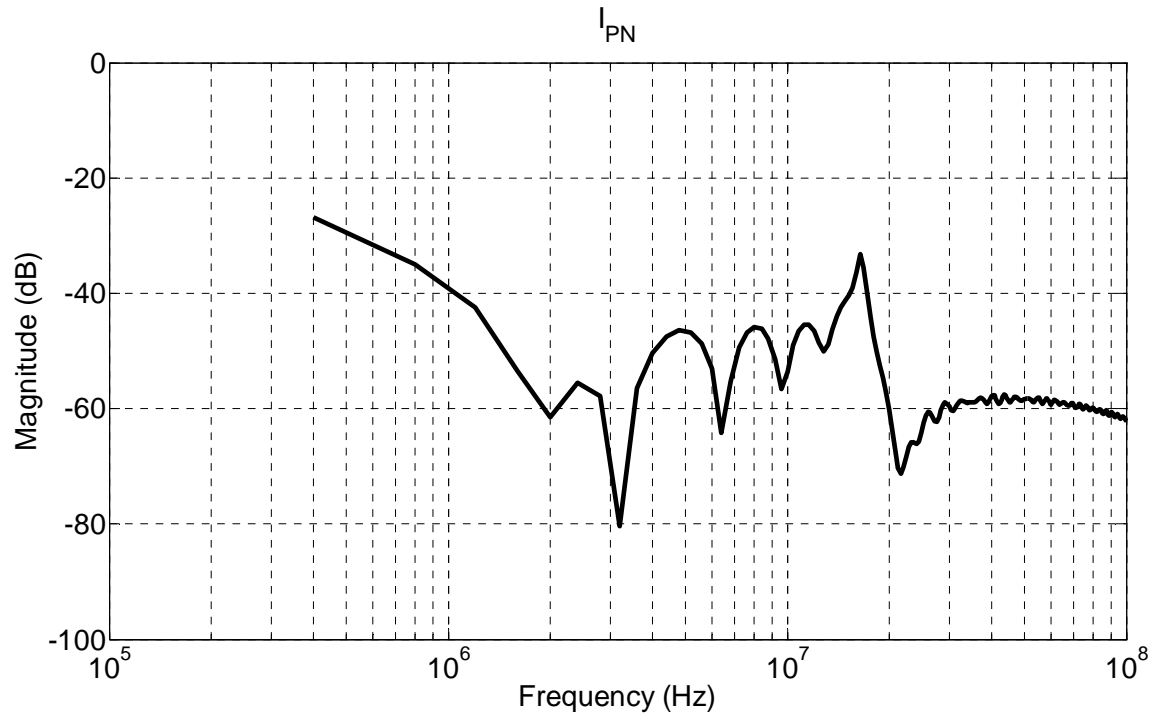
(a) Frequency spectrum calculated for the equivalent terminal current source.
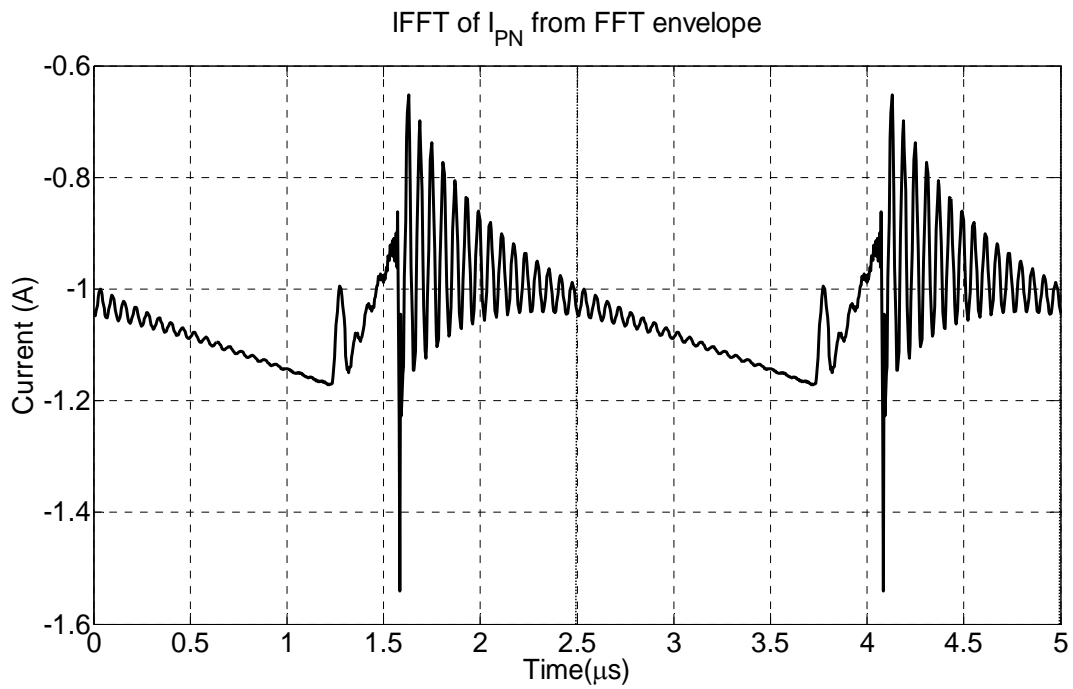
(b) IFFT of the modeled Norton current source.
Fig. 3.9: Equivalent terminal current source of the two-terminal boost converter.
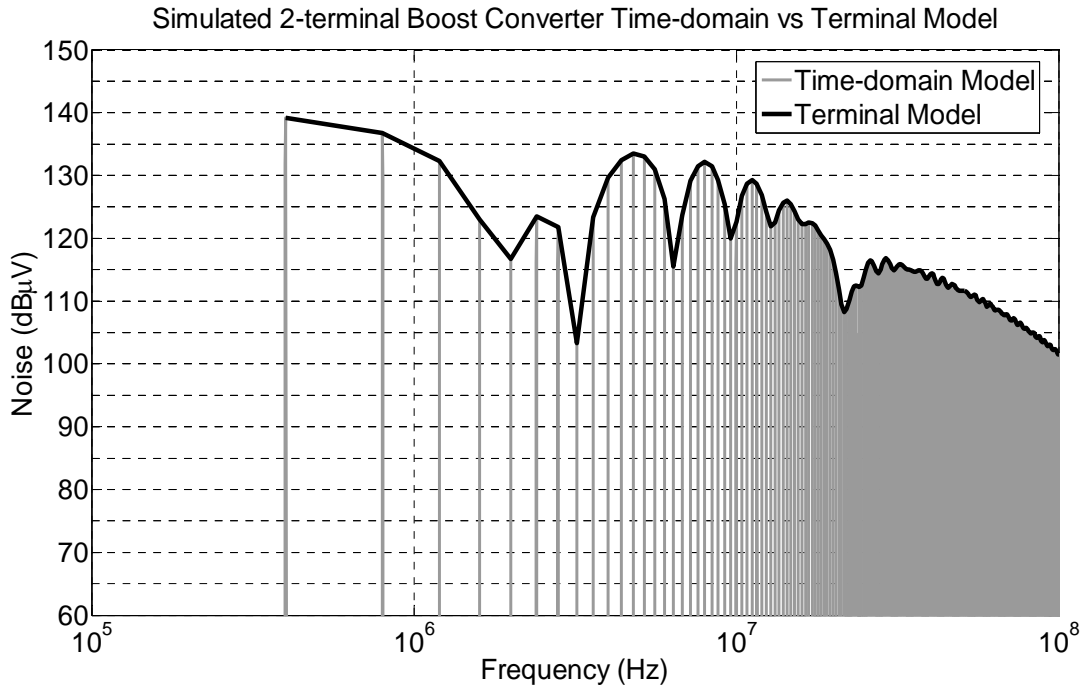
Fig. 3.10: Comparison of EMI for the original two-terminal boost converter defined in the time-domain (gray) and the terminal model (black envelope).

Uniqueness of Converter Model

The uniqueness of the model deserves a brief investigation. The first comparison is made when the shunt impedance changes; that is, the attenuation changes. Both the Norton impedance and current source for the boost converter are shown in Fig. 3.11. They are calculated when the shunt impedance changes by two orders of magnitude, i.e. when $R_{Shunt} = 100 \, m\Omega$ and $R_{Shunt} = 10 \, \Omega$. This impedance is 10 times smaller and then 10 times larger than the example shown in Section 3.1.1.2, respectively. The results are the same for all three attenuation conditions.

Finally, the equivalent model that is created using $R_{LISN} = 1 \, k\Omega$ is used with $R_{LISN} = 50 \, \Omega$. The terminal model is then compared to the time-domain simulation of the boost converter with $R_{LISN} = 50 \, \Omega$ in Fig. 3.12. The overall noise will obviously be less than when $R_{LISN} = 1 \, k\Omega$ and the model predicts this and remains very accurate for source impedances different than the impedance with which it was created.

41

(a) Norton impedance   **(b) Norton current source**
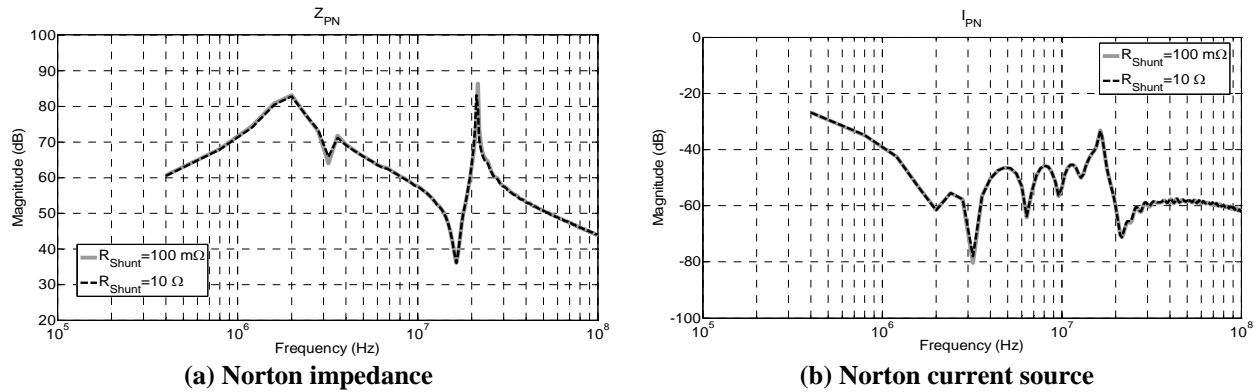
Fig. 3.11: Equivalent Norton parameters of the boost converter example when the shunt impedance varies by two orders of magnitude; R_{Shunt}=100 mΩ is the solid gray line and R_{Shunt}=10 Ω is dashed black line.
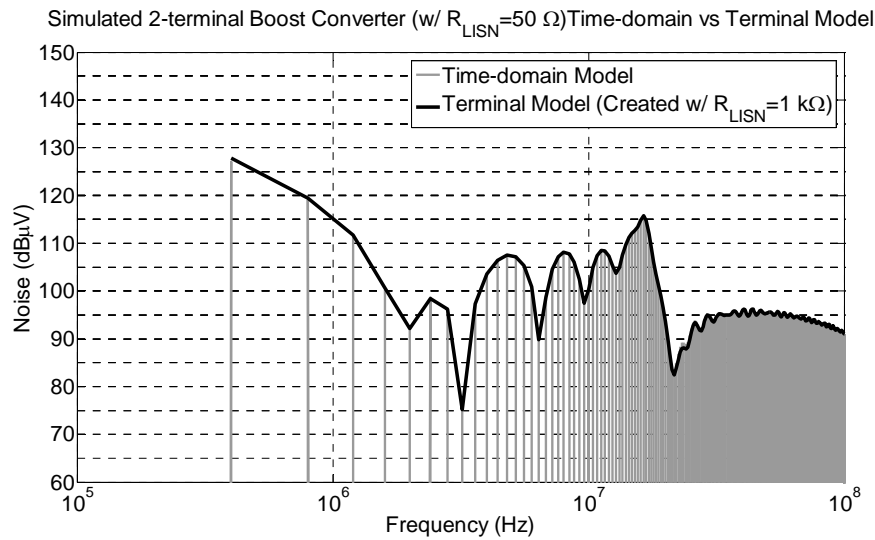
Fig. 3.12: Comparison of EMI when the source impedance is 50 Ω (R_{LISN}). The nominal detailed time-domain simulation is run with R_{LISN}=50 Ω (gray). The terminal EMI model was created with R_{LISN}=1 kΩ, then used in a model with R_{LISN}=50 Ω (black envelope).

Improvements over Previous Methods

A considerable improvement compared to other models is due to the accuracy of the noise source models. As mentioned in Chapter 1 a common method of characterizing the noise source is to assume a trapezoidal waveform. The boost converter modeled in the previous section is compared with using an ideal trapezoidal noise voltage source in Fig. 3.13. All the parasitics of output capacitors, switching elements (MOSFET and diode), any interconnect impedances, etc. causes additional ringing which is included in the noise source using this proposed modeling approach. The inclusion of these effects, in addition to discrepancies in the rise and fall times, improves the accuracy at the higher frequencies. However, Fig. 3.13 also shows some

inconsistencies in the lower frequency range. This is caused by differences in the duty cycle and precise magnitude values of the approximated switched voltage source. It is very difficult to know the exact duty cycle and voltage values and even small differences will cause the errors seen. This is a critical result to illustrate the usefulness for the proposed approach compared to other (and potentially quicker) methods. Additionally, the approximations presented in Section 2.2 that propose the ability to use this method for power electronic systems (regardless of the models switched impedance limitations) is validated with this example.
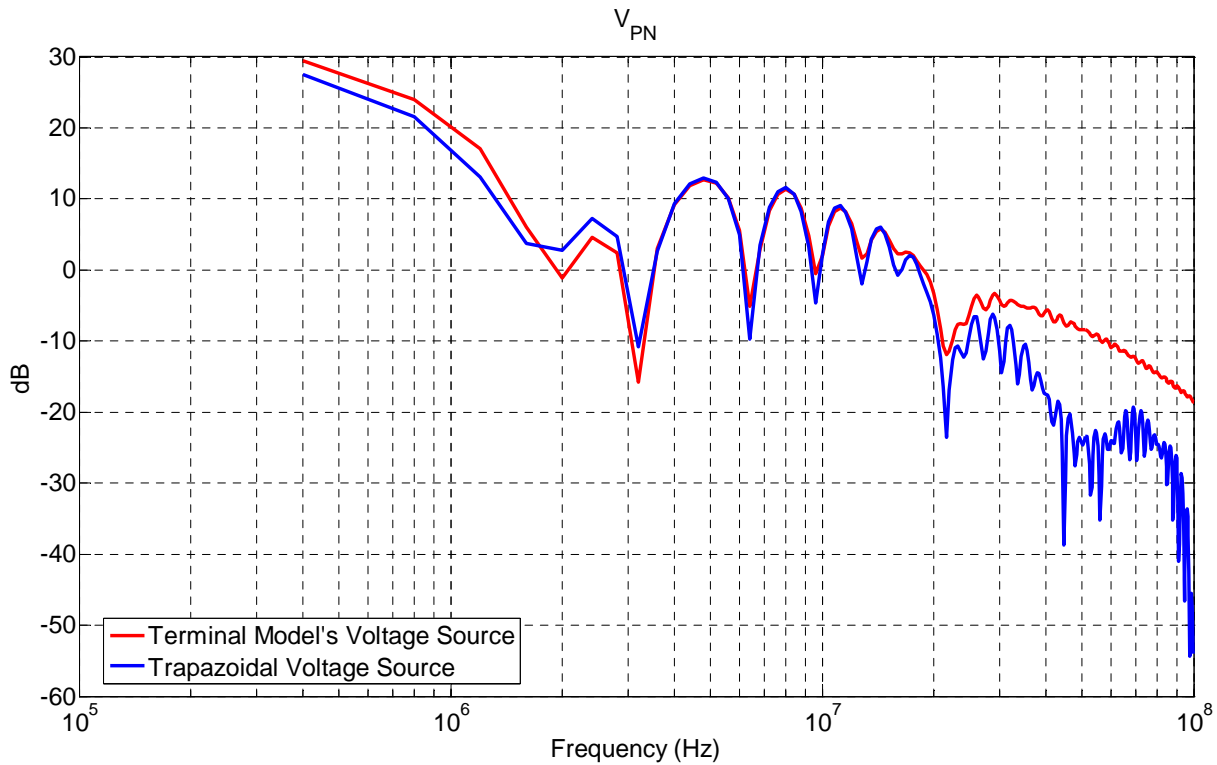
(a) Comparison of the terminal voltages using the two different noise voltage sources.
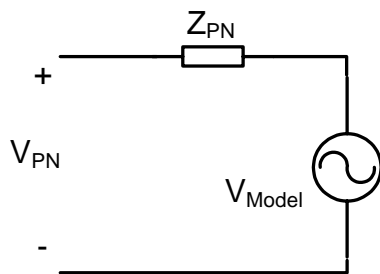
(b) Model using full voltage source from the terminal modeling methods in previous section.
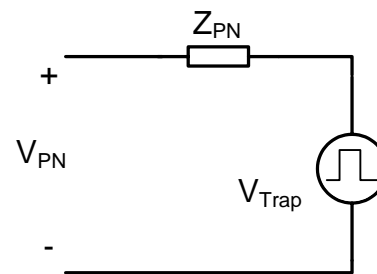
(c) Model using an ideal trapezoidal voltage source.

Fig. 3.13: Difference of the terminal voltage seen calculated using the terminal modeling method vs. an ideal trapezoidal voltage source.

Sensitivity Discussion

A sensitivity analysis provides an important understanding of how the EMI, or terminal voltage prediction, is affected by uncertainty in the model parameters. This section provides an example of how a sensitivity study could be done on various parameters; a complete analysis is not completed in this work. An initial requirement is to define the error of the model. Some work has been done to characterize the accuracy of a model or measurements using a defined cost function, figure of merit, or a norm between actual and modeled results [67-68]. A visual inspection that compares the actual noise to the modeled noise is typically done to determine the accuracy of the model and is used in this paper. This, however, does not provide an exact error (or accuracy) factor and an error determined by inspection can also be subjective.

Using the boost converter in Section 3.1.1.2 a few types of errors are demonstrated in Fig. 3.14 – Fig. 3.17. Four different types of errors are shown: a multiplicative and additive error for both the magnitude and phase. The first plot, Fig. 3.14 shows a multiplicative error of the Norton impedance created by the model. The second plot, Fig. 3.15 shows the affects of an additive error in the Norton impedance. Similarly, Fig. 3.16 and Fig. 3.17, respectively show the errors for multiplicative and additive effects to the Norton current source. A 10% error in the magnitude or phase is used to examine the sensitivity of the terminal voltage. The multiplicative error for either of the Norton parameters only causes a small discrepancy in the terminal voltage (< 2 dB throughout the spectrum). Additive errors can cause a much bigger discrepancy, specifically in the current source. The reason the impedance does not cause as large of an error is because it is in parallel to the source impedance, so the error is diminished by the source impedance. The ratio of the source impedance and the Norton impedance will affect the magnitude of the error. Additive errors in the phase of the current source are not a large factor since it already wraps around 2π many times. The largest error is due to the additive error of the current source's magnitude. A 10 mA error causes up to 20 dB discrepancy to the terminal voltage. Similarly to the impedance, the sensitivity of the current source will change for every system's modeled values. Additionally, sensitivity analysis was also done for input parameters such as Z_{Source} and Z_{Shunt} (not shown here) to find that the model is also very sensitive Z_{Shunt}. A detailed sensitivity analysis could be done to fully characterize the uncertainty in the model.
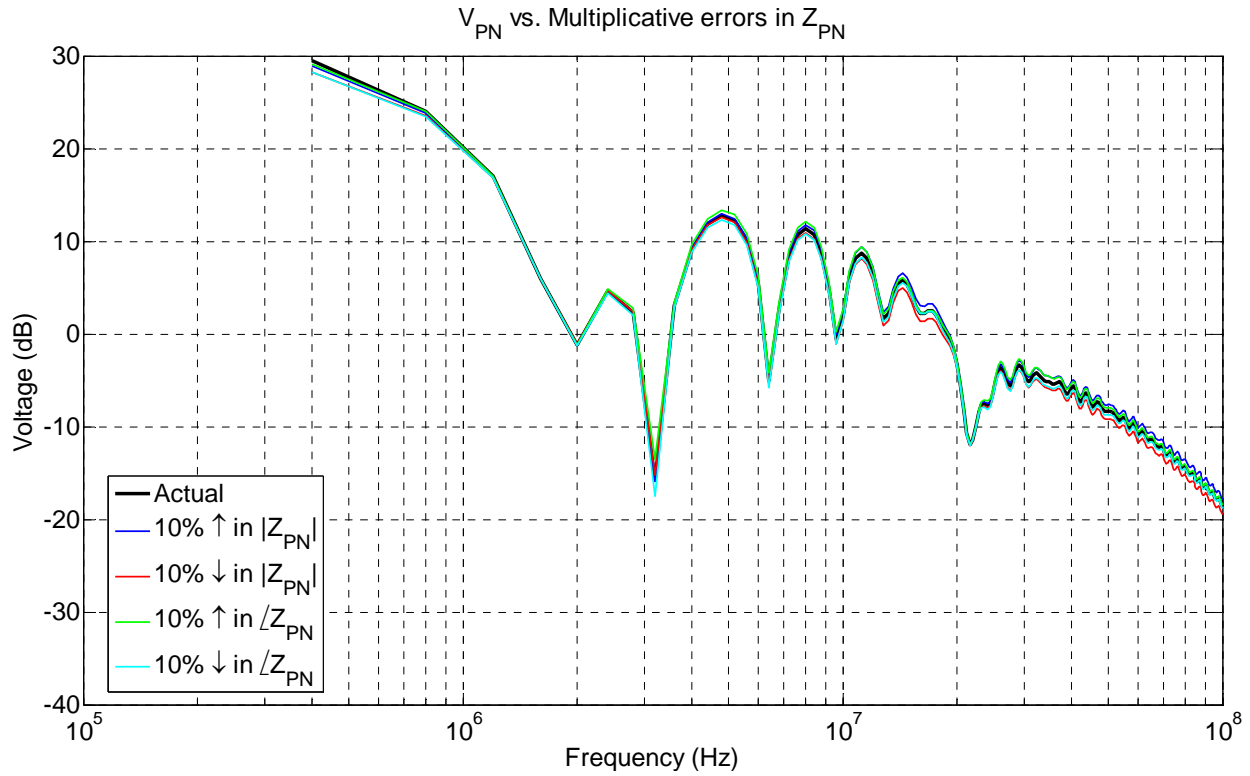
Fig. 3.14: **Discrepancies in terminal voltage as the Norton impedance's magnitude or phase varies by 10%.**
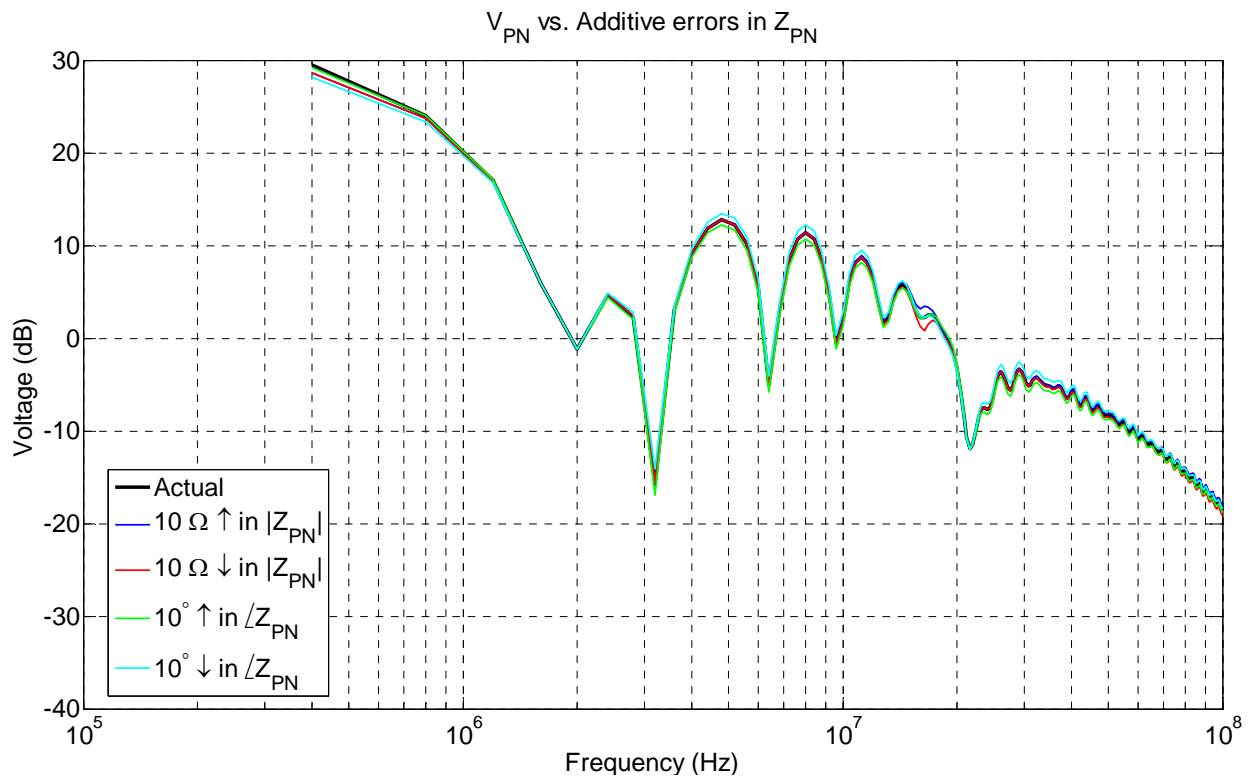
Fig. 3.15: **Discrepancies in terminal voltage as the Norton impedance's magnitude varies by 10 Ω or phase varies by 10°.**
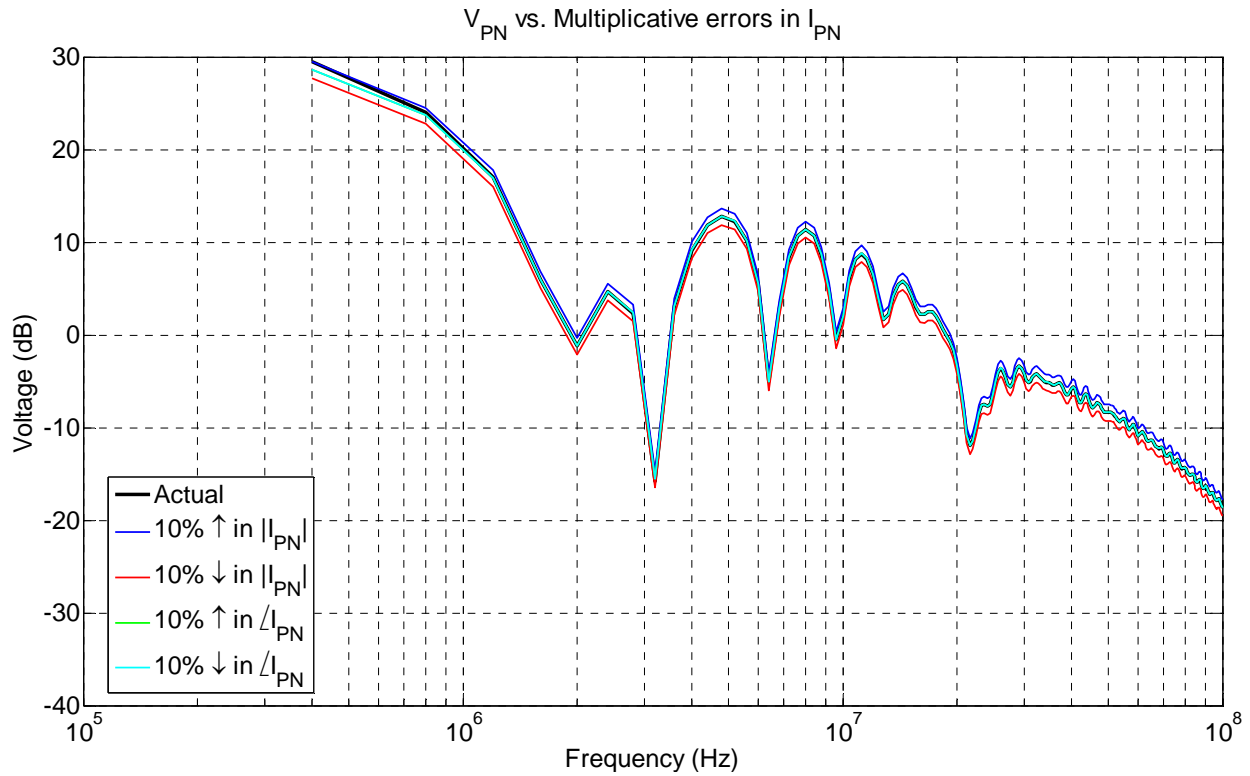
Fig. 3.16: Discrepancies in terminal voltage as the Norton current source's magnitude or phase varies by 10%.
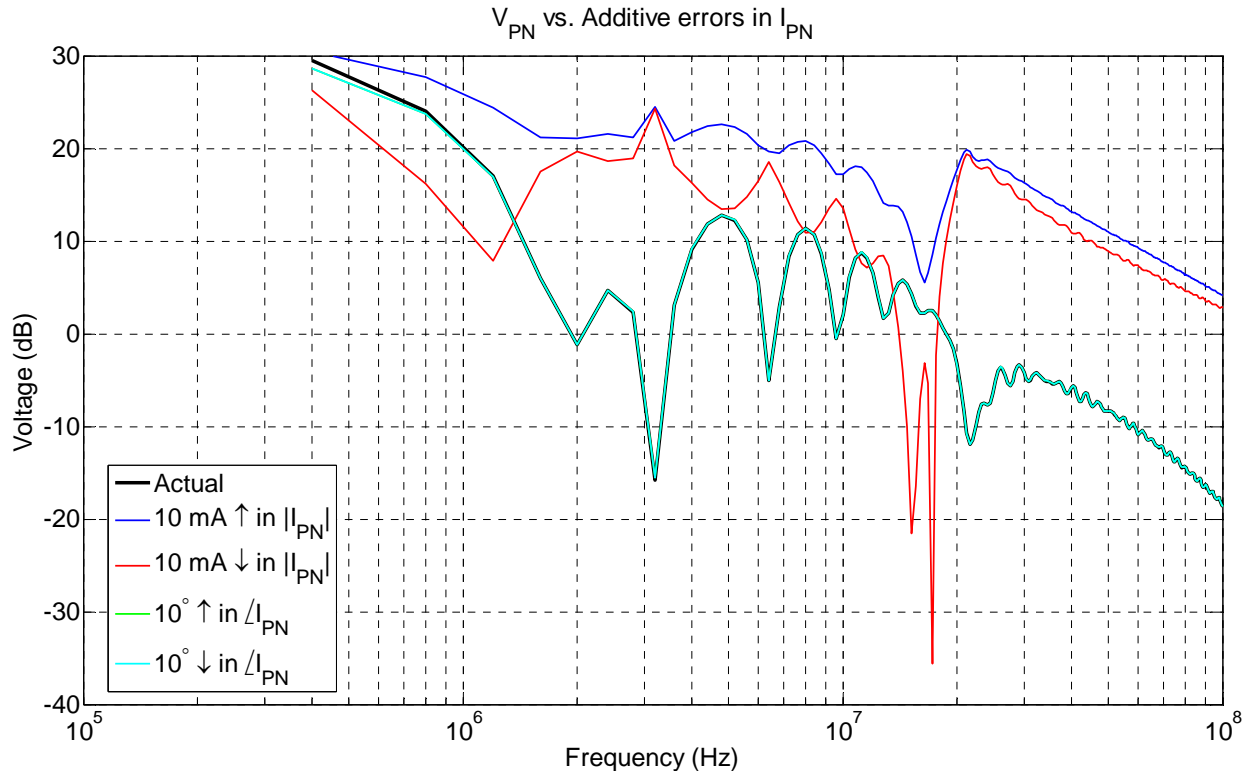
Fig. 3.17: Discrepancies in terminal voltage as the Norton current source's magnitude varies by 10 mA or phase varies by 10°.

46

3.1.2 Three-Terminal

3.1.2.1 Linear Example

In order to verify the three-terminal model, a completely linear time-invariant example is again demonstrated first. The linear system used is shown in Fig. 3.18, similar to Fig. 2.8, the nominal condition is in all black and an example attenuation case shows the shunt impedances in gray. The three impedances are a simple resistive-inductive (R-L) combination arbitrarily chosen, where $Z_{PG} = 4.5\Omega + 1\mu H$, $Z_{NG} = 12.5\Omega + 0.1\mu H$, and $Z_{PN} = 0.5\Omega + 6.5\mu H$. Similarly, the current sources are also arbitrarily chosen with various rise and fall times and magnitudes to provide a rich and complex frequency spectrum. Both of the current sources are periodic with a period of 2.5 µs (400 kHz). All impedances are labeled in the schematics and the two current waveforms are provided in Fig. 3.18b.
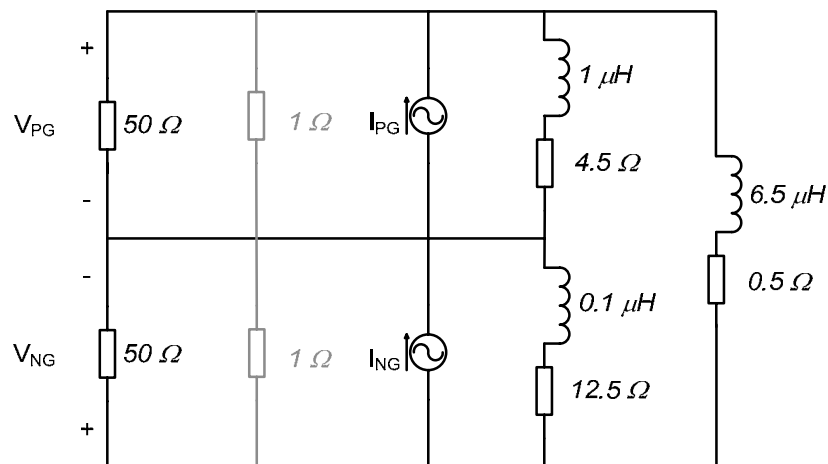
(a) Nominal system, example of one attenuated case shown with the gray shunt impedances.
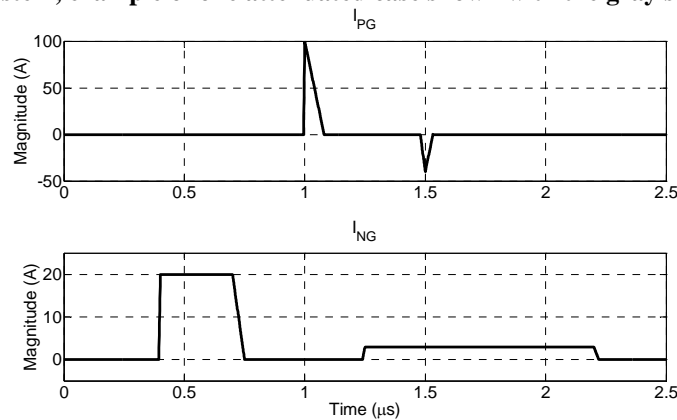
(b) Periodic current sources used in model.

Fig. 3.18: Linear system used for verification: composed of two periodic (400 kHz) current sources and three resistive-inductive impedances.

A source impedance of 50 Ω is used initially, and the shunt impedances for the attenuated conditions are all chosen to be 1 Ω. The simulation was also performed in Simplorer under the same conditions as the two-terminal examples. Five different cases were simulated: 1) nominal, one shunt between 2) positive - ground, 3) negative - ground, then between 4) positive - negative, finally 5) two shunts, one between both positive - ground and negative - ground.

Using the methods described in the previous section with the terminal voltage measurements in all five cases the equivalent terminal impedances and current sources are calculated. The impedances are plotted in Fig. 3.19. The plot has both the ideal impedance shown in Fig. 3.18a and the modeled terminal impedances. The two impedance curves overlap each other nearly perfectly up to 100 MHz. The current sources as a function of frequency are shown in Fig. 3.20. The solid gray line is the original current sources, and the thinner black line is the modeled terminal current source. It is clear that the two current waveforms overlap completely, verifying the accuracy of the model. Finally, the total noise seen at the terminals is compared; the noise between the detailed nominal condition (Fig. 3.18) and the terminal model is plotted in Fig. 3.21. Again, the entire frequency spectrum (gray) is provided for the original system's noise, while only the envelope (black line) is plotted for the terminal model. A nearly perfect agreement is seen throughout the spectrum up to 100 MHz.
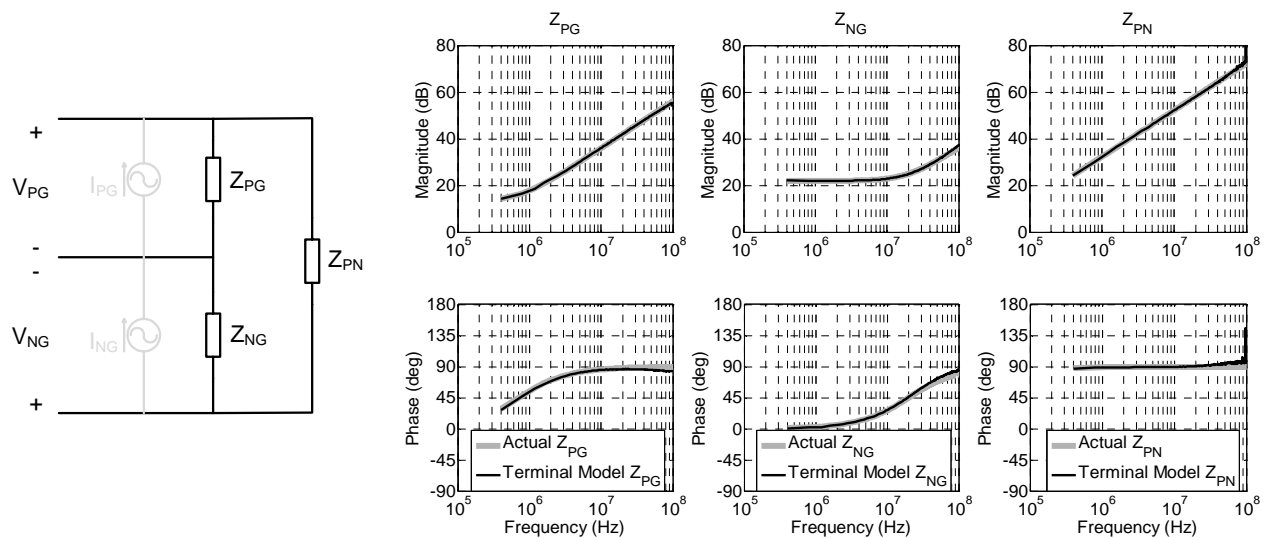
Fig. 3.19: Comparison of the calculated (modeled equivalent terminal) impedances and the actual impedances in the linear three-terminal system.
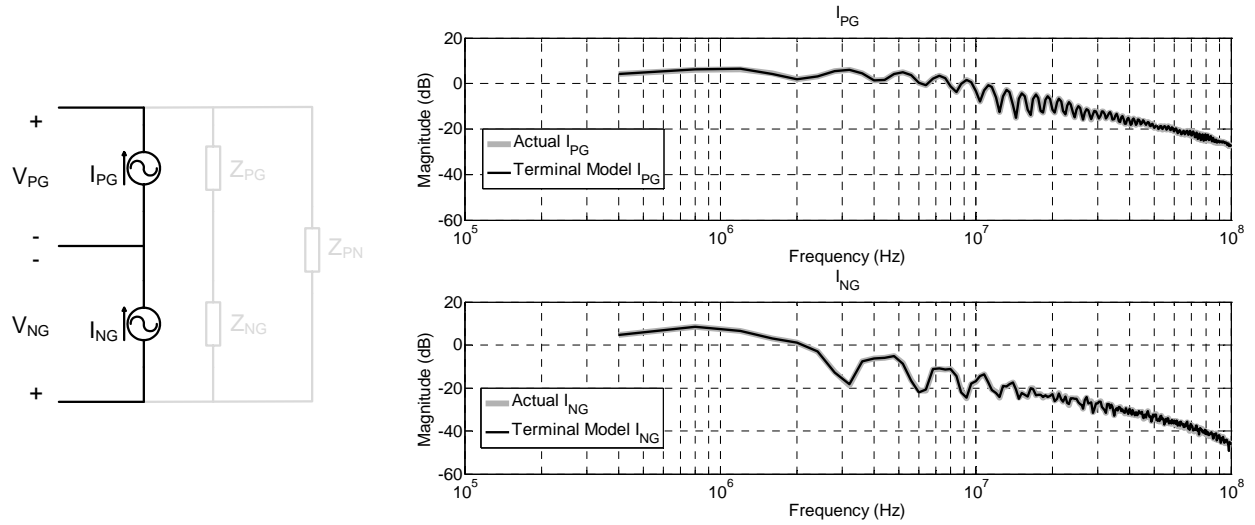
Fig. 3.20: Comparison of the calculated and actual frequency spectrums for the two current sources of the three-terminal linear system.
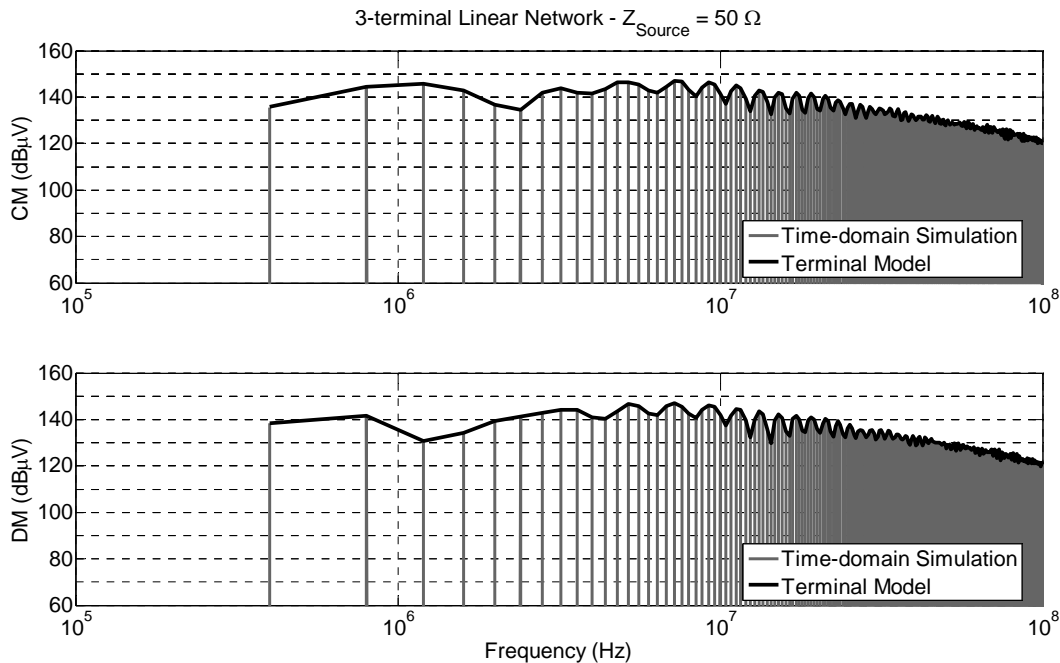
Fig. 3.21: Comparison of EMI for the original linear three-terminal system defined by the detailed time-domain simulation (gray) and the terminal model (black envelope).

There are many options in determining the terminal noise with the model created in Matlab. Two that were used in this work are to directly solve the equivalent circuit equations in Matlab. If it is desired to use this model in conjunction with other circuit elements, Matlab can be used to write a netlist with the current sources and impedances as a function of frequency. This netlist can then be used in Simplorer (or any other circuit simulator) as a black box model. This makes it simple for investigating multiple systems in one simulation.

3.1.2.2 Converter Example

A three-terminal boost converter is used to illustrate the model for a power electronic system; the schematic is shown in Fig. 3.22. The converter operates the same as in Section 3.1.1.2, however, with CM impedances. The nominal condition has an input voltage of 50 V and an output voltage of 400 V. The converter switches at 400 kHz with open loop control. There is an ideal voltage source with LISNs at the input. The converter operates in continuous conduction mode at roughly 50 W. The attenuated cases use shunt impedances comprised of a 1.5 µF capacitor to block the DC component and a 1 Ω resistor to attenuate at the desired frequencies.
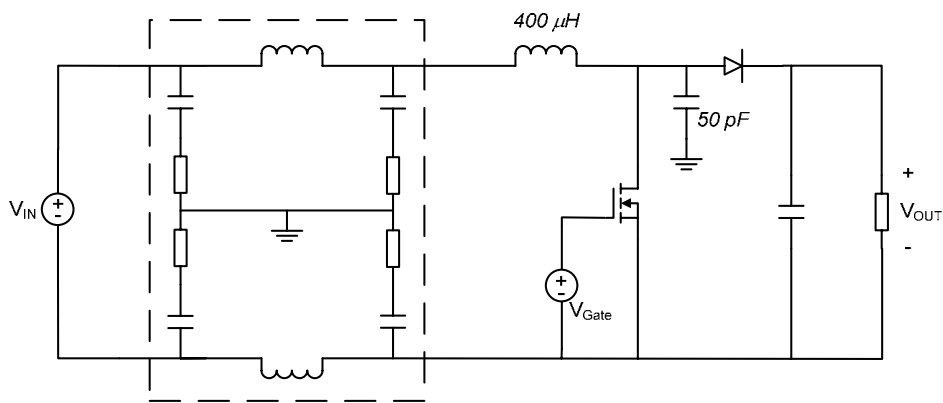
Fig. 3.22: Power electronic system used for verification: boost converter in open loop with V_{IN}=50 V,
V_{OUT}=400 V, f_s=400 kHz. The active and passive models represent an actual converter.

The modeled impedances are plotted in Fig. 3.23. The equivalent impedance across the positive and negative terminals starts out to be inductive, then resonates and is mostly capacitive with exception of a resonance at about 20 MHz; similar to the two-terminal impedance witnessed earlier. The impedance of Z_{PG} is the sum of the inductors impedance and the capacitive impedance, only there is some error that is discussed below. Z_{NG} is the impedance of the switch in series with the capacitance to ground. Since the impedance of the switch is very small (junction capacitance) compared to the ground capacitor at these frequencies, the 50 pF capacitance is seen as Z_{NG}.

This is an example when the source impedance used to determine the model is critical. The three impedances of the system range from 20 dB to 100 dB. The lower impedances (at higher frequencies) are most accurate when the source impedances are smaller (50 Ω). However, the higher impedances (at lower frequencies) are more accurate with a larger source impedance (1 kΩ). A couple options are available to reduce this error. A capacitive source

impedance can be implemented to cause the impedance to decrease as the frequency increases, although in general that may not always be the form of the unknown impedances. Furthermore, it will force a different source impedance to be manufactured for every model created. In order to keep the model acquisition process as simple as possible, only the two source impedances will be used 50 Ω and 1 kΩ. Measurements will be taken with both source impedances and a least squares approximation (still using *lsqnonlin*) will be performed on all the data sets. This is what is seen in Fig. 3.23. Even with the use of both source impedances, some errors are also seen in the model. Around 80 MHz there is a large error in Z_{PN}. Furthermore, there is some error in Z_{PG} as well. This is primarily due to the large magnitude of Z_{PG}; even with the source impedance of 1 kΩ (60 dB) the magnitude of Z_{PG} is 20-60 dB larger below 10 MHz. This error may be reduced by using an even larger source impedance. However, these models will primarily be used with a source impedance of 50 Ω, or smaller, for EMI purposes; impedances much larger than 10 kΩ would not impact the system greatly. One instance where this may have an impact is with an interaction with another system of similar impedance. For increased accuracy the model could also be created with the addition of a source impedance of roughly 10 kΩ.
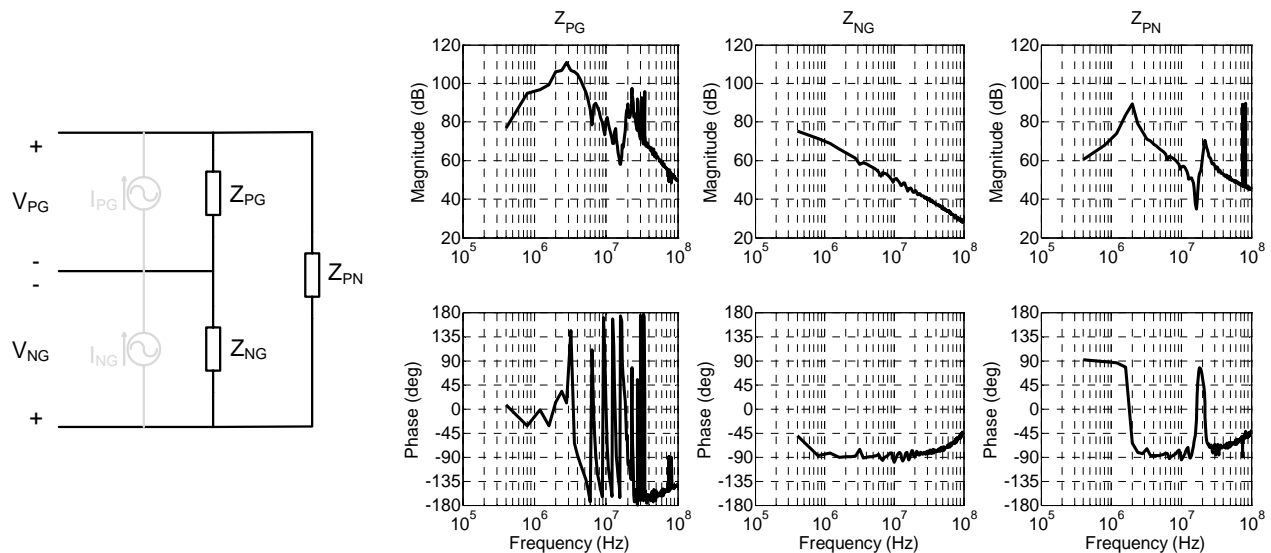
Fig. 3.23: Equivalent impedances of the simulated boost converter determined from the model.

The current source, as a function of time, is shown in Fig. 3.24. The IFFT of the equivalent current source is plotted for visual inspection of the waveform in the time-domain, and is very similar to the two-terminal example. As before the model solves for the full frequency spectrum and the time-domain information can then be determined from the frequency data. Finally, the

noise of the nominal condition using the detailed time-domain simulation (Fig. 3.22) is compared to the terminal model with $R_{LISN} = 50\Omega$ and plotted in Fig. 3.25. Again, the entire frequency spectrum (gray) is provided for the original system's noise, while only the envelope (black line) is plotted for the terminal model. A nearly perfect agreement is seen throughout the spectrum up to 100 MHz.
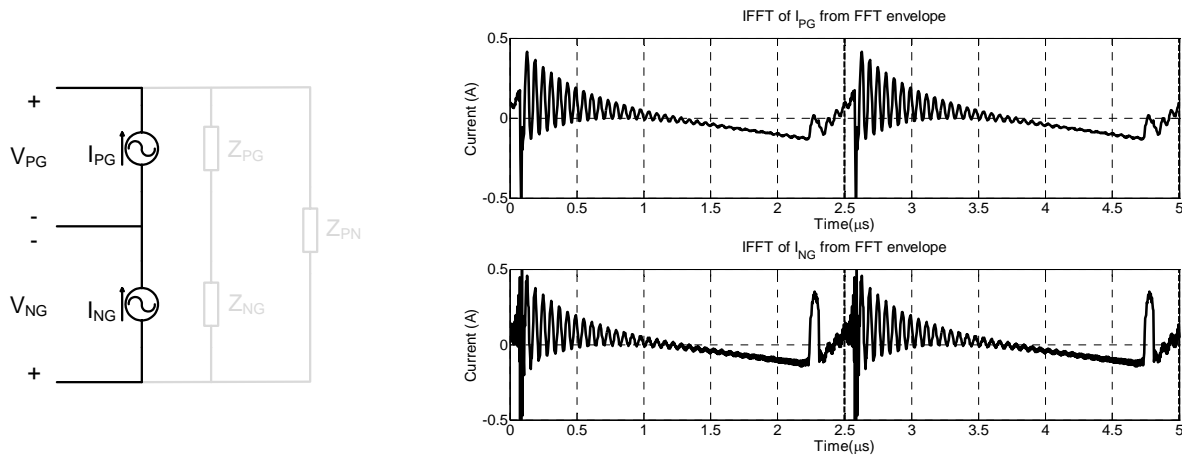
Fig. 3.24: IFFT of the equivalent current sources of the simulated boost converter.
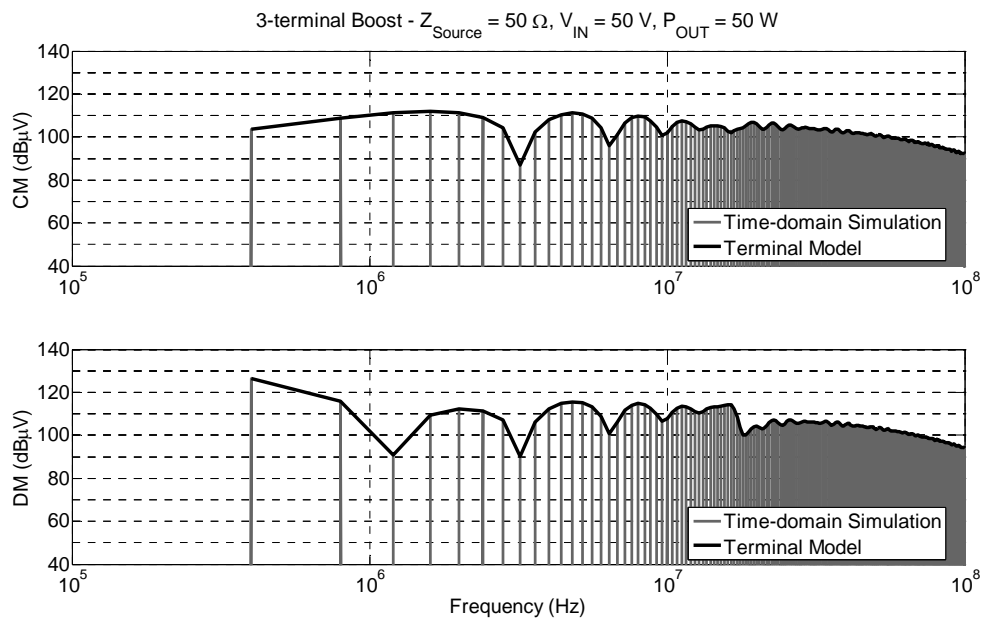
Fig. 3.25: Comparison of EMI for the detailed simulated boost converter defined in the time-domain (gray) and the terminal model (black envelope).

3.1.3 Four-Terminal

As mentioned in Section 2.4 the four-terminal model is not focused on in this work. Some preliminary results, however, will be shown and discussed in order to direct additional work with this modeling approach beyond the three-terminal examples. A simple four-terminal linear example is displayed in Fig. 3.26. The parameters in this example are chosen to somewhat resemble similar impedances and operations of a phase-leg module. The capacitances to ground, C_{PG}, C_{NG}, C_{OG}, are typical parasitic capacitances. Capacitors, C_{PO} and C_{ON} are chosen to resemble a junction capacitance. The final impedance Z_{PN} depicts a decoupling capacitor with typical ESR and ESL values. Finally, the current sources, I_{PO} and I_{ON}, are pulsed waveforms that might resemble switching while I_{OG} is a CM current source with sharp spikes. It is also worth noting that there are no fundamental issues with switched impedances, non-linearities, equivalent circuit differences, or measurement errors. Since this is a simulated example, each impedance and current source in the system should closely match the modeled parameters.
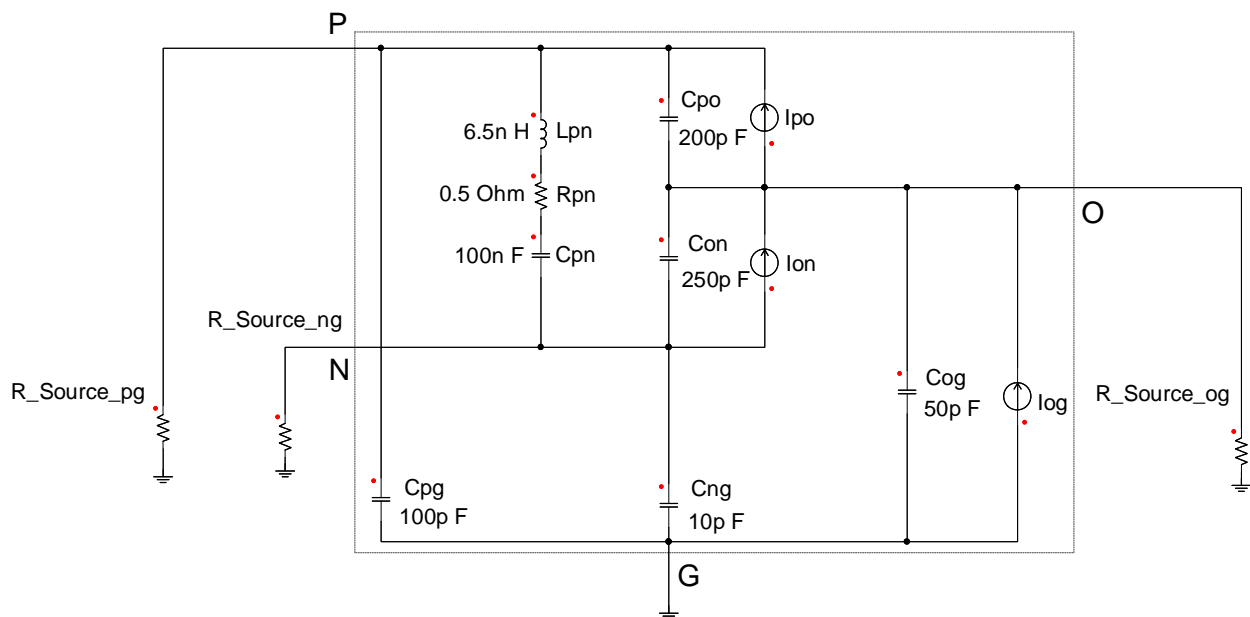
Fig. 3.26: Four-terminal example that shows some difficulties even in a simple linear network.

Several problems occurred in the initial modeling process. First, the value of the impedance Z_{PN}, among others, influenced the overall accuracy of the model. When Z_{PN} was much smaller than the other impedances in the system it dominated the flow of current. This caused for the other impedances in the system to become less significant in determining the terminal voltages; therefore, errors occurred in calculating all the impedances dwarfed by Z_{PN}. This was also found

to be true when there is a large difference between all the impedances in any modeling example. However, since the number of equivalent impedances in the four-terminal example increases drastically the errors are more pronounced and can occur more frequently than a three- or two-temrinal.

Another issue is the values of the current sources pictured in Fig. 3.26. Under nominal operating conditions I_{PO} and I_{ON} are defined by the operation of the converter's load. However, the value I_{OG} would ideally be zero since it is considered noise currents. The inherent nature of the converter design attempts to keep this current at a minimum. When I_{OG} was chosen to have two spikes of current equaling 1 A in amplitude extremely large errors occurred. The blue plots in Fig. 3.27 show the modeled impedances, with this small I_{OG}, compared to the black ideal impedances in the actual simulation of the network. Large errors are clearly seen in the impedances to ground, Fig. 3.27a. Again this is due to the fact that the ground impedances and current source (I_{OG}) at this operating condition do not significantly affect the terminal voltages. An example to illustrate this phenomena is performed with the current source, I_{OG}, modified to have peak current spikes of 100 A. This is shown as the red plots in Fig. 3.27. Although some errors still occur the only significant error is seen in Z_{NG}, again due to the fact that it is a considerably larger impedance than all other impedances and less significant.

The lack of significance in some parameters is a serious one that would need to be solved before proceeding further with the four-terminal model. This issue will only worsen as the number of terminals increases. These parameters that are insignificant do not necessarily need to be involved in the modeling process, however, in the general case it may not be possible to know which parameter should be excluded. Additionally, an impedance may be insignificant at some frequencies but not others, as can be seen in Z_{NG} in Fig. 3.27a, which makes it increasingly difficult to exclude certain parameters at only certain frequencies. Finding a particular method to systematically justify the appropriate modeling conditions is also needed for the four-terminal system as well as a general approach for n-terminal systems.
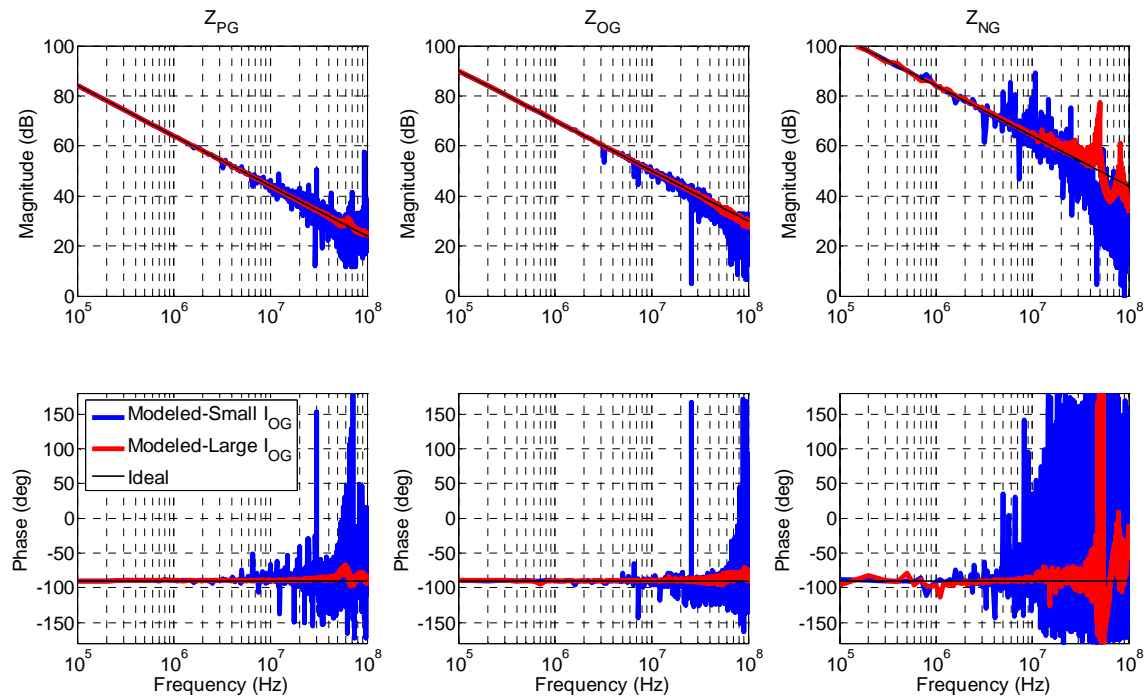
a) **Impedances from power terminals to ground.**
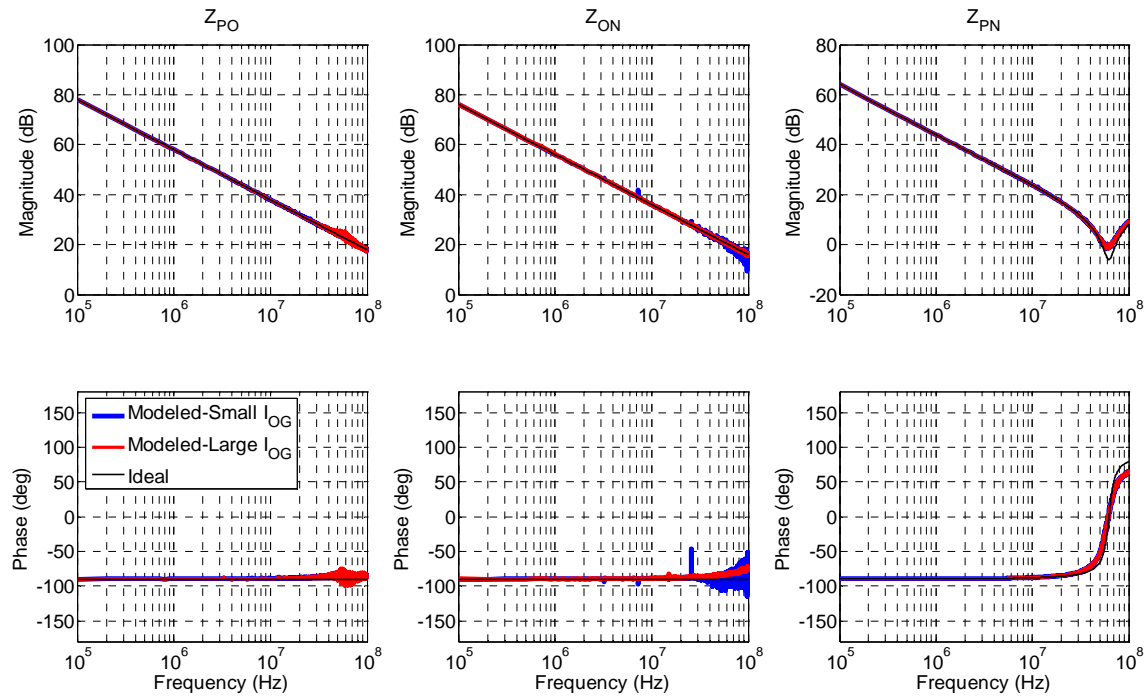
b) **Impedances between each power terminal.**

Fig. 3.27: Comparison between modeled impedances and ideal impedances in the four-terminal system.

3.2 MEASUREMENT VALIDATION

3.2.1 Procedure

In order to acquire accurate results through a universal method a measurement fixture was made. The fixture is shown in Fig. 3.28; it is based off of the design of a LISN. The inductance and capacitance seen in the schematic assist in blocking any outside noise from entering the system to be modeled. This also provides the ability to choose the source impedance that is desired. For this fixture a switch is used to change the source impedance from 50 Ω to 1 kΩ at the EMI frequencies. At lower frequencies the impedance is mostly inductive. The fixture also has a repeatable method of implementing the shunt impedances. This is critical since the shunt (and source) impedance needs to be precisely known up to 100 MHz in order to avoid large errors in the calculations of the unknown parameters. Any combination of shunt impedances is possible by inserting the appropriate jumpers. Using the switches and jumpers still allow the system to function under the same low frequency operating conditions.

Another requirement of the measurement fixture is to achieve repeatable and accurate measurements of the terminal voltages. Since different probes (and the connections of each probe) can produce different results a standardized method was adopted. A BNC connection is used to minimize the ground loop which can greatly affect results at high frequency. A Tektronix TDS 7054 Oscilloscope is used to measure the terminal voltages simultaneously from the fixture via a 10X passive probe in the same fashion every time. Finally, the metal enclosure of the fixture helps to further shield any outside noise from entering the system that should not be included into the model.

The source impedances of the fixture can accurately be measured using Agilent's 4295A Precision Impedance Analyzer through the BNC connections. The shunt impedance is more difficult, however, due to its small magnitude, and implementation into the system. To determine the net effects of the shunt impedances on the system, they are individually calibrated through modeling a known two-terminal impedance that is independently measured using an impedance analyzer. The two-terminal model is created using the same procedures described in Section 2.1. A two-terminal method is used since an impedance and source can be created to maximize accuracy of the model. The results of the model are then solved in reverse to determine the unknown Z_{Shunt} instead of Z_{PN}.

Only one period is captured from the oscilloscope. This helps simplify the modeling procedure and memory usage during the calculations. To further improve the accuracy an averaging of ~100 triggered waveforms is done on the oscilloscope prior to saving the data. This reduces the noise in the captured waveform, and therefore increases the fidelity of the model. Since each switching period is assumed the same in steady-state conditions this approach is valid. This is especially important since only one period is captured; it is similar to performing the FFT on 100 waveforms. Finally, the sampling time is set at the maximum of the oscilloscope, 400 ps. Furthermore, a third channel is used to trigger the oscilloscope at a consistent point. Since both of the LISN voltage measurements are changing due to the attenuation schemes, a different location is needed for the triggering. The output voltage is used throughout this study since it remains relatively consistent in all conditions.
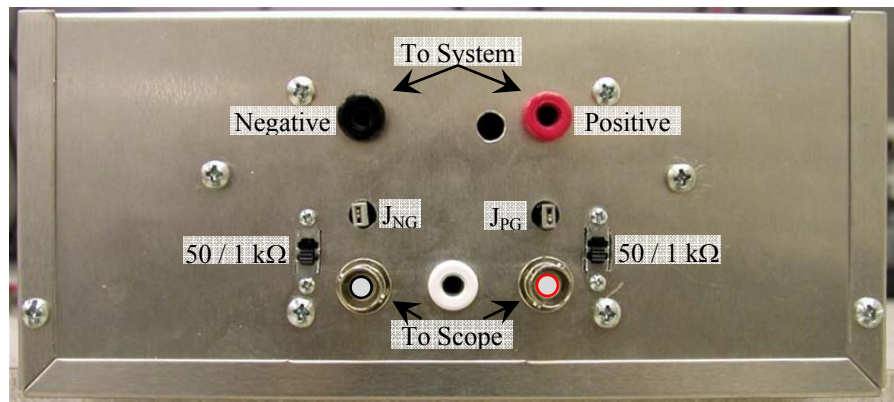
(a) Picture of the measurement fixture used to capture terminal voltage.
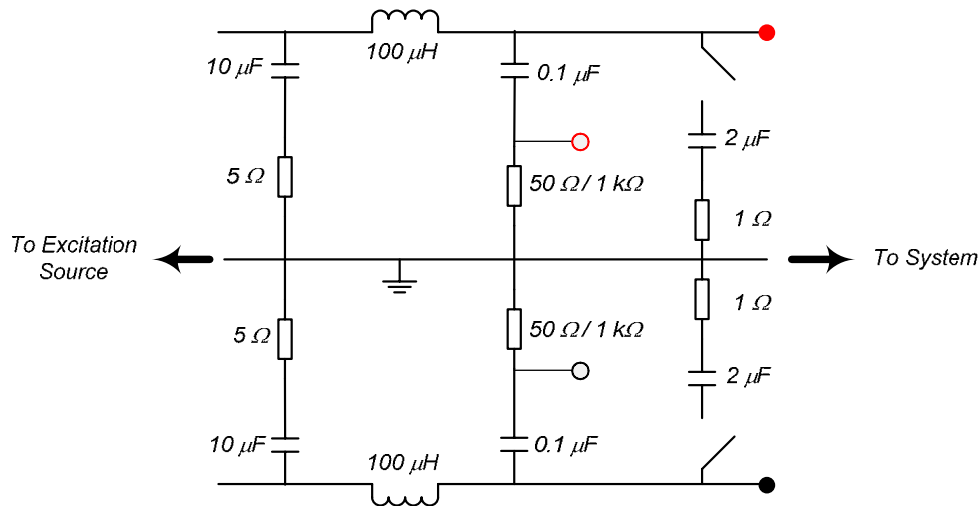
(b) Schematic of the measurement fixture.

Fig. 3.28: Measurement fixture provides a known source impedance (50 Ω or 1 kΩ) that is based off of a LISN. The shunt impedances can also be included by the using the appropriate jumper(s). To provide a consistent method of acquiring the waveforms, measurements are taken directly from the BNC terminals.

3.2.2 Boost Converter

The system used in the validation process is a power factor correction converter operating as a controlled dc-dc converter with 50 V input, 400 V output, 50 W output power, switching at 400 kHz. A simplified schematic of the converter is provided in Fig. 3.29. Additionally, the transformation the equivalent circuit represents is illustrated in Fig. 3.30, where the five equivalent parameters will characterize the complete hardware of the converter. The output voltage of the boost converter has a small ripple that is not greatly affected under the different measurement conditions; therefore, it was used as the trigger for all the measurements. Furthermore, the model was acquired with the source impedances of 50 Ω and 1 kΩ. Four measurements were performed for each source impedance: nominal, and attenuated across P-G, N-G, and finally P-G & N-G at the same time. As mentioned earlier all eight measurements are used simultaneously to solve the model.
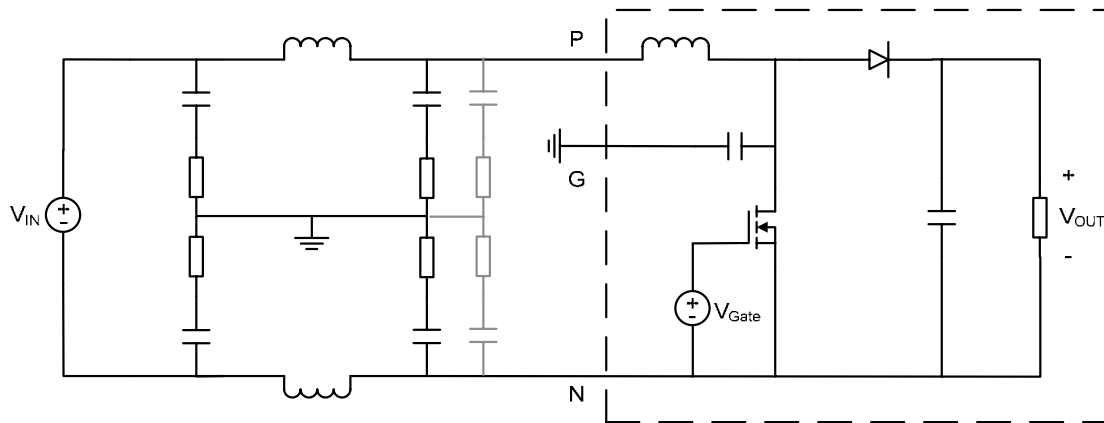
Fig. 3.29: Schematic of boost converter used in experimental measurement validation. Operating at V_{IN}=50 V, V_{OUT}=400 V, P_{OUT}=50 W, f_s=400 kHz.
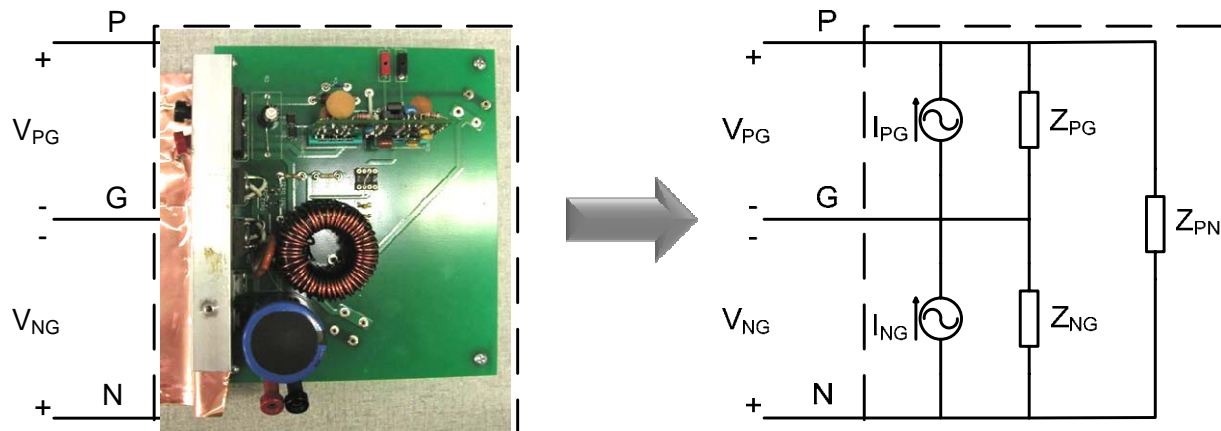
Fig. 3.30: Picture of boost converter modeled and an illustration what the equivalent circuit represents.

The model results are shown below: equivalent impedances in Fig. 3.31, equivalent current sources in Fig. 3.32, and the comparison of the overall EMI seen at the LISN is provided in Fig. 3.33. First, the results above 50 MHz are not very accurate. This is due to the voltage measurements; the magnitude of the voltage at these frequencies is very low and on the order of the background noise, causing a low signal-to-noise ratio. Therefore, accurate measurements are not attainable. Below 50 MHz, however, the results are very accurate, within a couple dB.

It is difficult to compare the impedance and current measurements to an ideal case. This is an equivalent circuit so no one component makes up an equivalent impedance; that is, all components – including, but not limited to, the discrete passives, actives, control, and layout – in the system are lumped together into the three equivalent impedances and two current sources. However, noise seen at the terminals can directly be compared to the measured values, with high accuracy. Both of the simulated systems were modeled accurately. This example shows that with care in the measurement procedures and accurate calibrations the modeling procedure for an actual power electronic system is valid.
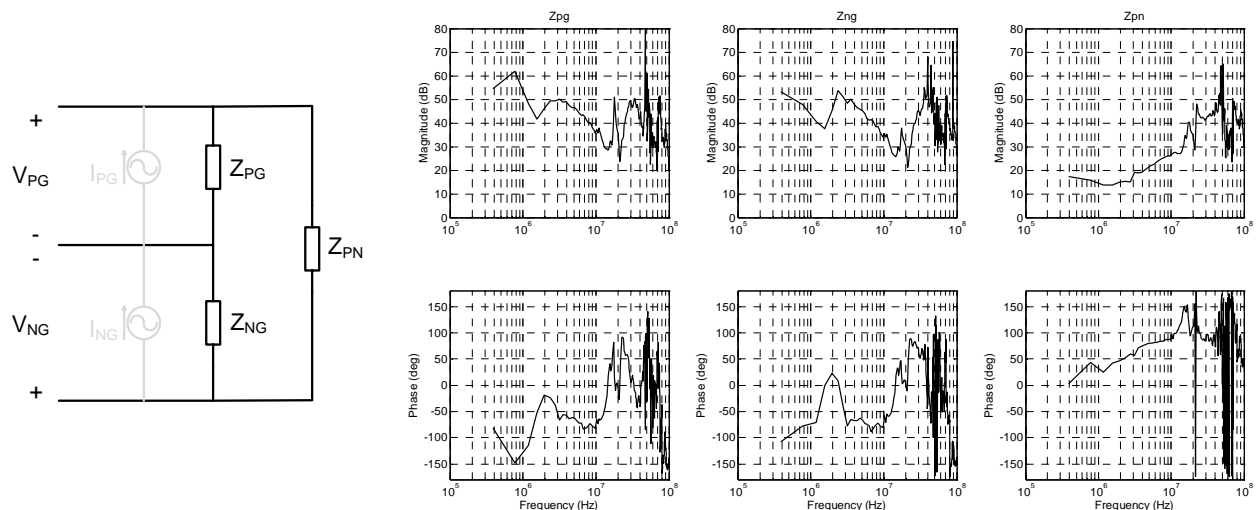
Fig. 3.31: Equivalent impedances of the boost converter determined from the model.
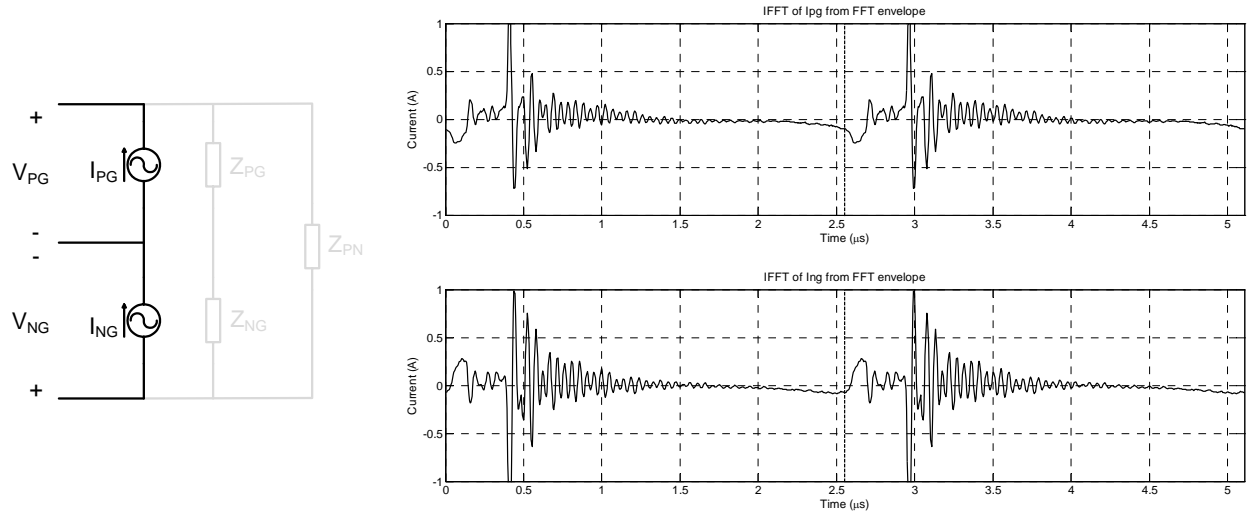
Fig. 3.32: IFFT of the equivalent current sources of the boost converter.
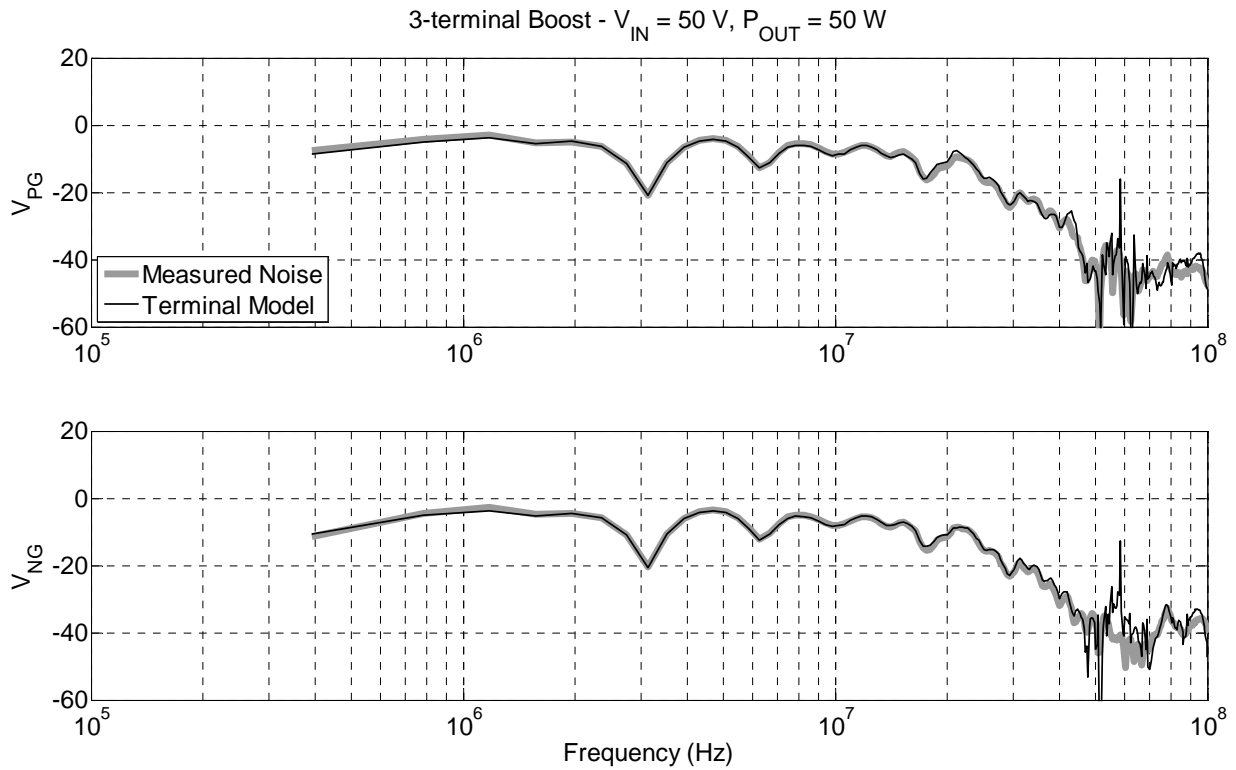
Fig. 3.33: Comparison of EMI for the boost converter's measured noise (gray) and the terminal model (black envelope).

60

3.3 FILTER MODEL CASCADED WITH TERMINAL MODEL

As stated, filter design is a major application for EMI models. With a full noise source and impedance model an optimal filter can be designed to achieve the desired attenuation for the specific system. The terminal model will need to be validated with a filter model to ensure the model predicts the noise accurately. In addition, the system can be connected with any other system to see the interaction between them. This will also be the first system-level demonstration and confirmation of an application using this behavioral model. An EMI filter can be represented as shown in the left of Fig. 3.34. However, all the parasitics of this model may be difficult to model as lumped elements, so a terminal approach will also be adopted for the passive network. The method derived in [69] finds the CM or DM impedance of an EMI filter. This can be expanded to find the Z-parameter matrix of any given passive network. A single phase EMI filter is then characterized as a four-port network, Fig. 3.34; where [Z] is a 4 x 4 matrix. This allows the Z-parameter representation of the filter to fully characterize the filter for all frequency points of interest and be easily cascaded with the terminal model of a converter.
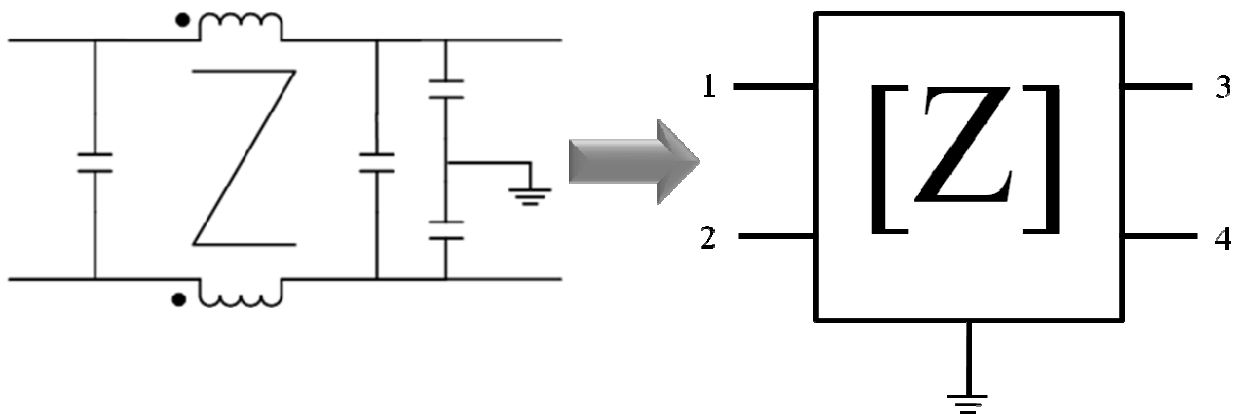
Fig. 3.34: Z-parameter (terminal) representation of a classic EMI filter.

In general, any passive system can be expressed as an n x n matrix, where n is the number of ports in the system. The matrix is inherently symmetric due to reciprocity of linear passive networks. As Fig. 3.34 demonstrates, a single-phase EMI filter has four ports associated with it. The matrix to be defined for each EMI filter is provided in (3-1). As illustrated the lower left half of the matrix is symmetric with the upper right, therefore only 10 impedances are required: 4 diagonal elements and 6 off-diagonal elements. Each diagonal element is a driving point impedance of the system and can be directly measured accurately using an impedance analyzer.

The definitions for each diagonal impedance is illustrated in Fig. 3.35a. The off-diagonals, however, are difficult to accurately measure at high frequencies due to the need of measuring open circuit voltages. When at higher frequencies, small parasitics can greatly affect the measurements. Using the method in [69], these errors are avoided by using a well known impedance instead. An example connection used to calculating the off-diagonal, or transfer impedance, of Z_{13} is provided in Fig. 3.35b. The insertion gain (IG) between two ports is defined in Fig. 3.36. A network analyzer is assumed to have an accurate impedance of 50 Ω over a wide frequency range; therefore, the insertion gain accurately measures the attenuation of the two ports in question. Assuming the diagonal impedances and all the possible IG are measured, the off-diagonal impedance are calculated using (3-2), assuming R= 50 Ω. The equation for the off-diagonals uses a +/- of a square root function. This can be classified by reviewing the real part of A_{XY}. When real(A_{XY})>0 use plus, and likewise when real(A_{XY})<0 use a minus sign.

$$\begin{pmatrix} Z_{11} & Z_{12} & Z_{13} & Z_{14} \\ & Z_{22} & Z_{23} & Z_{24} \\ & & Z_{33} & Z_{34} \\ & & & Z_{44} \end{pmatrix} \qquad (3\text{-}1)$$
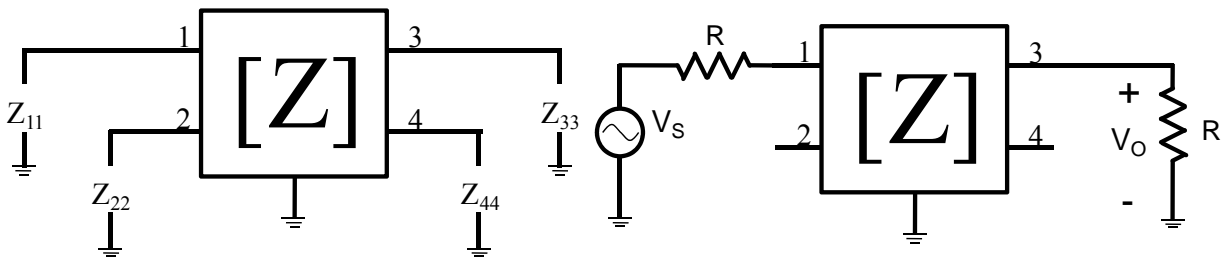
(a) Driving point impedances

(b) Off-diagonal impedances, example showing measurement of A_{13}

Fig. 3.35: Measurements setups to acquire Z-parameter model of passive network.

$$Z_{XY} = -R \cdot A_{XY} \pm \sqrt{(R \cdot A_{XY})^2 + R^2 + R \cdot (Z_{XX} + Z_{YY}) + Z_{XX} \cdot Z_{YY}} \qquad (3\text{-}2)$$

$$IG = \frac{V_2}{V_1}$$
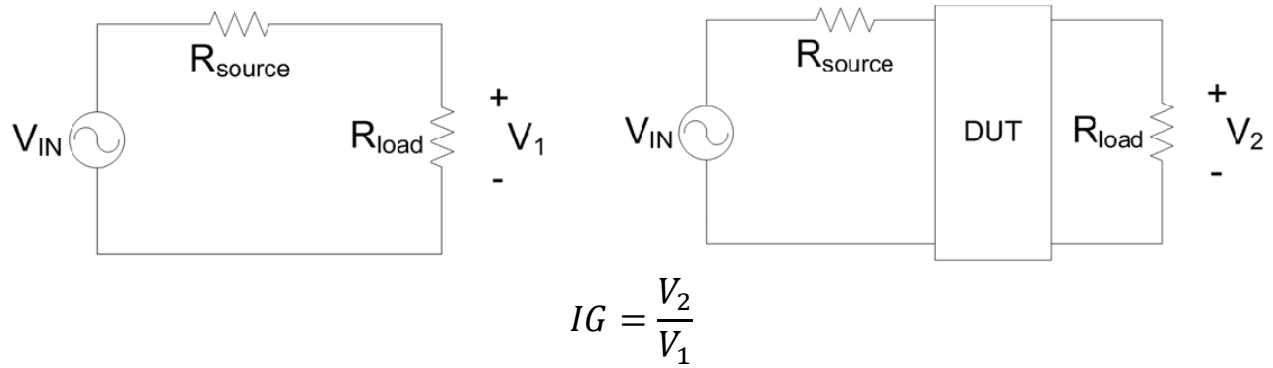
Fig. 3.36: Definition for insertion gain.

An issue, however, with this approach is that the inherent symmetry of an EMI filter causes some errors to surface. These errors cause large discrepancies in the DM properties of the filter. For example, Z_{11}, Z_{12}, Z_{22} are all very similar impedances. The equivalent input impedance for DM operation is defined as $Z_{11} + Z_{22} - 2 \cdot Z_{12}$. If small errors are present in the individual measurements then a large error is witnessed in the resulting DM impedance. Likewise, small errors cascade to larger errors in all DM attenuation predictions. Since the purpose is for EMI filtering evaluations a modified approach is created. Two port Z-parameter systems are created for DM, CM and a few additional measurements from the full filter four-port system, pictured in Fig. 3.37(a, b, c), respectively. Using both DM and CM models to assist in the Z-parameter model creation of an EMI filter ensures the model accurately characterizes the filtering properties. The relationships between the DM and CM two-port parameters and the four-port model are listed in (3-3). Solving the system of equations provides seven of ten total parameters for the full model as summarized in (3-4). The final three parameters, Z_{11}, Z_{44}, A_{13} (Z_{13}) are measured directly from the four-port EMI filter.

(a) Two-port DM Z-parameter network

(b) Two-port CM Z-parameter network

(c) Four-port full EMI filter Z-parameter network
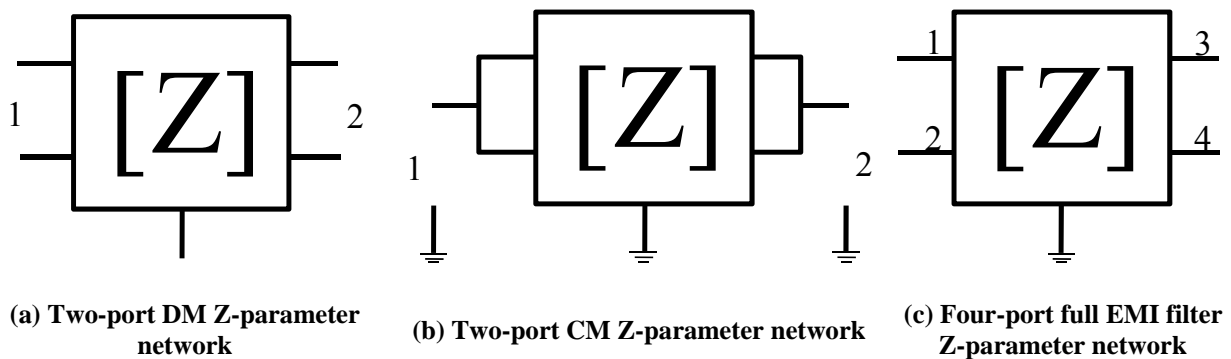
Fig. 3.37: Modified Z-parameter extraction method to enforce EMI filtering characteristics in the Z-parameter model.

$$Z_{11,DM} = Z_{11} + Z_{22} - 2 \cdot Z_{12}$$

$$Z_{22,DM} = Z_{33} + Z_{44} - 2 \cdot Z_{34}$$

$$Z_{12,DM} = Z_{13} - Z_{23} - Z_{14} + Z_{24}$$

$$Z_{11,CM} = \frac{Z_{11} \cdot Z_{22} - Z_{12}^2}{Z_{11} - 2 \cdot Z_{12} + Z_{22}}$$

$$Z_{22,CM} = \frac{Z_{33} \cdot Z_{44} - Z_{34}^2}{Z_{33} - 2 \cdot Z_{34} + Z_{44}}$$

$$Z_{12,CM} = \frac{Z_{13} \cdot (Z_{44} - Z_{34}) + Z_{14} \cdot (Z_{33} - Z_{34})}{Z_{33} - 2 \cdot Z_{34} + Z_{44}}$$

$$Z_{12,CM} = \frac{Z_{23} \cdot (Z_{44} - Z_{34}) + Z_{24} \cdot (Z_{33} - Z_{34})}{Z_{33} - 2 \cdot Z_{34} + Z_{44}}$$

$$(3\text{-}3)$$

$$Z_{12} = \sqrt{Z_{11,DM} \cdot (Z_{11} - Z_{11,CM})} + Z_{11}$$

$$Z_{22} = \frac{2 \cdot \sqrt{Z_{11,DM}} \cdot (Z_{11} - Z_{11,CM})^{3/2} + Z_{11}^2 + Z_{11} \cdot (Z_{11,DM} - Z_{11,CM}) - Z_{11,CM} \cdot Z_{11,DM}}{Z_{11} - Z_{11,CM}}$$

$$Z_{34} = \begin{cases} \sqrt{Z_{22,DM} \cdot (Z_{44} - Z_{22,CM})} + Z_{44}, when\ Z_{22,DM} \le 0 \\ -\sqrt{Z_{22,DM} \cdot (Z_{44} - Z_{22,CM})} + Z_{44}, when\ Z_{22,DM} > 0 \end{cases}$$

$$Z_{33} = \begin{cases} 2 \cdot \sqrt{Z_{22,DM} \cdot (Z_{44} - Z_{22,CM})} + Z_{22,DM} + Z_{44}, when\ Z_{22,DM} \le 0 \\ -2 \cdot \sqrt{Z_{22,DM} \cdot (Z_{44} - Z_{22,CM})} + Z_{22,DM} + Z_{44}, when\ Z_{22,DM} > 0 \end{cases}$$

$$(3\text{-}4)$$

$$Z_{14} = \frac{Z_{12,CM} \cdot (Z_{33} - 2 \cdot Z_{34} + Z_{44}) + Z_{13} \cdot (Z_{34} - Z_{44})}{Z_{33} - Z_{34}}$$

$$Z_{23} = \frac{Z_{12,CM} \cdot (Z_{33} - 2 \cdot Z_{34} + Z_{44}) + (Z_{12,DM} - Z_{13} + Z_{14}) \cdot (Z_{34} - Z_{44})}{Z_{33} - 2 \cdot Z_{34} + Z_{44}}$$

$$Z_{24} = \frac{Z_{12,CM} \cdot (Z_{33} - 2 \cdot Z_{34} + Z_{44}) + (Z_{12,DM} - Z_{13} + Z_{14}) \cdot (Z_{33} - Z_{34})}{Z_{33} - 2 \cdot Z_{34} + Z_{44}}$$

An example EMI filter's schematic can be seen in Fig. 3.38. This filter is simulated in Simplorer to mimic the acquisition of the Z-parameter model using the measurement procedures described above. The full impedance matrix of the filter is provided in Fig. 3.39. Notice the high frequency effects, due to all the parasitics, are included in the matrix model where the lumped model may fail to capture. This example is fairly simple where 14 lumped elements are modeled using the 10 impedances in the 4 x 4 Z-parameter matrix. However, a much more complex model with additional parasitics – such as mutual impedances, parallel capacitances and resistances of the inductors, etc. – can also be modeled with the 10 impedances and still incorporate all higher frequency effects.
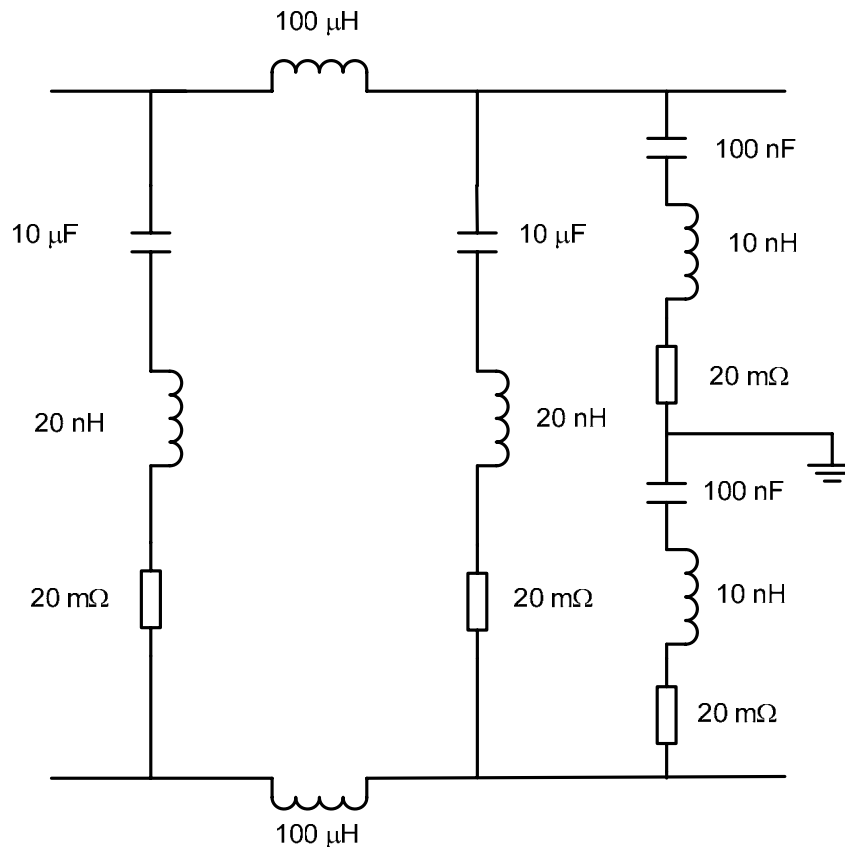
Fig. 3.38: Example EMI filter used in simulation to illustrate the model's acquisition and prediction capabilities.
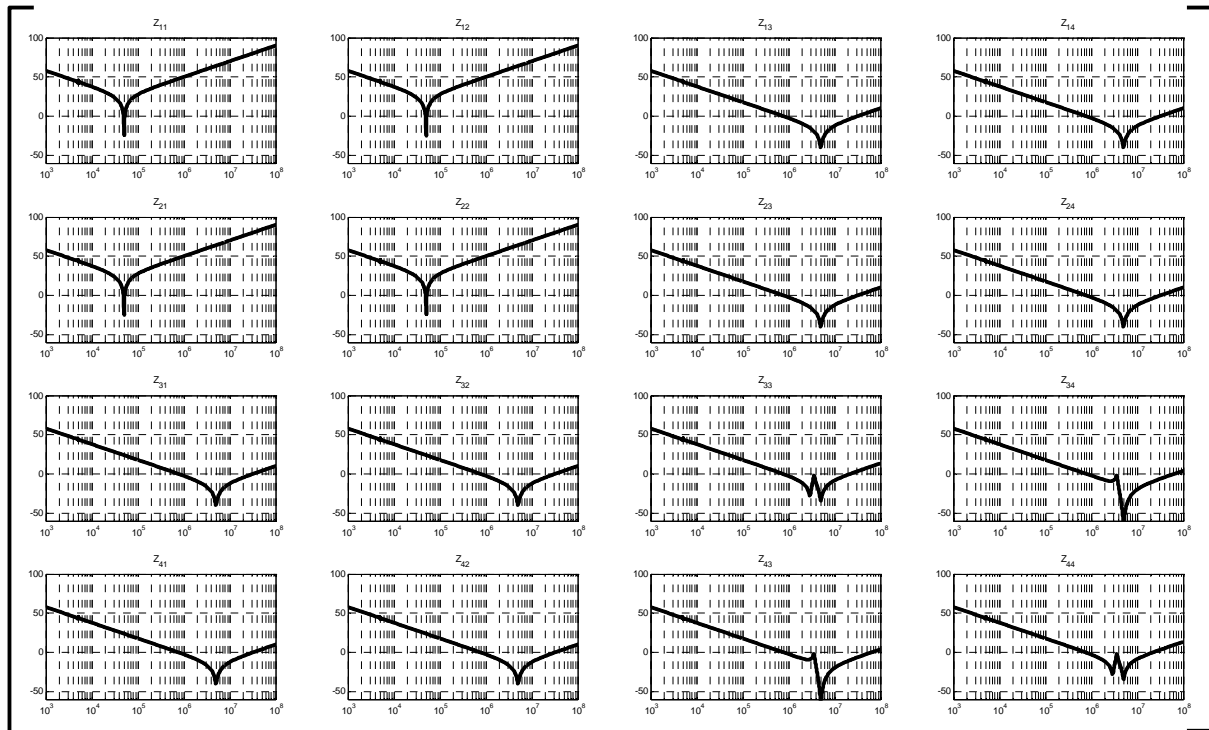
Fig. 3.39: Z-parameter matrix of EMI filter shown in Fig. 3.38.

The insertion gain of a filter is typically the metric used for how well it will attenuate noise in a converter. However, the insertion gain is found using a network analyzer; as mentioned it uses a source and load impedance of 50 Ω. The filter will not necessarily have a source or load impedance of 50 Ω when implemented with a converter. Therefore, the attenuation seen with the converter will usually differ from the small signal insertion gain determined by the network analyzer. The insertion gains for DM and CM are used to compare how the network analyzer measurement predicts the actual attenuation versus the terminal model cascaded with the filter's Z-parameter model. The DM and CM insertion gain for the same filter characterized in Fig. 3.39 is provided in Fig. 3.40(a, b), respectively. These plots are then used to estimate the filtered noise.

The CM and DM noise for a boost converter is plotted in Fig. 3.42. The red line is the noise spectrum of the converter, where the blue line is the terminal model for the noise spectrum of the same boost converter, which verifies that the terminal model is accurate. The magenta line is the projected filtered noise when using the insertion gains from Fig. 3.40. However, the black line is the actual filtered noise using the filter. Similarly, the green line is the terminal model cascaded with the filter Z-parameter model. To visualize the different configurations for each plot, Fig. 3.41 provides a schematic for each curve. The colored boarder in the schematics correlates to the

plot colors described in Fig. 3.42 - Fig. 3.44. In this example, the actual filtered noise is predicted more accurately with the converter's terminal model and filter's matrix model. The actual in-circuit filtered noise is less than the insertion gain projected noise, so it is possible to overdesign a filter using the insertion gain only. It could also be possible that the insertion gain measured with a network analyzer shows the filter meets the desired standard when the actual filtered noise does not meet the same standard. That is, when the filter is implemented the source and load impedances in the system will mismatch differently with the filter's input and output impedance than it did with the network analyzer's $50\,\Omega$ impedance. The largest difference between the cascaded terminal models and the insertion gain model is roughly 10 dB when the source impedance of the converter (and likewise the source impedance of the filter) is $50\,\Omega$ (same as insertion gain measurement and similar to a LISN). When the impedance at the input of the filter is different form $50\,\Omega$ the accuracy of the terminal models over the insertion gain model is more prevalent. The difference between the two methods is roughly 40 dB when the source impedance is $1\,\mathrm{k\Omega}$, Fig. 3.43. Similarly, when the source impedance is $1\,\Omega$, Fig. 3.44, the difference is up to 20 dB. In this case, the small signal insertion gain predicts more attenuation than the actual in circuit simulations. That is, the actual noise in the system will be higher than expected meaning the filter may not meet the standard. Meanwhile the terminal models almost identically predict the noise with and without the filter for any excitation source impedance.
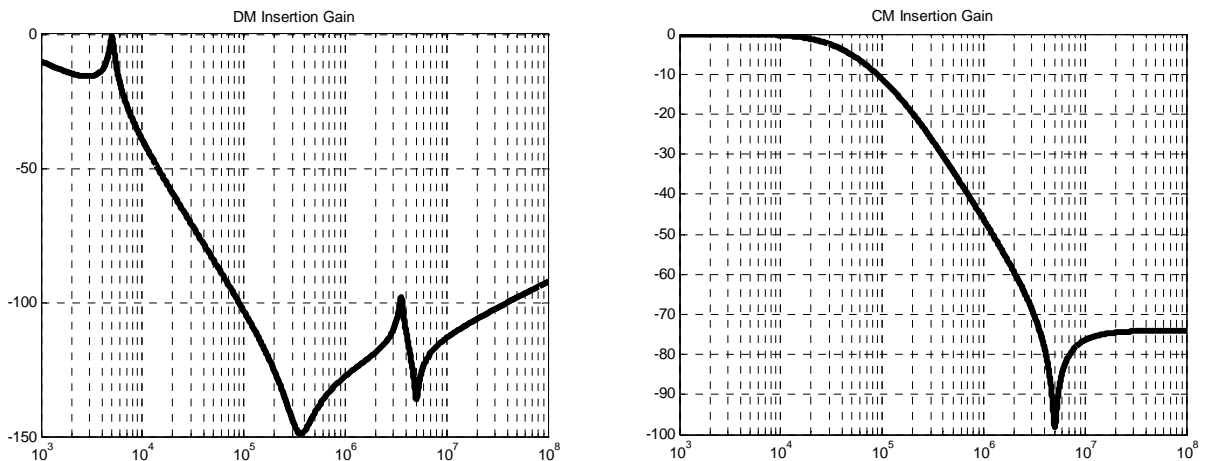
(a) DM insertion gain of EMI filter, with R_{source} and R_{load} equal to $50\,\Omega$.

(b) CM insertion gain of EMI filter, with R_{source} and R_{load} equal to $50\,\Omega$.

Fig. 3.40: Small signal insertion gains of EMI filter.
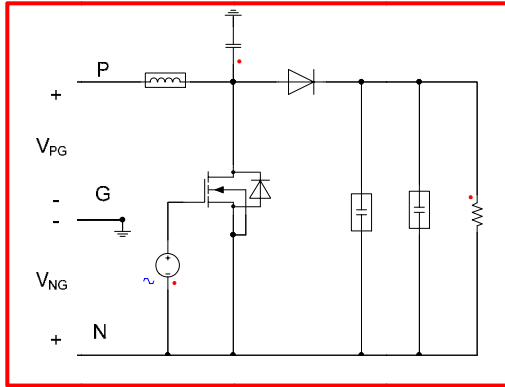
(a) Simulated time-domain model of detailed boost converter, same as in Section 3.1.2.2.
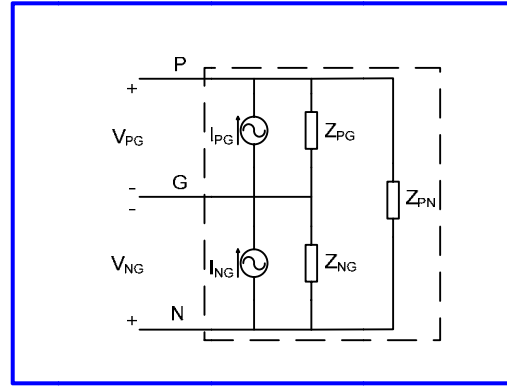
(b) Terminal equivalance model of the boost converter from (a)
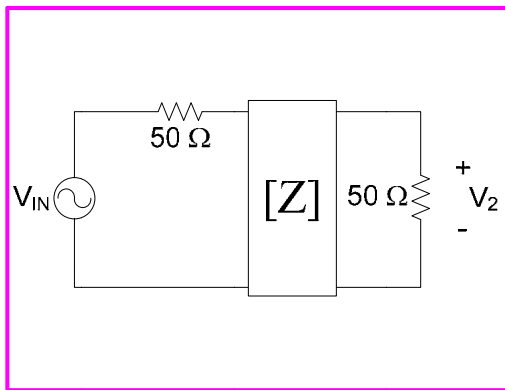
(c) Small signal insertion gain measurements using standard source and load impedances. Also used to create Z-parameter models.
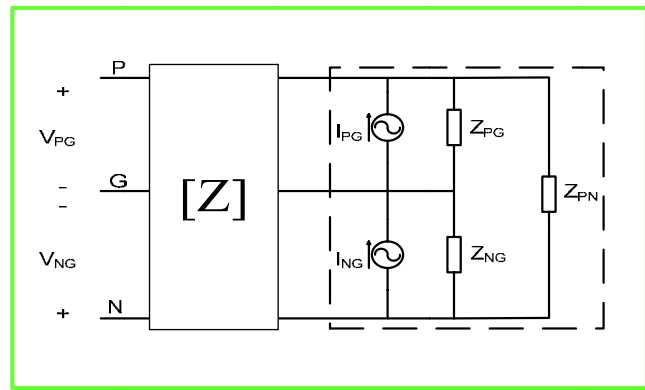
(d) Cascaded terminal models used to predict interactions and filtered EMI.
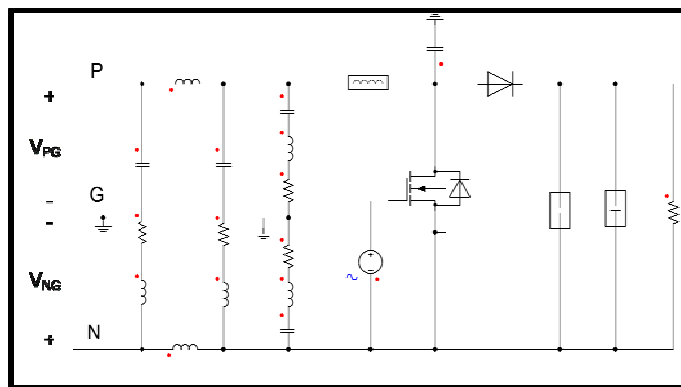
(e) Simulated time-domain model of detailed filter and boost converter; used to compare to (d).

Fig. 3.41: Circuit description used for comparison of terminal models to detailed circuit simulations and small signal attenuation to in-circuit attenuation. The color of the boarder around each circuit correlates to the color of the curve in the Fig. 3.42 - Fig. 3.44.
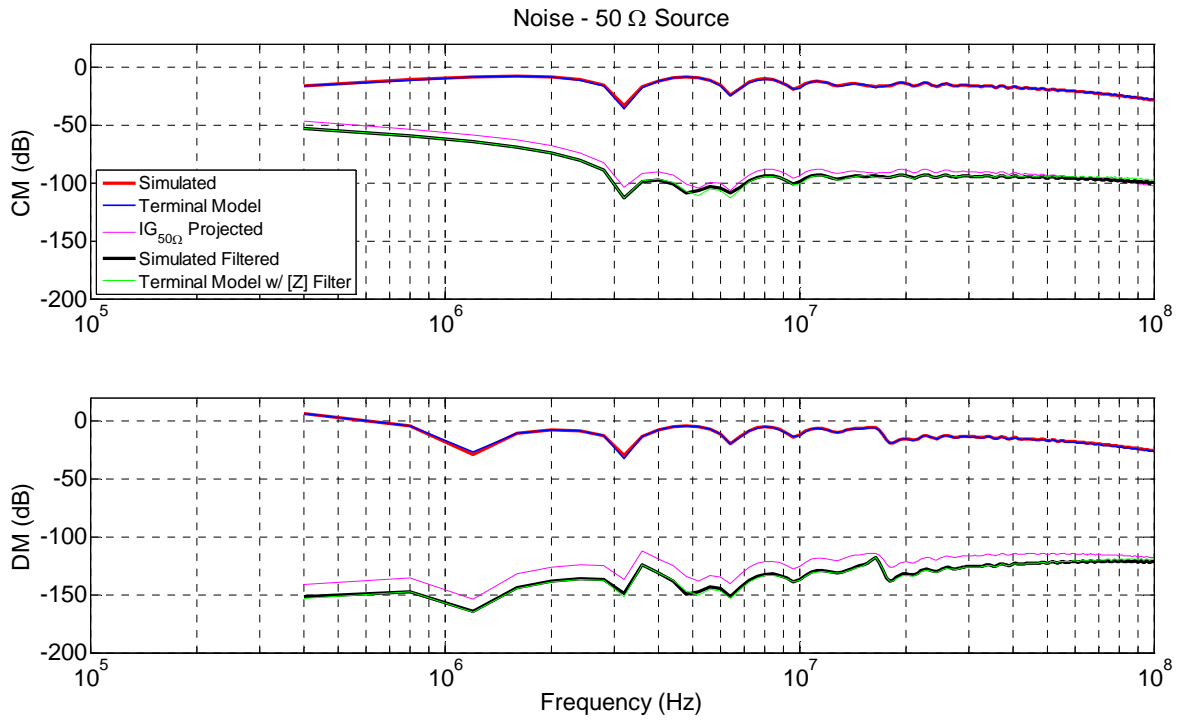
Fig. 3.42: **Comparison of noise produced by a boost converter with and without an EMI filter and the projected noise using the small signal insertion gain. Source impedance is 50 Ω.**
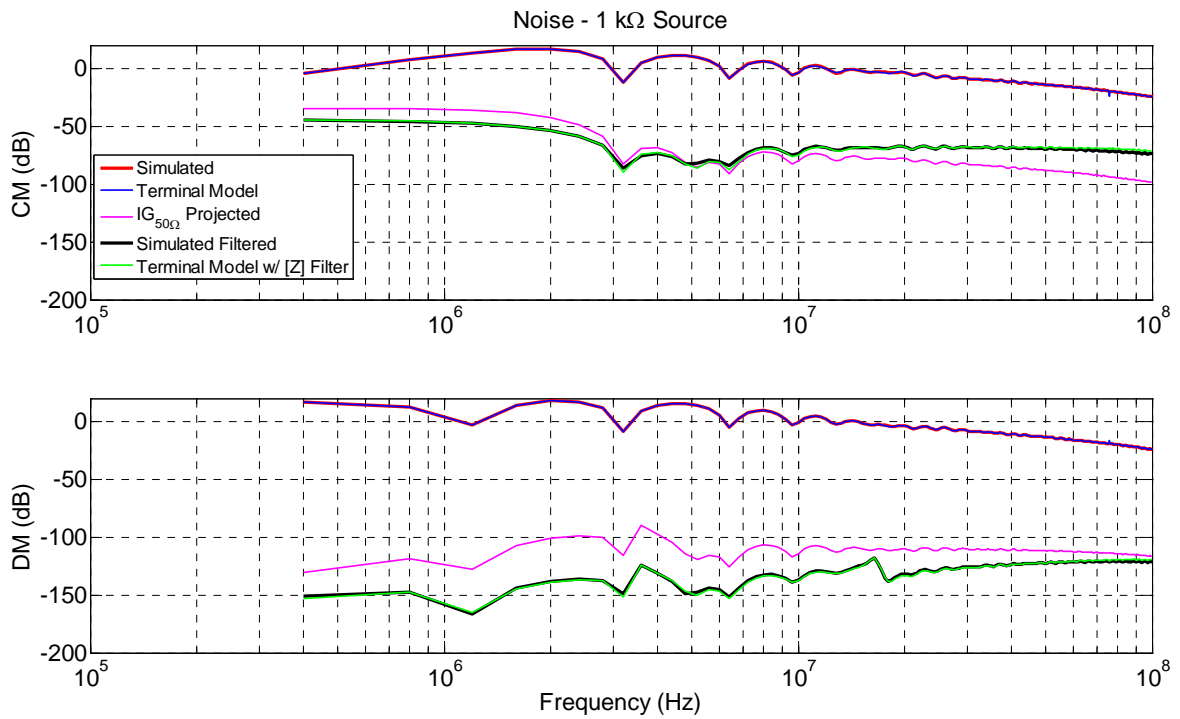
Fig. 3.43: **Comparison of noise produced by a boost converter with and without an EMI filter and the projected noise using the small signal insertion gain. Source impedance is 1 kΩ.**
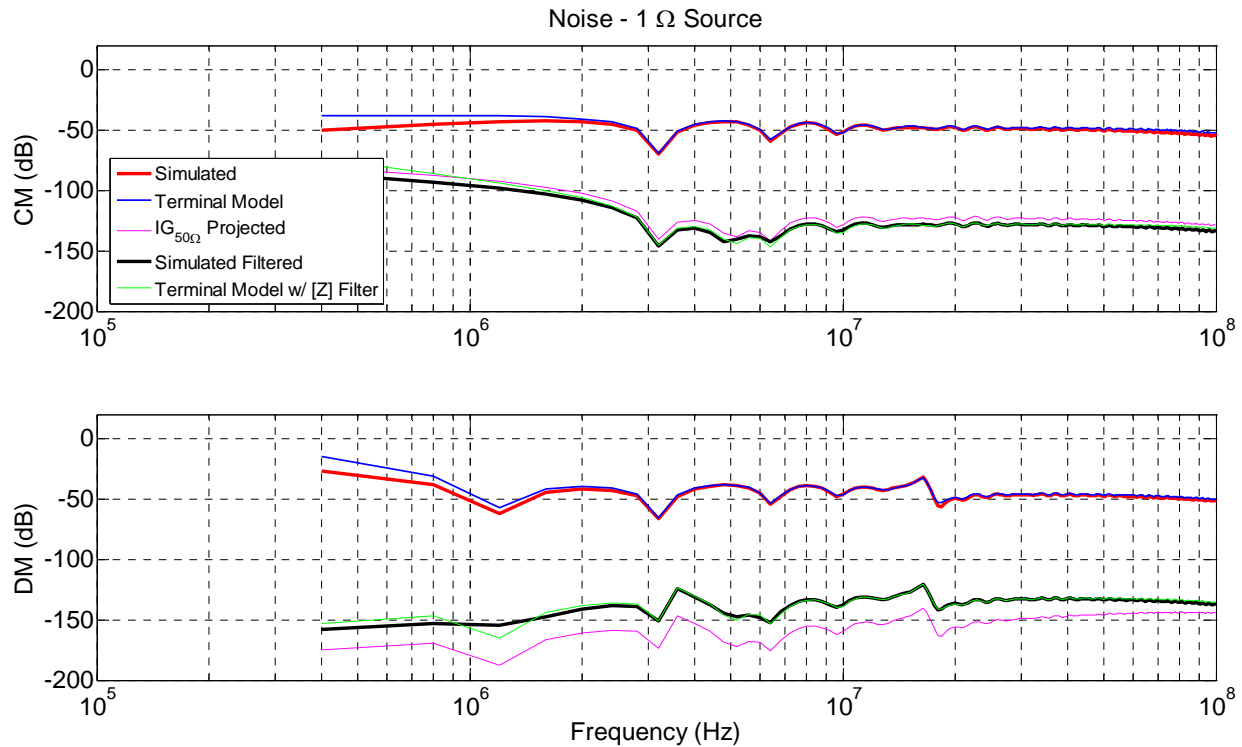
Fig. 3.44: Comparison of noise produced by a boost converter with and without an EMI filter and the projected noise using the small signal insertion gain. Source impedance is 1 Ω.

The above results are for a simulated converter. An experimental boost converter, Fig. 3.30, tested with a filter is also investigated to show the benefits and application of cascading a filter model and converter terminal model. EMI plots for the boost converter are provided in Fig. 3.47. The black plot is the noise of the converter without a filter, same as in Fig. 3.33. The blue line is the filtered noise of the converter using a basic EMI filter; the measured impedance matrix of the filter using the above method is seen in Fig. 3.45. The light green line is the resulting prediction of the noise from the small signal insertion gain measurements, plotted in Fig. 3.46. Finally, the red line graphs the prediction of the terminal modeling parameters cascaded with the filter's Z-parameters. The filtering shows obvious improvement in the EMI noise over only the converter in all examples. The insertion gain predictions clearly overestimate the attenuation by up to 40 dB. This can cause many issues in the design of the filter. One issue with the measurements is that the noise floor is much larger compared to the simulations. The measured filtered noise, blue curve, is either larger than or in line (< 10 dB difference) with the terminal modeling prediction, red curve. It is quite probable that the actual noise is around the red curve; however, the measurement capabilities do not allow the ability to capture it due to the signal-to-

noise ratio. One point to mention is that the noise level of the blue and red are both below typical standard lines, and the procedure should be adequate for meeting a standard. Using the terminal model should provide more insight to the interactions and actual attenuation over the small signal insertion gain predictions.
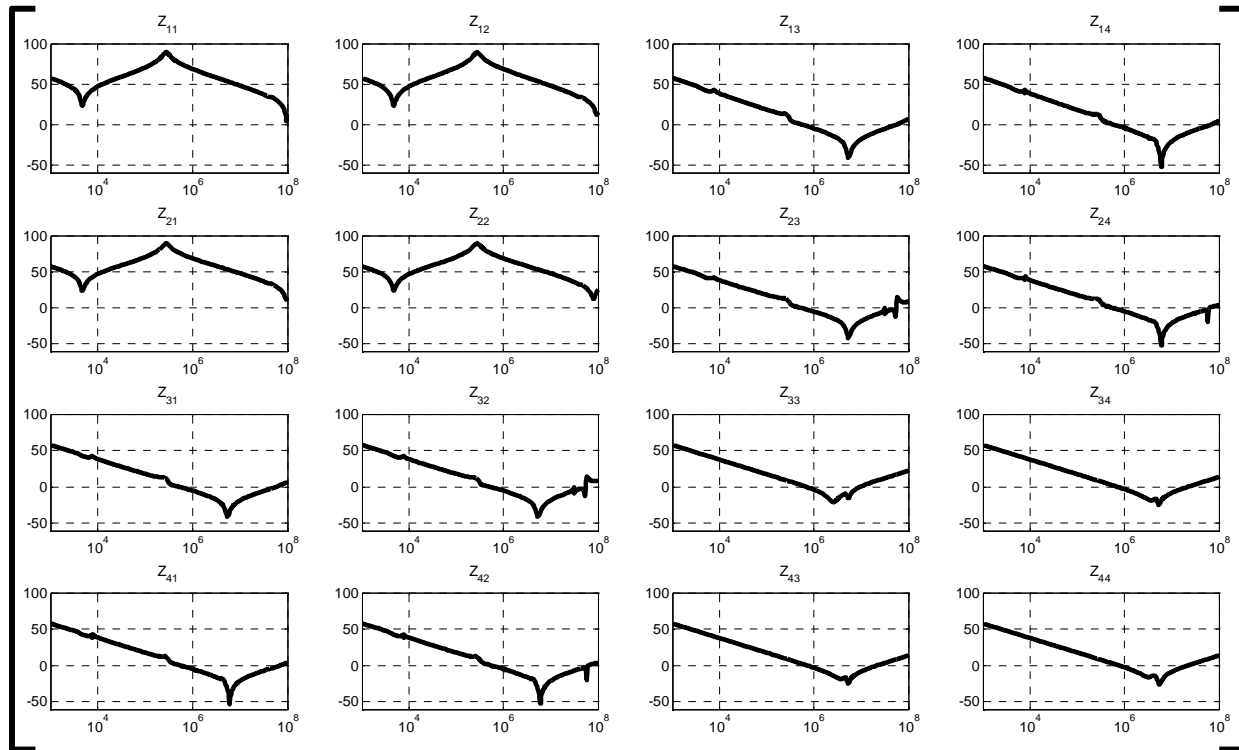
Fig. 3.45: Z-parameter matrix of EMI filter used in measurements with boost converter.
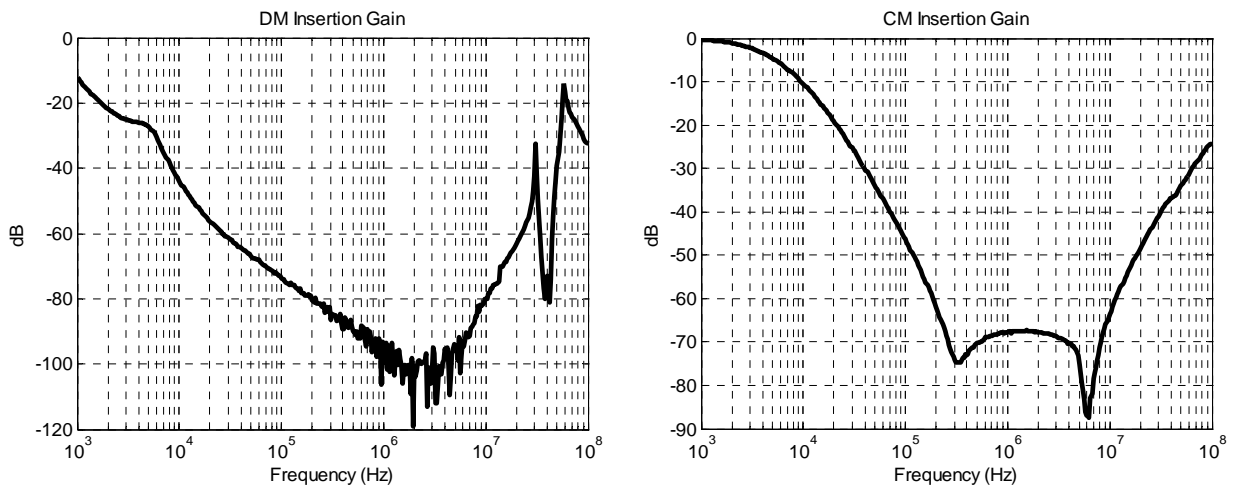
(a) DM measured insertion gain of EMI filter, with R_source and R_load equal to 50 Ω.

(b) CM measured insertion gain of EMI filter, with R_source and R_load equal to 50 Ω.

Fig. 3.46: Small signal insertion gains of EMI filter used with boost converter.
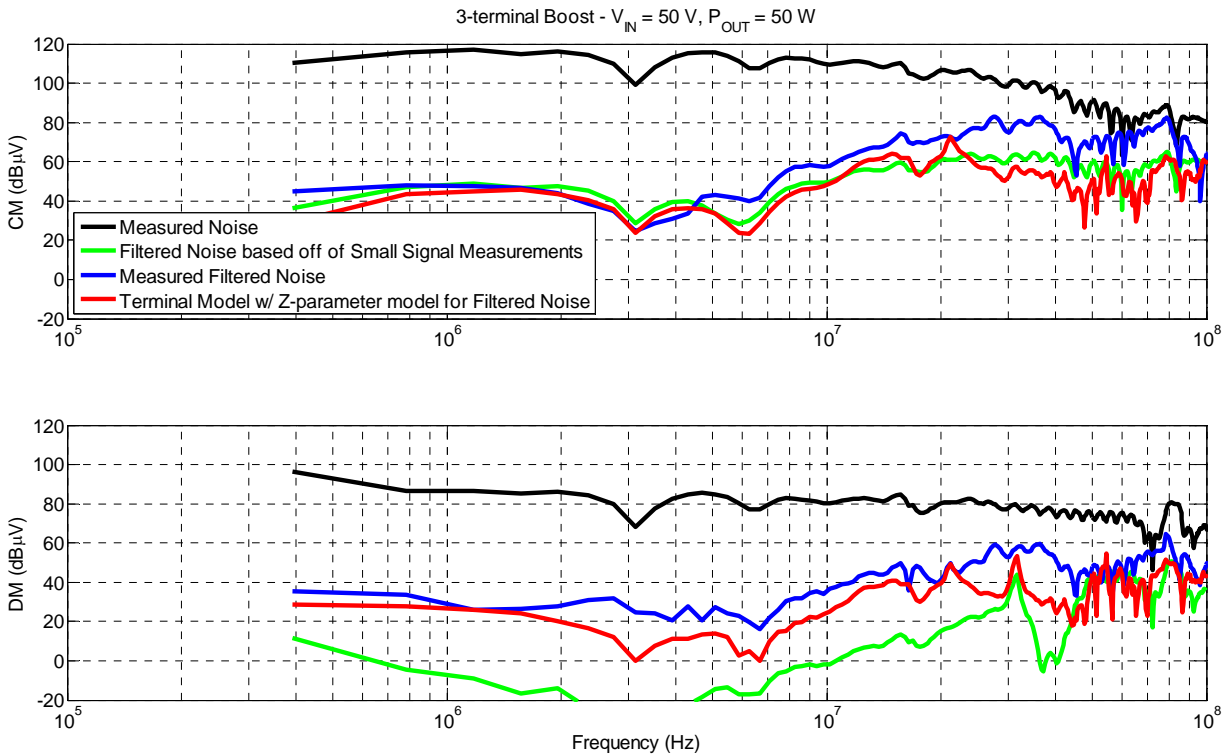
Fig. 3.47: Measurement results comparing noise of a boost converter (from Fig. 3.30). Noise measurements with and without filter are compared with small signal insertion gain prediction and terminal model's prediction.

The impedance matching between the converter and filter can also lead to a filter design throughout the frequency spectrum as opposed to designing one corner frequency well below the EMI spectrum. Unique techniques could be implemented to filter the noise differently at different frequencies since a full model is now available.

This procedure of cascading a converter's terminal model is not limited to a filter. This can be extended to other converters as well. For example, two (or more) converters could be on a single bus and share an EMI filter. Many converter models could be placed together to predict the noise of all converters and any interactions between them, while designing one filter for the entire system.

4 MODEL VARIATIONS

4.1 PHASE-LEG MODULE

The modeling process does not have to contain an entire converter. It is possible to characterize sub-systems. The same measurement fixture will be used to measure the terminal model of a phase-leg module. Since an entire converter is not modeled but rather only a few components of the converter, a double pulse signal is sufficient to capture the characteristics of the module under particular operating conditions. One difference occurs when measuring a component using a double pulse method. A large bulk capacitor is required to store enough energy for the pulses, represented as '[Z]' in Fig. 4.1a. This impedance will be included in the equivalent circuit. Fortunately, since it is simply a passive network it can be removed through simple algebra using a similar (but reverse) approach as incorporating the passive filter matrix network in the previous chapter. The final equivalent circuit only contains the information desired. A three-terminal system still exist – positive, negative, and ground (heatsink) – and the same sets of attenuated measurements will be performed to create the model.

The module used to create the model is shown in Fig. 4.1b. A single phase-leg from a three-phase module will be modeled with a gate driver, interconnection board and decoupling capacitor along with an inductive load. The impedances are provided in Fig. 4.2 and the current sources are in Fig. 4.3. The resonance at 10 MHz in the impedances correlates to the series inductance of the decoupling capacitor. The model was created with a source impedance of 50 Ω and 1 kΩ to increase the accuracy of the impedances throughout the spectrum.

A comparison of the terminal model results are shown in Fig. 4.4. The terminal model is compared to the measured values at source impedances of both 50 Ω and 1 kΩ. The largest error is a difference of less than 5 dB seen around 13 MHz when the source impedance is 50 Ω. However, with a source impedance of 1 kΩ there is a nearly identical comparison between modeled and measured noise.
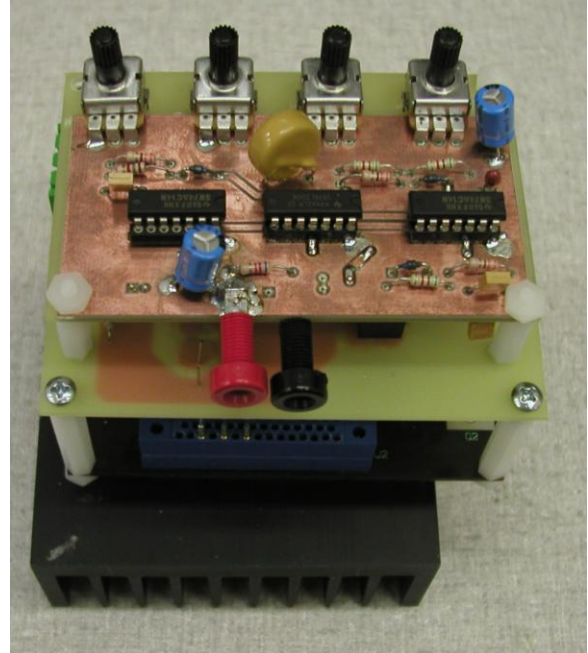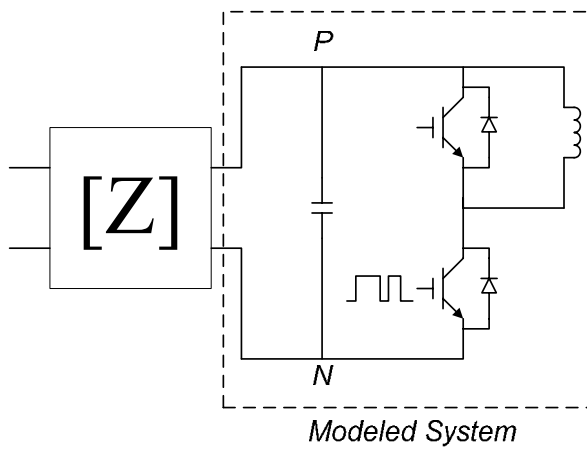
(a) Schematic of a phase-leg power module with interconnection board and heatsink (as the common path).

(b) Three-phase power module with gate drive board and double pulse generator board.

Fig. 4.1: Test setup for a phase-leg power module using double pulse test.
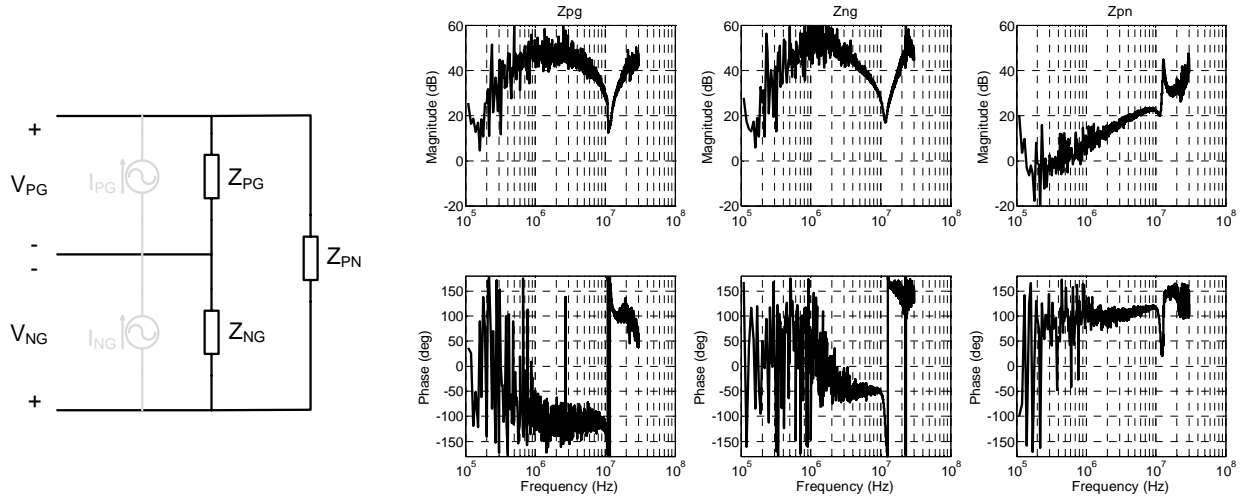
Fig. 4.2: Equivalent impedances of the phase-leg system determined from the model.
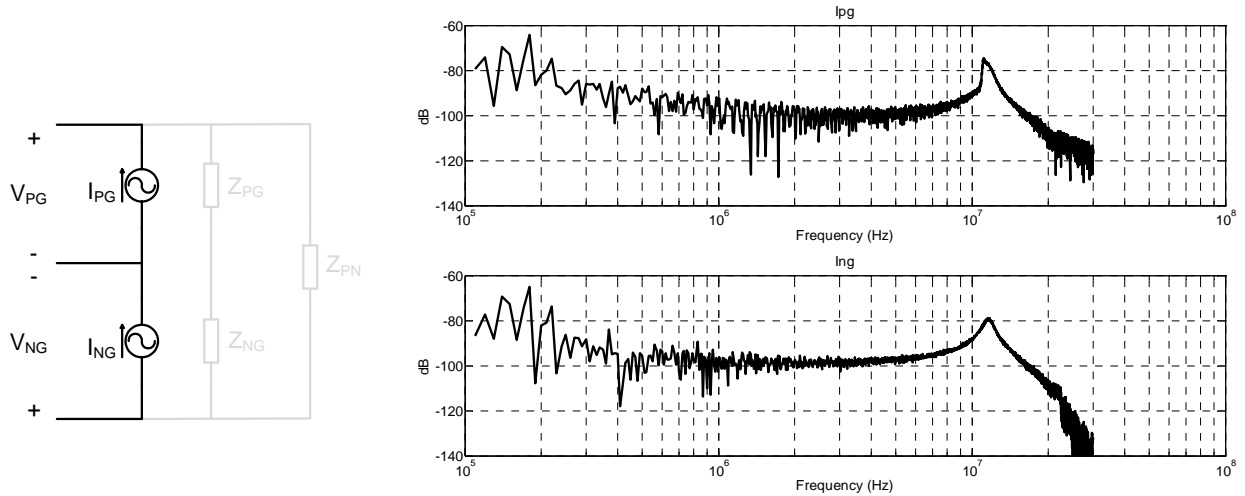
Fig. 4.3: Equivalent current sources of the phase-leg system determined from the model.
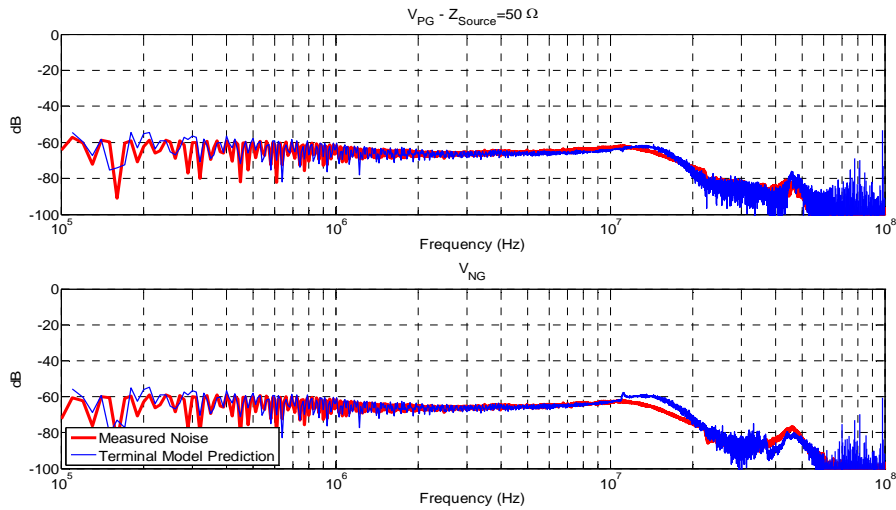
(a) Source impedance of 50 Ω.
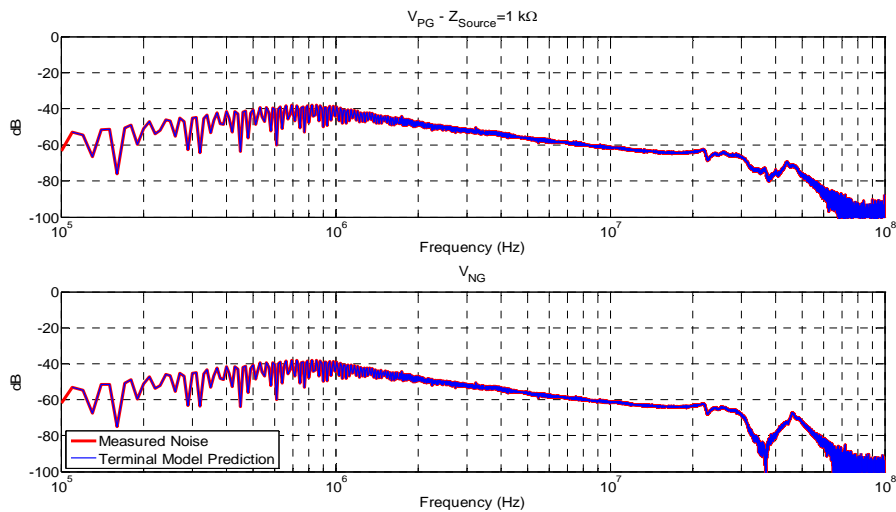
(b) Source impedance of 1 kΩ.

Fig. 4.4: Comparison of EMI for the phase-leg system's measured noise (red) and the terminal model (blue envelope).

The double pulse measurements and modeling are also completed for many different operating conditions to study the effects of operating point on the EMI generation of the phase-leg. The first operating condition investigated is the input voltage. The input voltage is also the blocking voltage across the phase-leg switches. The equivalent impedances and current sources are plotted in Fig. 4.5. The impedances of the system change very little as the input voltage increases, Fig. 4.5a. As the voltage increased, the impedances appear to be more defined. At lower input voltages there is what appears to be a band of impedance instead of a single line. It can also be seen as noise, or errors, associated with the impedance decreases as the voltage increases. This can be true since the overall noise increases with the input voltage, the signal-to-noise ratio also increases and the errors in the measurements are less dominant in the system. Since the overall noise increases with the input voltage the equivalent current sources will likewise increase, as is seen in Fig. 4.5b.

The impedance had minor effects from the input voltage variation; it also has very little effect from the load current, or switched current, Fig. 4.6a. In frequencies below 30 MHz there are no changes; however, some changes occurred in the higher frequencies. These changes occurred at currents above 2 A, but then remained constant up to 10 A. This affect is also dominated by the increased noise at these frequencies; also seen in the equivalent current sources, Fig. 4.6b. In a more general trend the noise, and likewise the current sources, increases as the load current increases in the lower frequencies.

Following the same logic as the other operating points varying the gate resistor had little effect on the equivalent impedances, Fig. 4.7a. Some differences were seen when the overall noise increased; again, probably due to a better signal-to-noise ratio. The equivalent current sources, shown in Fig. 4.7b, increase at frequencies above 1 MHz as the gate resistor decreases. This is also expected since as the gate resistor decreases, the switching speed increases and therefore cause larger di/dt and dv/dt transients. In summary, the equivalent impedance, or propagation path, does not vary with the operating point as expected. However, with increased noise, some errors are removed from the modeled results due to a higher signal-to-noise ratio. The main effect the operating point has on the model is in the equivalent current sources. These few examples illustrate one application of the model to predict the effects various parameters have on the system.
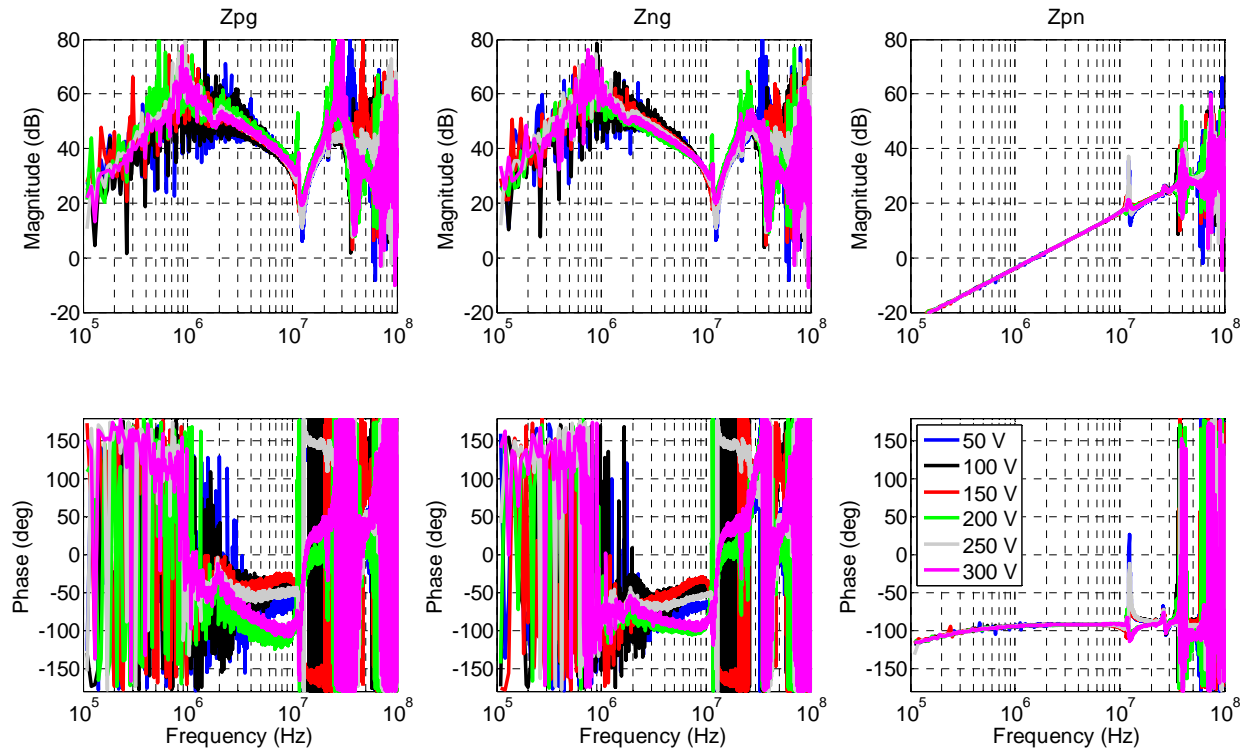
(a) **Modeled equivalent impedances of phase-leg. Not greatly affected by input / blocking voltage variations.**
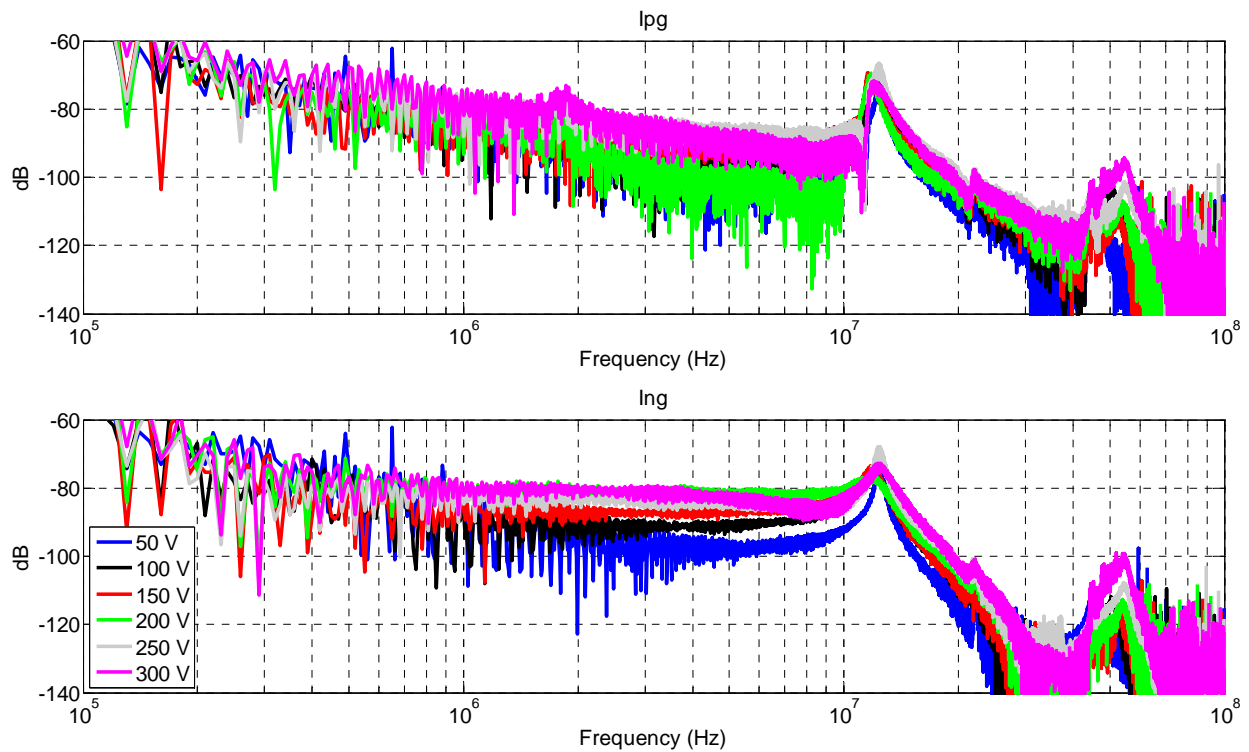
(b) **Modeled equivalent current sources of phase-leg. Noise source increase as input / blocking voltage increases.**

Fig. 4.5: Effects of modeled parameters as input / blocking voltage changes.
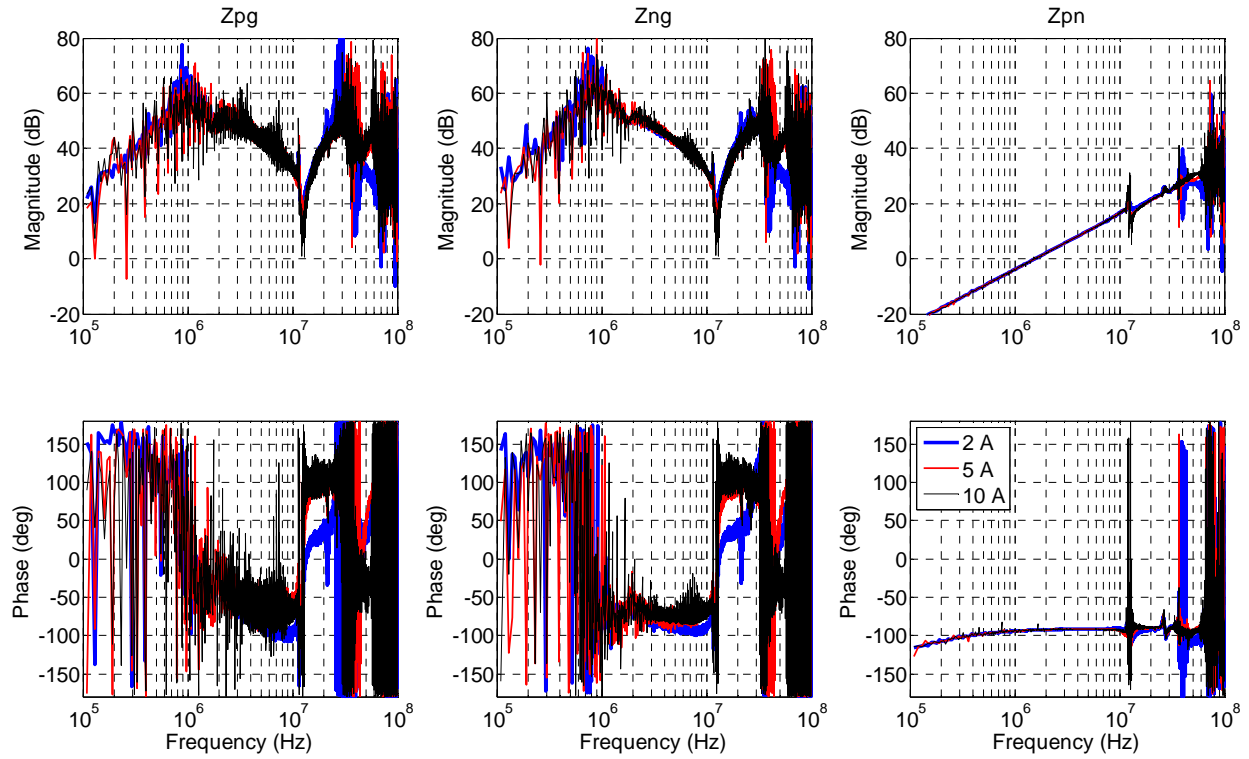
(a) Modeled equivalent impedances of phase-leg. Not greatly affected by load / switched current variations.
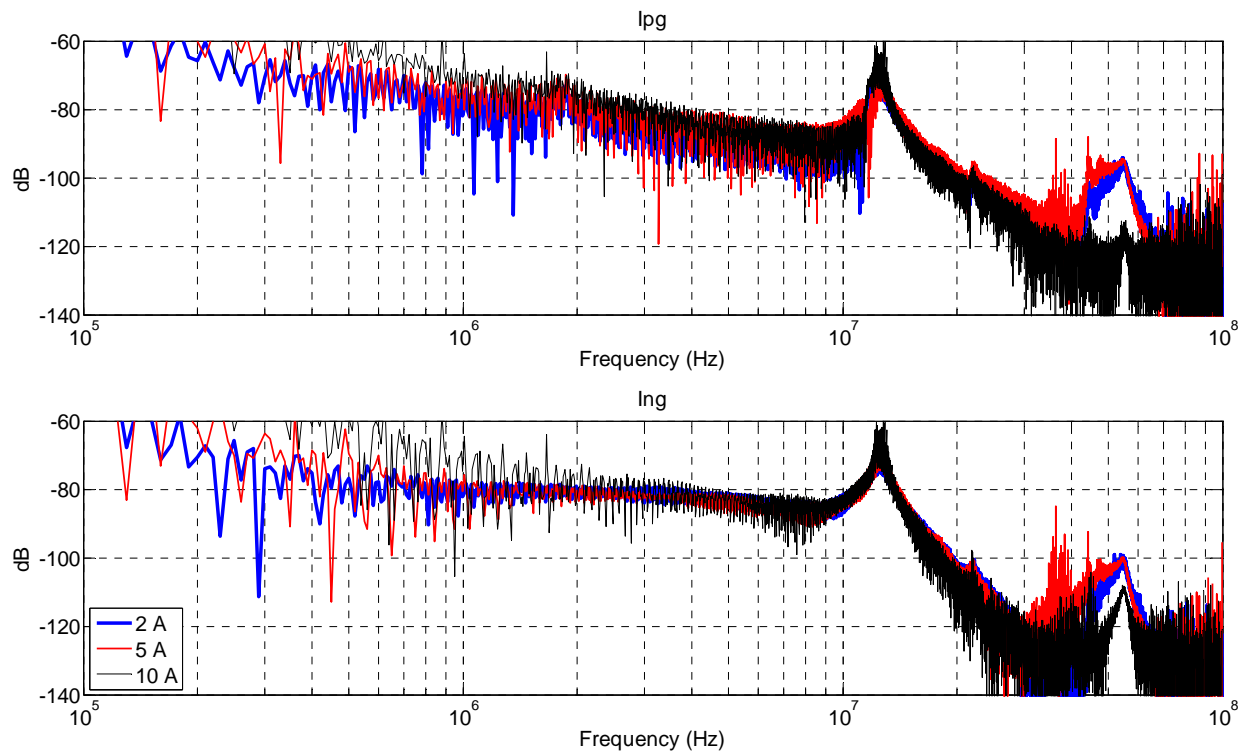
(b) Modeled equivalent current sources of phase-leg. Noise source increases at lower frequencies as load / switched current increases.

Fig. 4.6: Effects of modeled parameters as load / switched current changes.
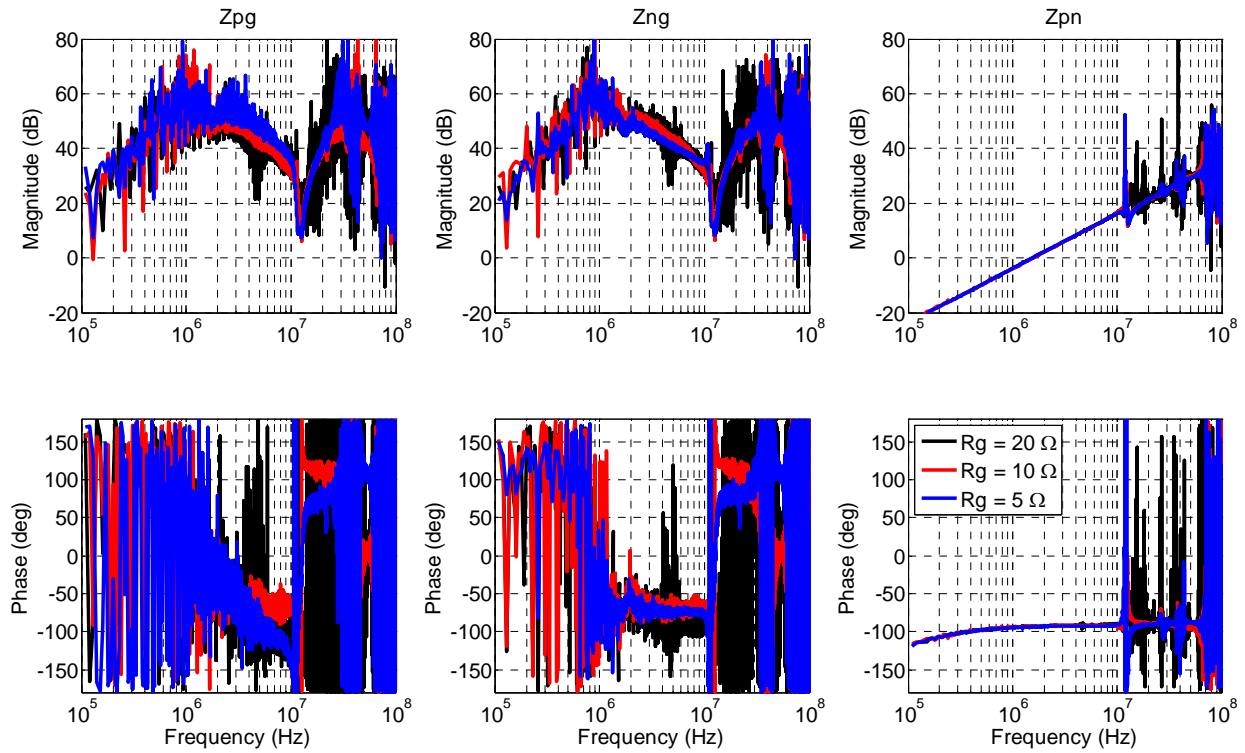
(a) Modeled equivalent impedances of phase-leg. Not greatly affected by gate resistor variations.
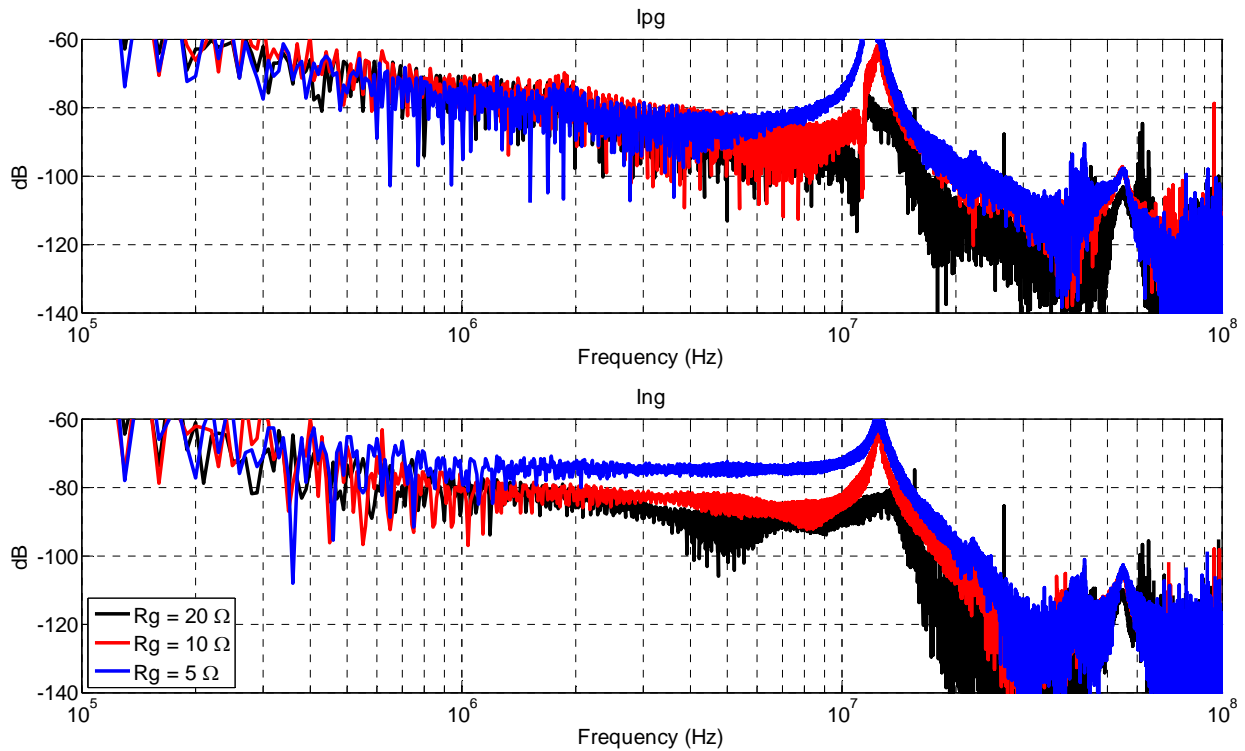
(b) Modeled equivalent current sources of phase-leg. Noise source increases at higher frequencies as gate resistor decreases.

Fig. 4.7: Effects of modeled parameters as gate resistor changes.

Furthermore, the phase-leg model can be used together with other sub-system models to create an entire system, in the event the system is not available as a single unit. Finally, modeling only a phase-leg module will provide insight on the limitations of the model. As mentioned earlier, modeling a switched impedance (or only an active switch) is not valid as a terminal model in this format. This is the reason to include the input decoupling capacitor and output inductive load. The phase-leg allows for easy modeling of different configurations: a series of switches with passive components (as in this example), or a complete buck/boost converter, or other more complicated systems such as inverters which are investigated in the next section.

4.2 AC OPERATION

The previous section provides some understanding of the effect of the operating condition on the phase-leg. A converter is now studied under varying operating points, or an AC load. In order to model a converter with an AC operation the entire length of the low frequency signal needs to be included into the FFT. If only one switching cycle is used, as with the DC converter examples, it is not known whether the event occurs at a zero crossing, peak, rising or falling edge, etc. Furthermore, the operation of one switching period will not necessarily define the system parameters at another operating point. Therefore all operating conditions are required. However, if the entire line frequency signal needs to be captured with a small time step the model becomes unreasonable to solve. For example a 60 Hz line frequency with a 1 ns sampling would require almost 17 million data points. Some form of data reduction or simplification is needed in order to manipulate the data efficiently.

A few different approaches to reducing the data are investigated in this section. The first reduction approach is to divide the line cycle into many partitions. In each of these partitions the operating point can be considered constant allowing for only one measurement. This assumes that all other switching instances within that partition are identical and approximates the operating point as a stair step function. Furthermore, when the stair step approximation is not accurate enough an interpolation approach within the partition is used to manipulate the single measurement to better match the actual converter's function. Finally, symmetry is explored to determine if only a fraction of the operating region is needed to predict the entire data set.

A half bridge inverter will be investigated first. A schematic of the inverter is provided in Fig. 4.8. The half-bridge inverter is initially examined since it is composed of one phase-leg, which insight from the previous section can be used to investigate the noise issues. Furthermore, the AC operation is on the load side and the measurement acquisition remains across DC excitation, therefore varying as few parameters as possible from the DC/DC converter examples. The half-bridge inverter operates with 100 V at the input. The switching frequency is 100 kHz with and output line frequency of 60 Hz. This causes approximately 1666 switching periods per the output line period.
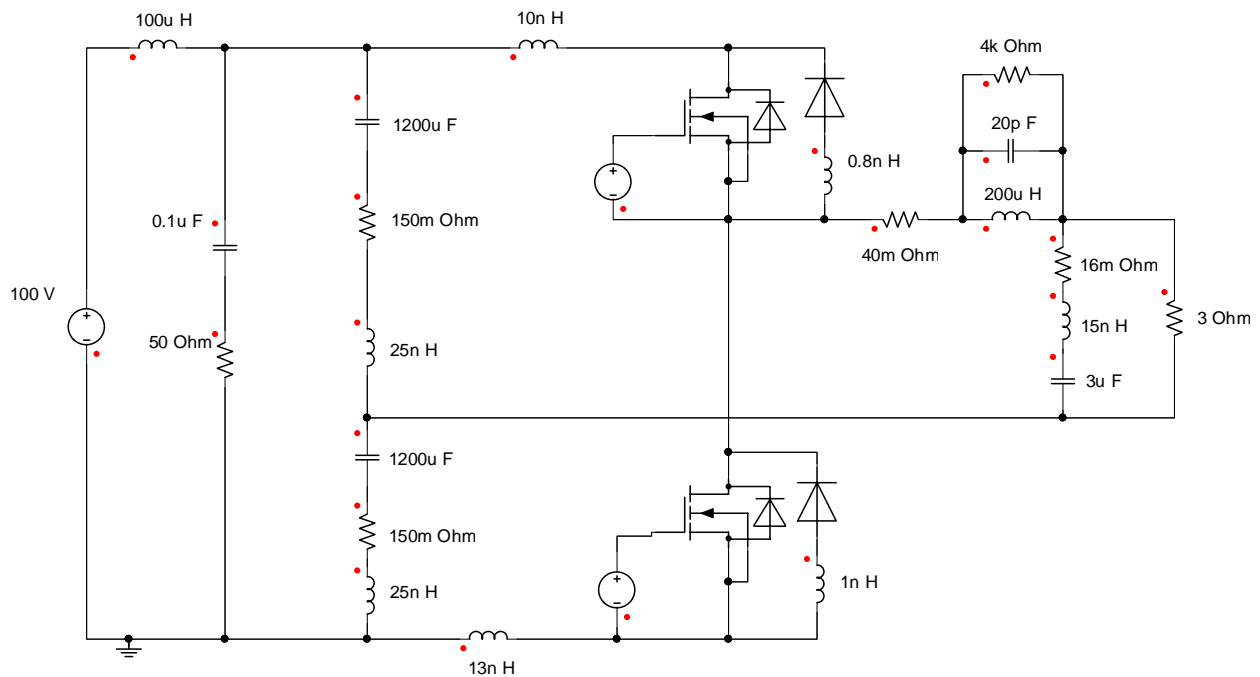
Fig. 4.8: Schematic of the simulated half bridge inverter.

4.2.1 Partitioning

Dividing a sine wave into different discrete operating points as opposed to an infinitesimal number of operating points could allow a significant reduction in the switching cycles required. For example, if a full sine wave is divided into eight partitions then the model only needs to solve for eight switching periods as opposed to 100s or 1000s if all periods are required. This is illustrated in Fig. 4.9 where (a) is a complete model and (b) assumes the switching event in the middle of each partition is repeated for the entire length of that partition. The mathematics that defines a partitioned line period is described in the flowchart of Fig. 4.10. Implementation of the

partitioning in Matlab is provided in APPENDIX B. Furthermore, definitions for a few parameters used in AC operation modeling are given in (4-1).

Partitioning will obviously cause an error in the final FFT. Two types of commutation strategies are examined to quantitatively determine the errors of this approximation: center aligned and edge aligned. These commutation strategies define when the switches turn on and off in reference to the beginning and end of the switching cycles. Center aligned defines the turn-on and turn-off events centered about the middle of the switching period. Edge aligned is defined as either the turn-on or turn-off events occurring at the beginning or end of the switching period, respectively. An example comparing the two commutation strategies of the half bridge inverters noise are displayed in Fig. 4.11. Three switching periods are plotted, the beginning of the line cycle, halfway up the rising edge, and the first peak of the line cycle. These three peaks also occur at the beginning and end of the cyan color and the end of the blue partitions in Fig. 4.9, respectively.

(a) Full model; includes all switching instances   **(b) Approximation of model into 8 partitions; assumes the same switching instance repeats within its partition**
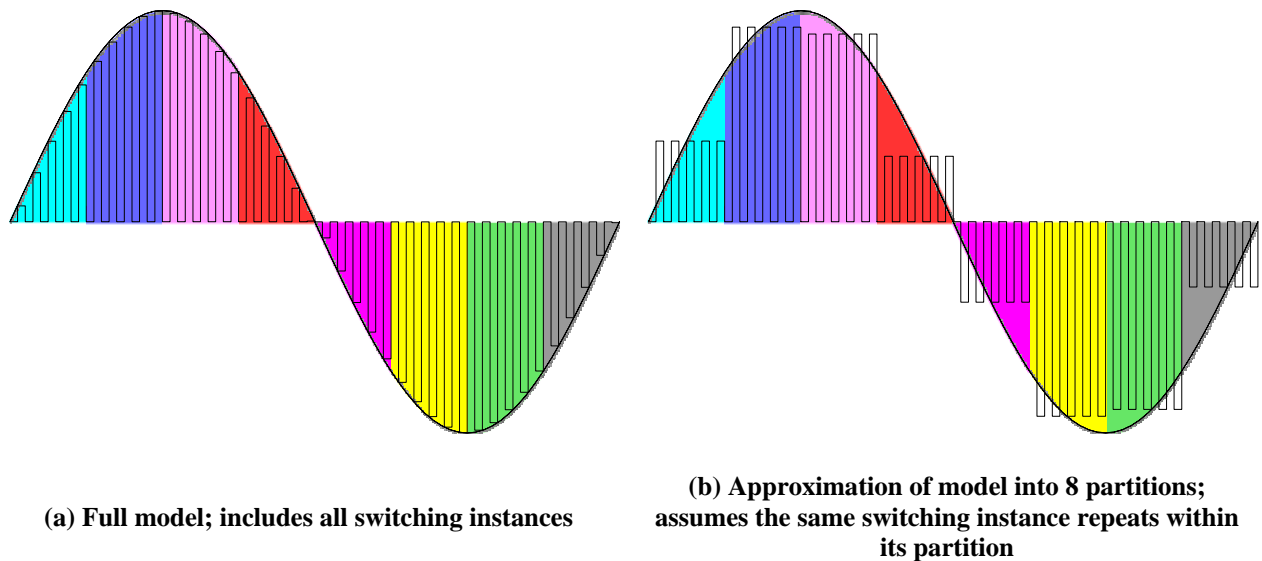
Fig. 4.9: Illustration of dividing an AC signal into a number of partitions to approximate the total noise. The sine wave depicts the operating point.

$$\text{P} := Total \ \# \ of \ periods$$

$$\text{P} = Integer\left(\frac{f_s}{f_l}\right)$$

$$\text{N} := \# \ of \ points \ per \ switching \ period$$

$$T := Total \ \# \ of \ partitions$$

$$Duty := Duty \ cycle \ of \ each \ switching \ period$$

(4-1)
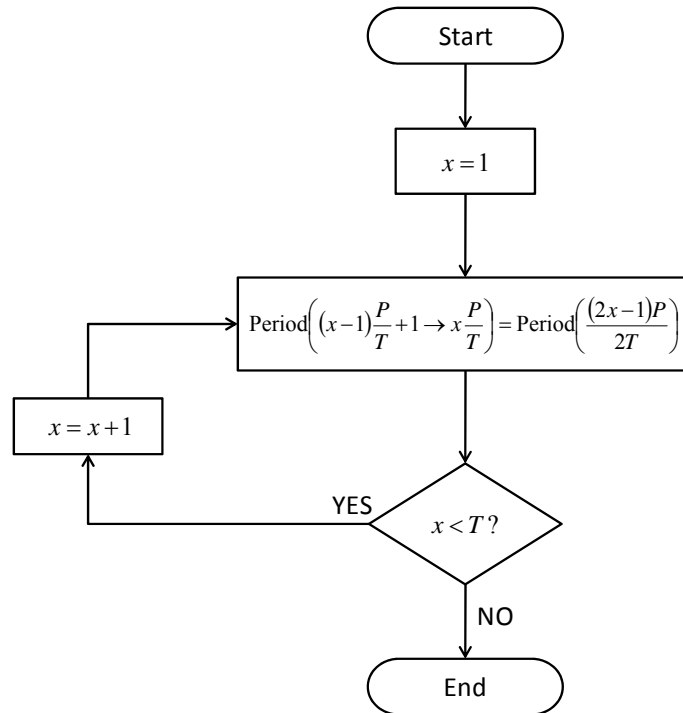
Fig. 4.10: Flowchart describing the process used to build the partioned dataset.
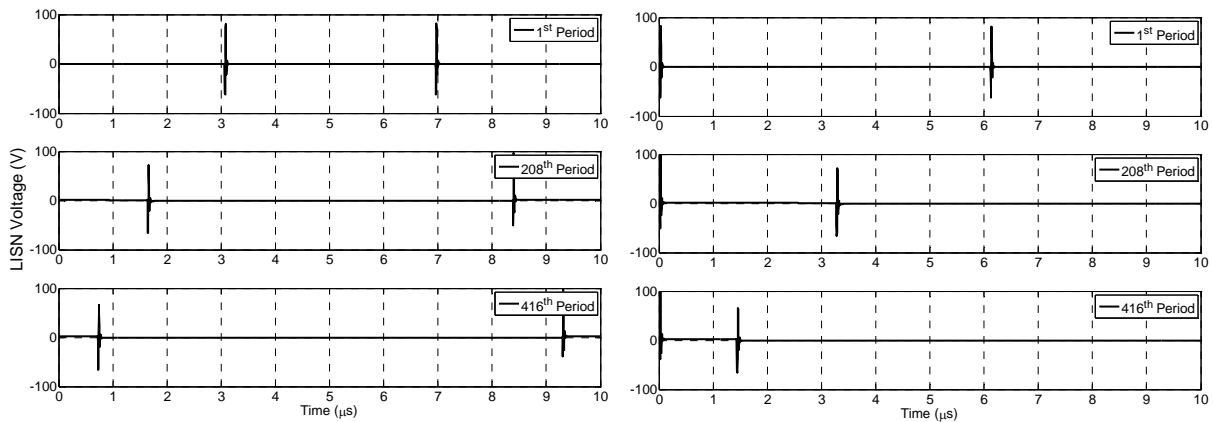
(a) Center aligned   **(b) Edge aligned**

Fig. 4.11: Switching periods in the first quadrant of the operating point. The three periods show the duty cycle changing as the operating point increases, as well as the alignment of each commutation strategy.

A series of voltage spectrums of the half bridge rectifier for different number of partitions are plotted in Fig. 4.13. The error clearly increases as the total partitions decrease. However, the errors in the center aligned case are drastically worse compared to the errors of the edge aligned. The Fourier series of each center aligned switching period is out of phase with the others. This causes a smaller noise value since the combination of all switching periods, which are out of

phase, partially cancel out. This can be seen in Fig. 4.13 for the full line cycle of data, 1666 partitions; the center aligned is considerably lower than the edge aligned. However, as the number of partitions decrease the center aligned partitioning examples move closer to the edge aligned noise values since fewer cancelations occur. The edge aligned switching periods are in phase with each other, therefore no canceling occurs and the approximations from partitioning are very accurate. The errors for the center aligned case are summarized in Fig. 4.12. The maximum error is around 18 dB if the sine wave is divided into only four partitions and approaches the ideal case as the number of partitions is increased.

The approximation errors of the terminal voltages propagate through the calculations that determine the modeled parameters. The equivalent current sources and impedances of the half-bridge inverter using the center aligned commutation strategy are plotted in Fig. 4.14 vs. the number of partitions. The errors of the terminal voltage approximation directly propagate to the current source calculation. However, the terminal impedance remains fairly constant as the approximation varies. As the operating point changes the propagation path does not change, only the current and voltages switched vary. Similarly, the minimal errors of the terminal voltage in the edge aligned case are also seen in the current source of Fig. 4.15a. Likewise, the impedance of the edge aligned case seen in Fig. 4.15b does not vary with the partitions, nor does it differ from the center aligned modeled impedance. The propagation path did not change with the commutation strategy.
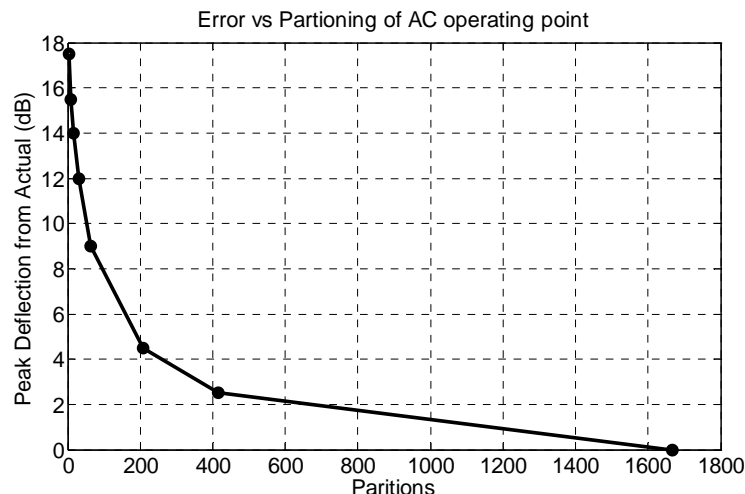
Fig. 4.12: Error vs. the level of approximating the operating point variation into discrete partitions. No approximation (ideal case) has 1666 partitions.
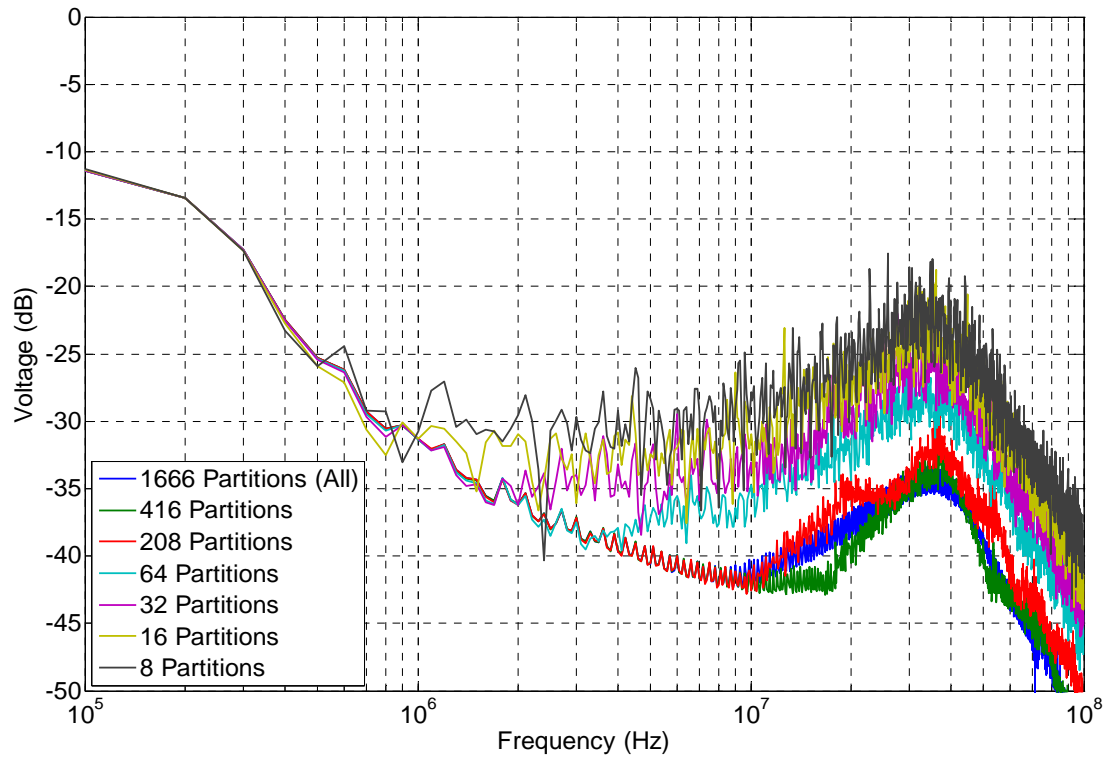
(a) Center aligned
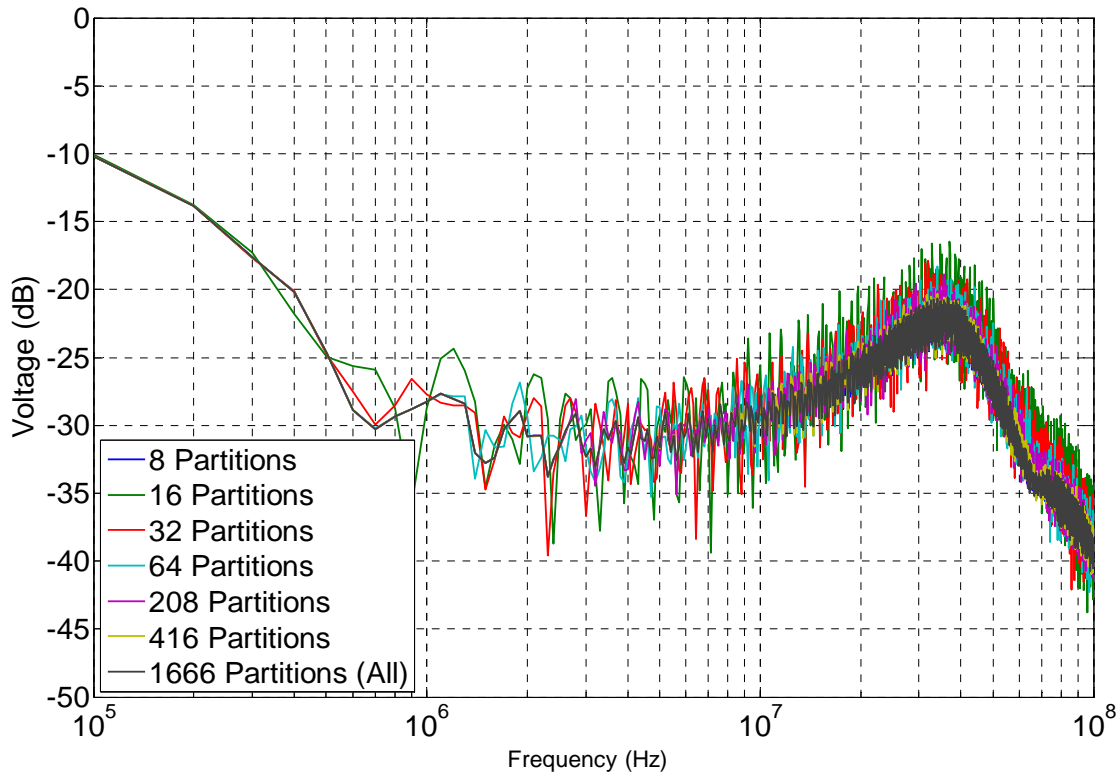
(b) Edge aligned

Fig. 4.13: Frequency spectrum of terminal voltage over a complete low frequency operation (60 Hz);
compares the full set of data with an approximation of the operating point as varying widths of discrete steps.
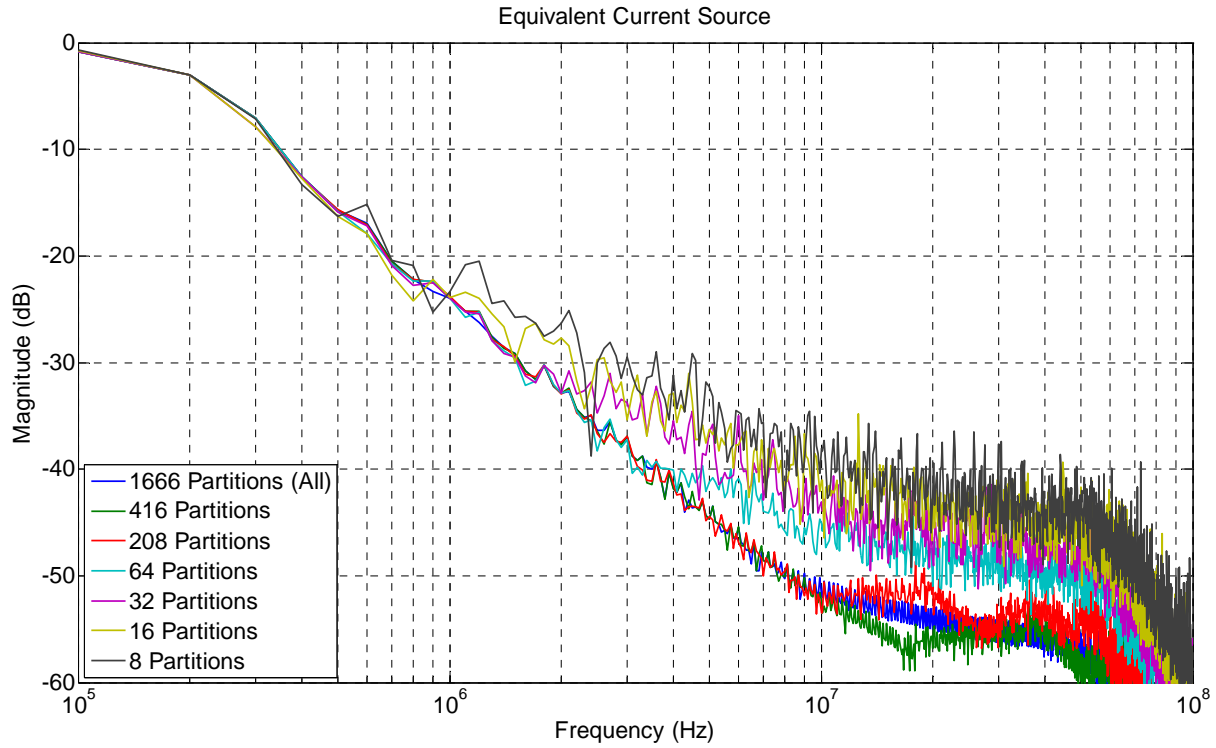
(a) Modeled equivalent current sources. Errors related to terminal voltage errors.
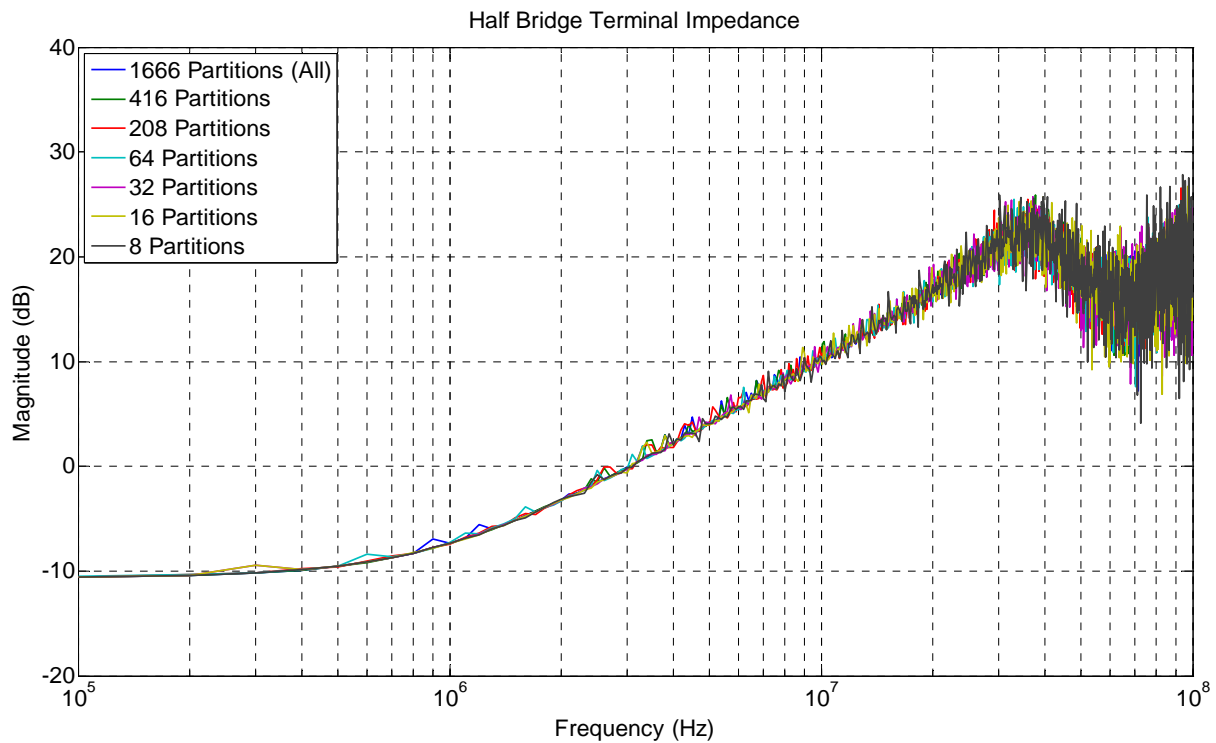
(b) Modeled equivalent impedance. Not greatly affected by terminal voltage approximations.

Fig. 4.14: Modeled parameters of half bridge inverter using center aligned commutations as the number of partitions varies.
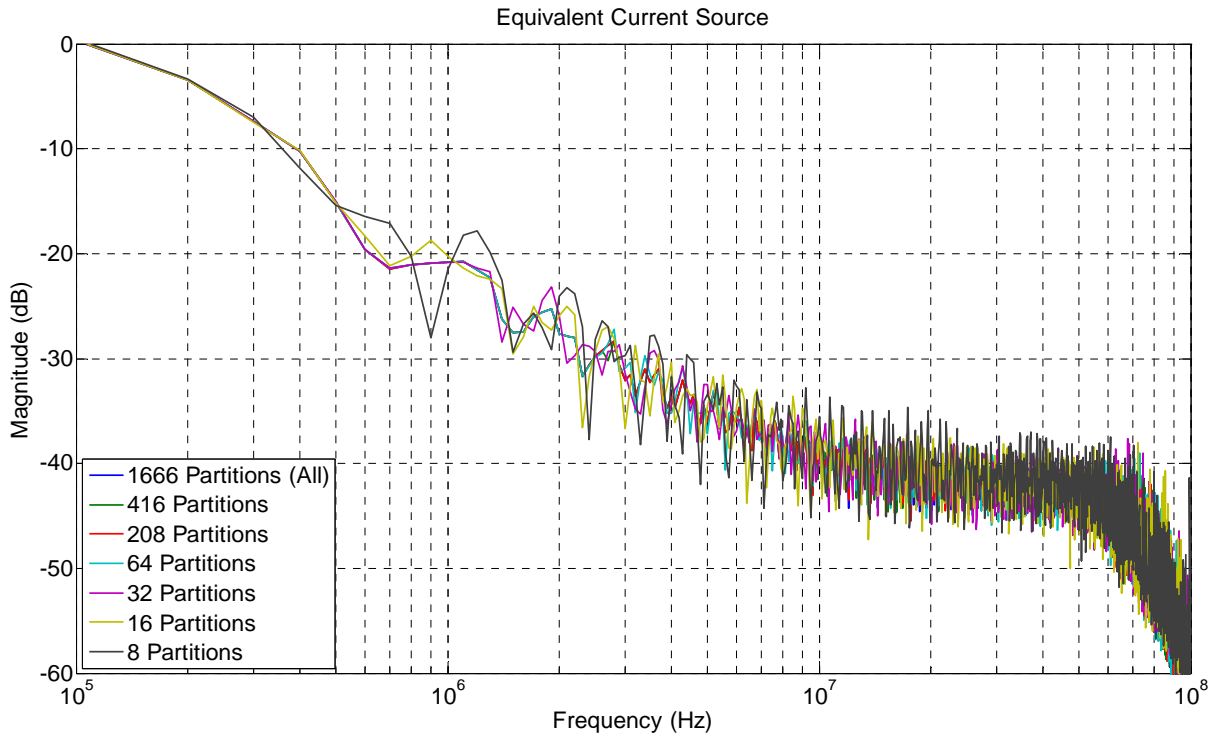
(a) Modeled equivalent current sources. Errors related to terminal voltage errors.
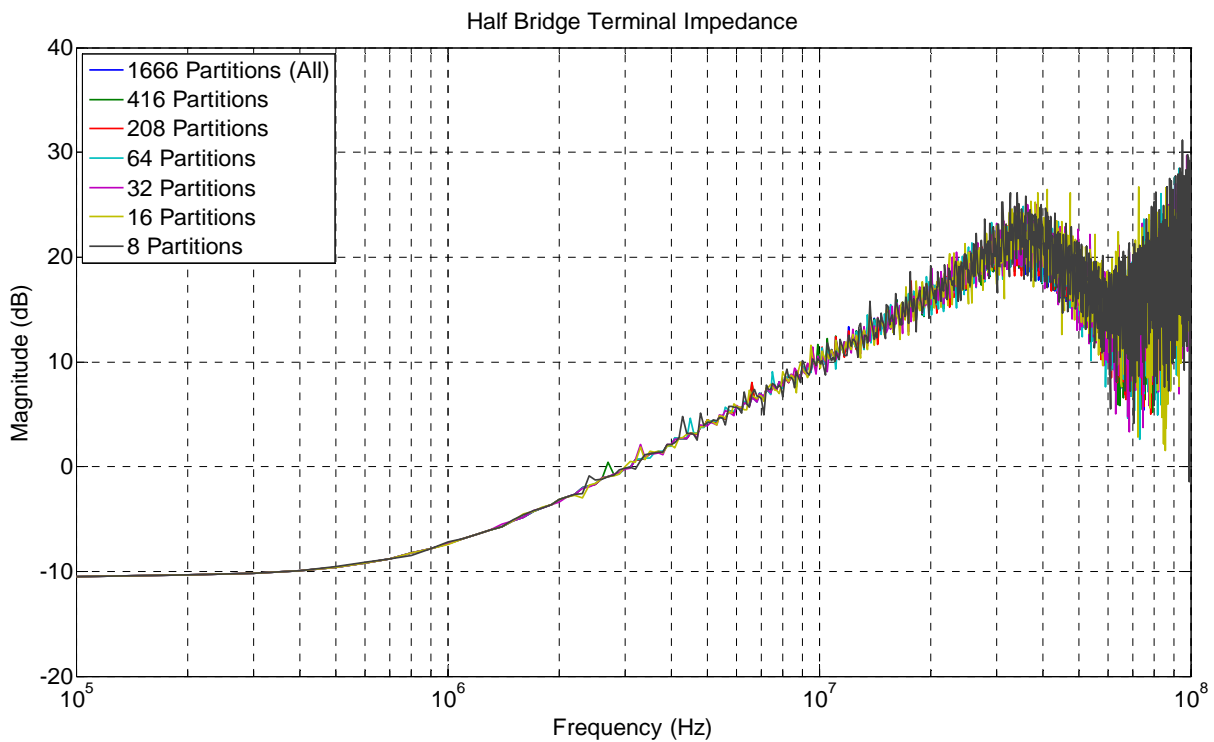
(b) Modeled equivalent impedances. Not greatly affected by terminal voltage approximations or commutation strategy.

Fig. 4.15: Modeled parameters of half bridge inverter using edge aligned commutations as the number of partitions varies.

4.2.2 Data Manipulation

One critical issue is the ability to know the commutation methods at the terminals of the system. This is needed in order to have some confidence on the accuracy of the partitioning approximation. By comparing a few switching cycles to each other, the location of turn-on and turn-off switching instances can be investigated and distinct enough to verify center or edge aligned commutations. For the purposes of this work only center and edge aligned commutation strategies are considered. The previous section illustrated how edge aligned remains very accurate even for a course approximation. However, the center aligned case became inaccurate very quickly. Assuming the switching strategy is known to be center aligned, this section proposes two techniques that can assist in improving the approximation. As mentioned, the center aligned case is often used to reduce the harmonics and EMI of the system due to the phase differences of each switching period. This same phenomenon is what reduces the accuracy of the partitioning approximation.

Before the two approaches are covered, a closer look into the errors involved with the center aligned case is investigated. A zoomed in illustrated view of the first partition is shown in Fig. 4.16. Only five switching periods are shown for simplicity in Fig. 4.16(b, c); additionally, the height of the pulse do not necessarily change, it is only pictured this way for illustrative purposes. As seen in Fig. 4.16b, the duty cycle of the periods change as the operating point changes, however, every period is approximated as the same duty cycle in Fig. 4.16c. As mentioned in the previous section, the middle ($^{\#}2$) switching period is assumed to repeat for all periods within its partition. A closer look at the first, middle, and last switching period of the first partition is plotted in Fig. 4.17. Part (a) illustrates how the switching commands appear in the actual (red) center aligned case compared to the approximation (black). The terminal voltages during each of those periods in the first of 16 partitions are also provided in part (b). Two main differences occur in this approximation: the duty cycles are different and the turn-on / turn-off times do not correlate. The first, or α, technique used to improve the approximation will attempt to eliminate both differences.
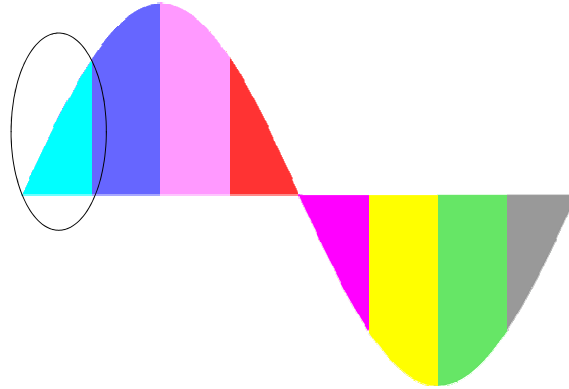
(a) Full AC operation divided into partitions; the first partition is expanded below
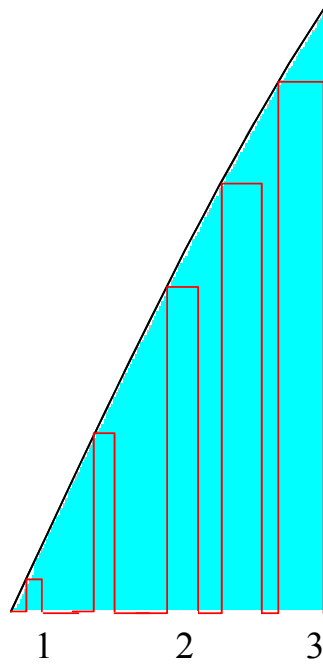
(b) Original switching periods
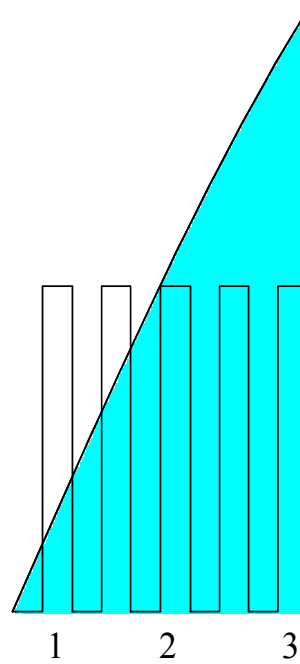
(c) Approximated switching periods assuming one period is identical to the others

Fig. 4.16: Illustration of the errors when partitioning; looking at the first partition.

Using only the middle ($^\#$2) switching period an interpolation can be used to predict when the turn-on instance should occur. Commutations created from comparing a triangle or sawtooth carrier with a sinusoidal will result in a sinusoidal duty cycle throughout the line cycle. Knowing how the duty cycle will (or should) change allows for an interpolation of the single captured period to better approximate the other periods within the partition. The interpolation within the first partition is illustrated in Fig. 4.18a. The period is shifted by the appropriate amount to align the turn-on instances using the sinusoidal duty cycle as the reference. One

problem with this approach is there will be missing information. For example, when period 2 is shifted to better align with period 1 (in Fig. 4.18a) part of the on-time will need to be truncated; which should not be much of an issue. However, the off-time needs to be expanded and no information exists to approximate this data. When decreasing the duty cycle off-time data is needed and when increasing the duty cycle (ie. using period 2 to predict period 3) more on-time data is needed, and unknown. In this example, the ringing occurring between turn-on and turn-off is very short, which causes most of the other data to be zero, or close to it. Therefore, to predict the unknown data, a linear interpolation is used between the two known points. The green lines in Fig. 4.18a simply connect the points with a straight line, which assumes no ringing occurs. The approximated periods of the simulated terminal voltages are compared to the actual voltages in Fig. 4.18b; very close agreement is seen. The frequency domain information of the approximations are also plotted in Fig. 4.19 for 8 and 16 partitions. The course approximation of only 8 partitions for the center aligned case – using data collected from one period and interpolated – is very close to the entire data set of the line cycle. That is, only one switching period in each partition is collected then interpolated to match the actual noise; when as high as 14 dB error was seen in Fig. 4.13a when no interpolation is used.

(a) Illustration   (b) Actual data (red) compared to approximation (black)
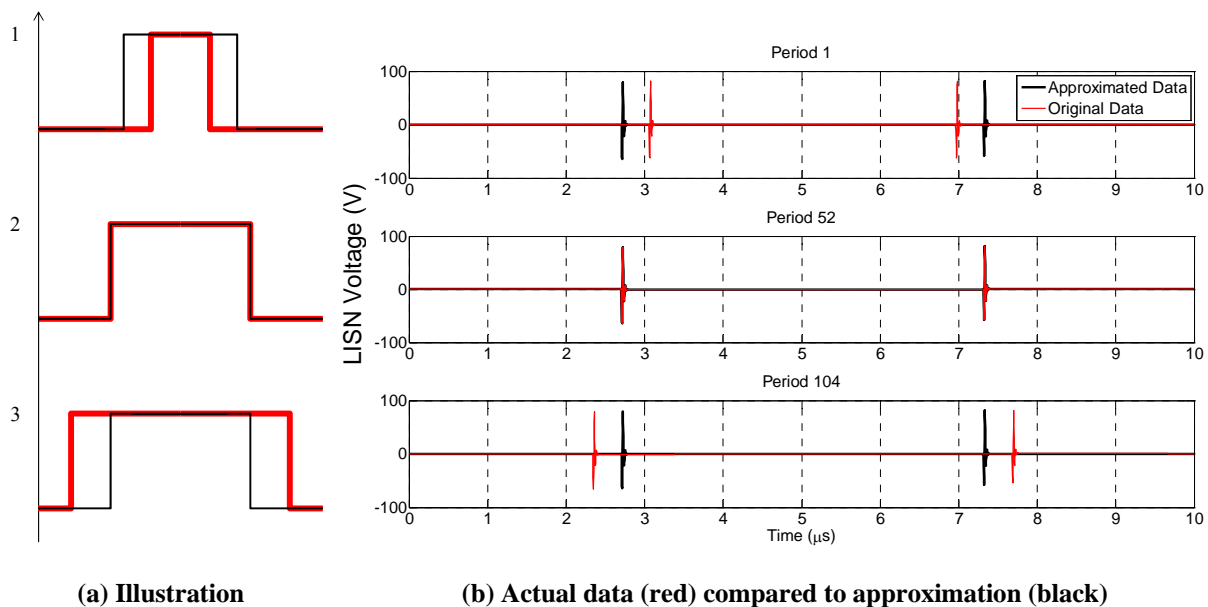
Fig. 4.17: Error between the approximated switching periods and actual data for the center aligned case.
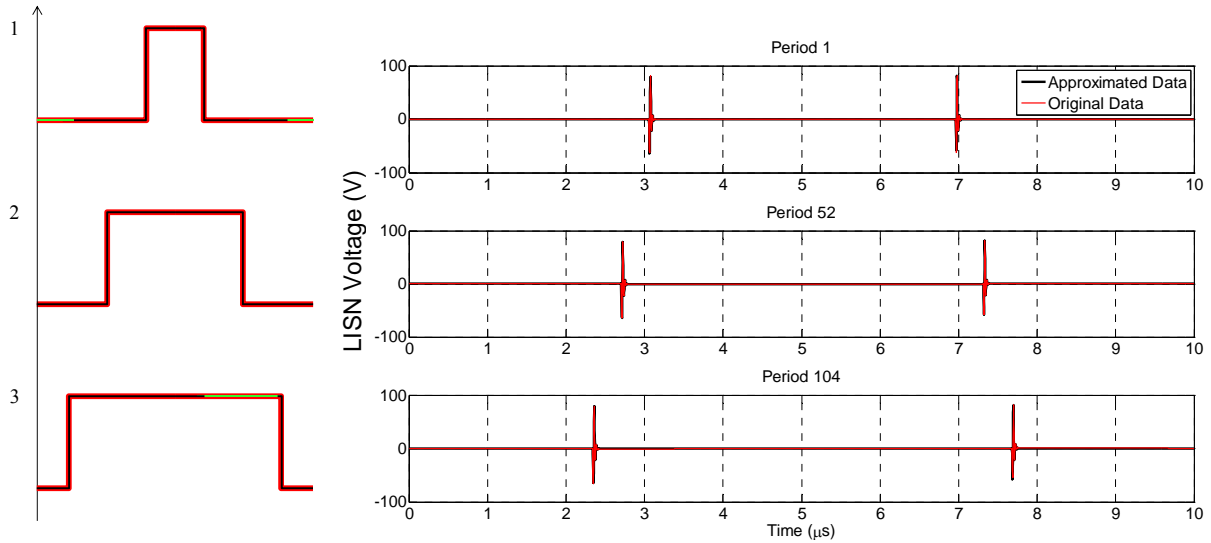
(a) Illustration how one period approximates the others

(b) Actual data (red) compared to approximation (black)

Fig. 4.18: Results of first (α) method to manipulate one switching period to predict the behavior of the rest.
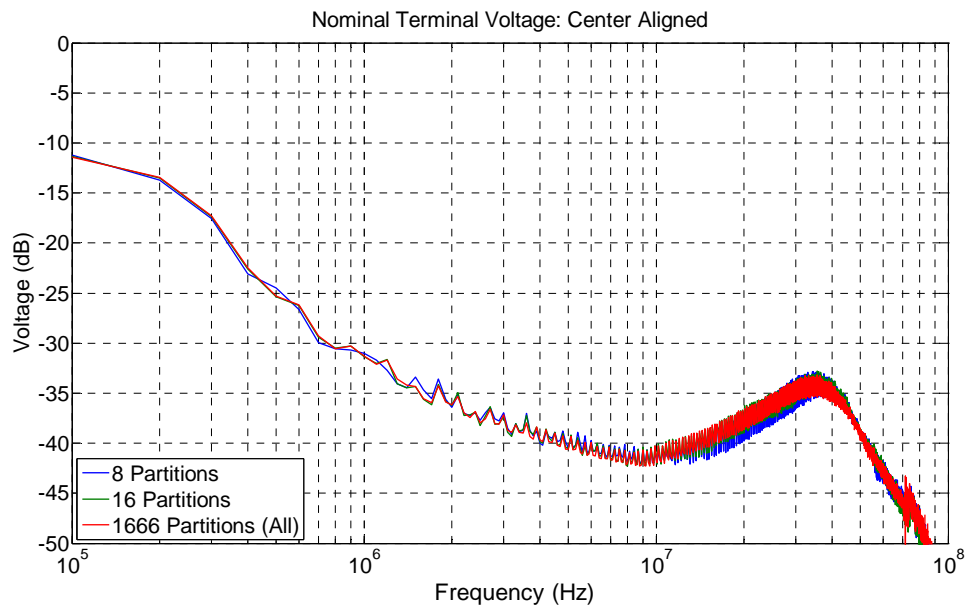
Fig. 4.19: Results of the first (α) method that uses one period to predict the behavior of the rest. Accurate results are seen for 16 and 8 partitions; without the additional prediction up to 14 dB error was seen.

Since it may not always be valid to assume a straight line between the two missing data points another method is also investigated. The edge aligned examples, Fig. 4.13b, show promising results using partitioning even though the duty cycle varies since the phases of each switching period are still aligned. The second, or β, method to predict the other switching period is to align the phases without changing the duty cycle. This allows for easier manipulation of the data since it is only a shifting of the turn-on points and no missing data is required. The process is illustrated in Fig. 4.20a. Again the middle ($^\#$2) period of the partition is acquired and used to predict the other periods. In this case the entire period will either shift forward or backwards to align the turn-on instance. As Fig. 4.20a shows for period 1 the acquired period is shifted right to align the turn-on times. When this is done the information at the end of the period will be shifted to the beginning. This is a safer assumption since the periods are cyclic and two adjoining periods are very similar. Likewise, period 3 shifts the acquired period to the left and moves the beginning portion of the period to the end. The black periods in Fig. 4.20a show the shifted data aligning the turn-on times with the red, and the green portion is moved from one end to the other. In this method if ringing is still occurring during this green portion then it will remain in the signal and therefore also in the Fourier series information.

The approximated periods of the simulated terminal voltages are compared to the actual voltages in Fig. 4.20b; close agreement is seen in terms of the alignment of each approximated period in phase with the actual data. The frequency domain information of the approximations are also plotted in Fig. 4.21 for 8 and 16 partitions. More error is seen with this interpolation method as compared to the first one since the duty cycles are not as accurate. However, this second method provides a more general solution to interpolating the data to better fit the actual results. The approximation of 8 and 16 partitions using the second interpolation method within each partition are within a few dB of the full data set, compared to Fig. 4.13a when as high as 14 dB error was seen. The flowchart that describes these mathematical manipulations is delineated in Fig. 4.22. Implementations of the two manipulation methods in Matlab are provided in APPENDIX B.
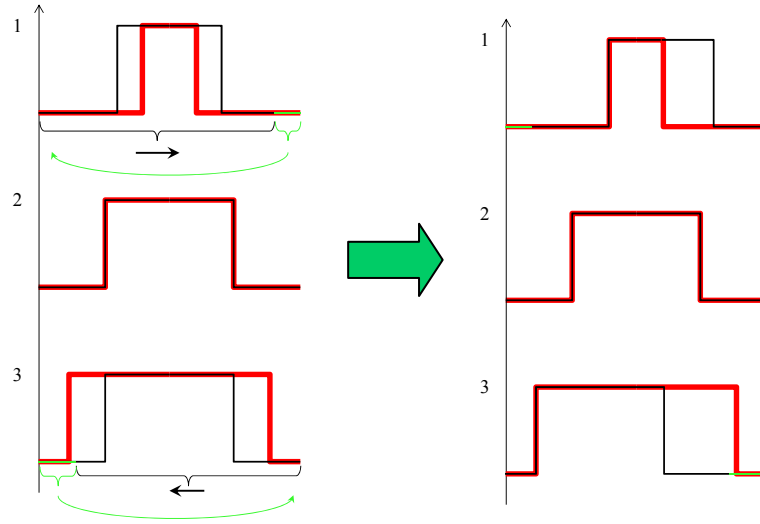
(a) Illustration of how one period is used to approximate the others
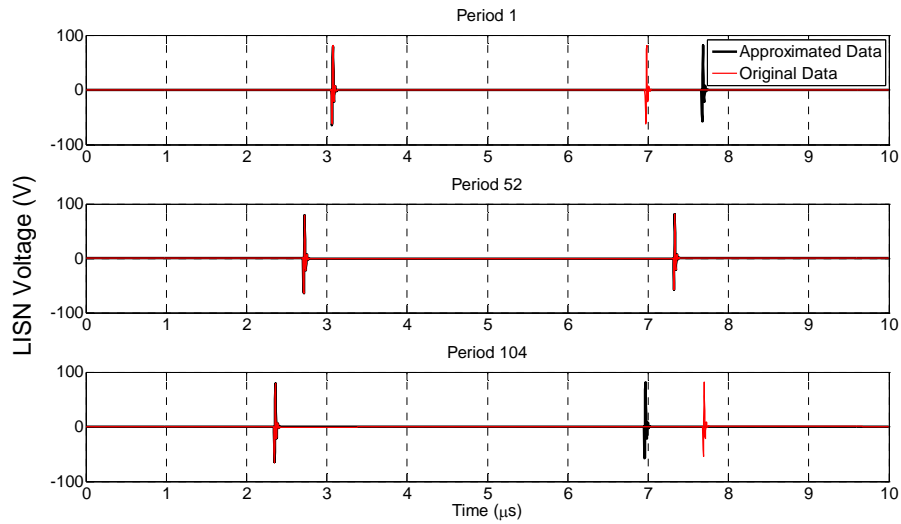
(b) Actual data (red) compared to approximation (black)

Fig. 4.20: Results of second (β) method to manipulate one switching period to predict the behavior of the rest.
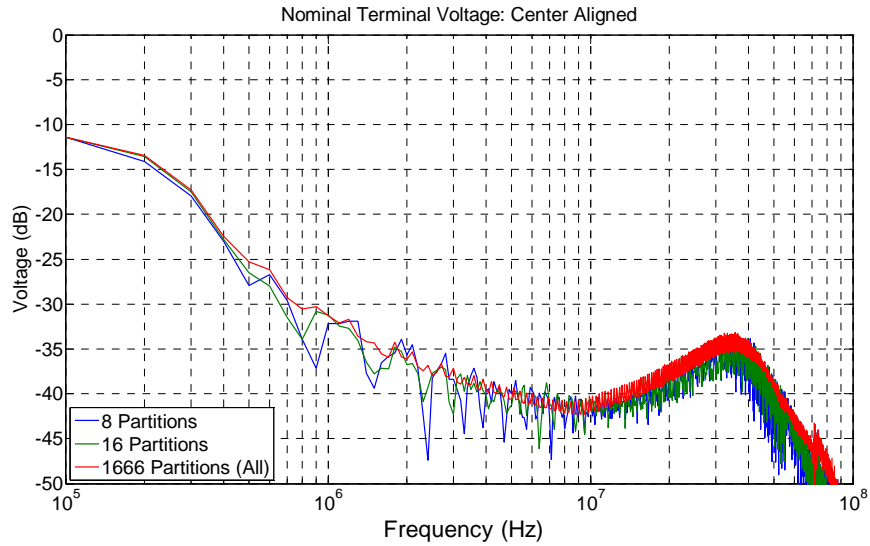
Fig. 4.21: Results of the second (β) method that manipulates one period to predict the behavior of the rest. Results with only a few dB error is seen for 16 and 8 partitions, where without the additional prediction method used up to 14 dB error was seen.
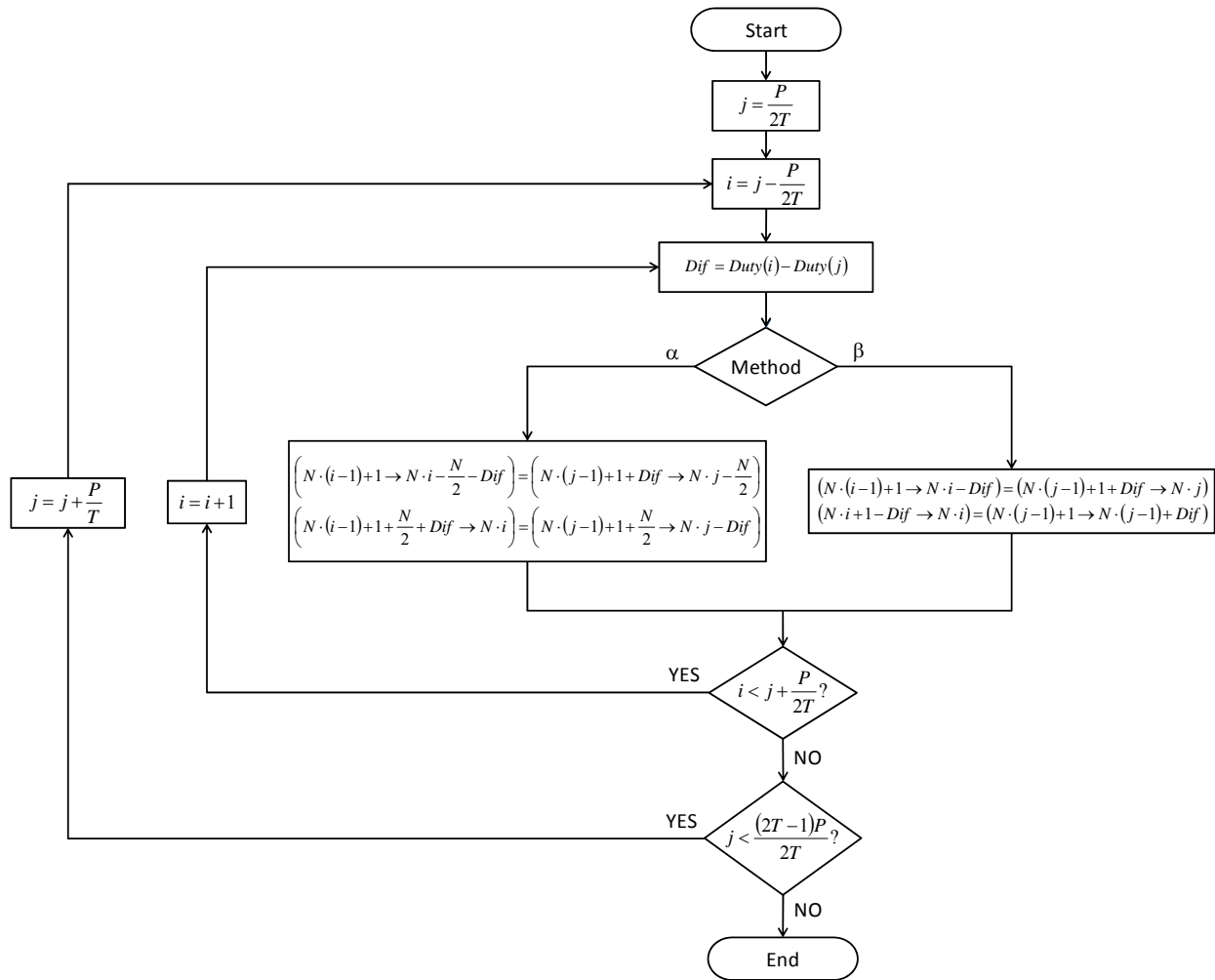
Fig. 4.22: Flowchart describing the process used to manipulate the center aligned dataset to improve the portioned approximations.

94

4.2.3 Symmetry

Provided the partitioning of the line cycle can reduce the number of data collection points, even 16 or 8 partitions are needed for the best case scenarios. This is still a large number of measurements that are needed. For each partition, one nominal and 2-3 attenuated cases are measured; that is, up to 64 measurements may be required if the operating region is divided into 16 partitions. A method to further reduce the data collection process is desired. Therefore, the influence of using symmetry to reduce the required amount of information while maintaining accuracy is also investigated.

4.2.3.1 Single-phase

Three types of symmetry are examined for single phase systems; all are summarized in Fig. 4.23. First, is to assume the rising and falling edge of the operating region produce the same values, Fig. 4.23b. In order to implement this assumption the first quadrant – or rising edge in the positive region – of the operating region is mirrored about the peak to the second quadrant. Similarly, the third quadrant is mirrored about the minimum to the fourth quadrant. The results of this symmetry for both center and edge aligned systems are plotted in Fig. 4.25. The edge aligned system has a nearly identical agreement between the full data set and that using symmetry, where the center aligned is still within 1-2 dB.

The next two symmetry options involve the entire first half of the operating point predicting the second half. Next, the mirroring concept is adapted to the entire first half to reproduce the second half of the operating region, Fig. 4.23c. The final symmetry method investigated is copying the first, positive, region to the second half, Fig. 4.23d. These assume that the top side switching is identical to the bottom side switching in the half bridge inverter example. The results for the symmetry implemented as in Fig. 4.23(c, d) are shown in Fig. 4.26 and Fig. 4.27, respectively. Although both options show to be accurate, copying the first half to the second half is more accurate. This makes sense, since when copied the increasing / decreasing in the magnitude of the load current are the same. Additionally, the center aligned systems are more accurate than the edge aligned for both Fig. 4.23(c, d). Finally, a combination of the different methods can be implemented for the symmetry in the single-phase system. First, mirror the first quadrant to the second, and then copy that first half to the second half. This only requires the

first 1/4th of the operating region to be known. Simplified symmetry equations are given in (4-2) that correlate to each example in Fig. 4.23.
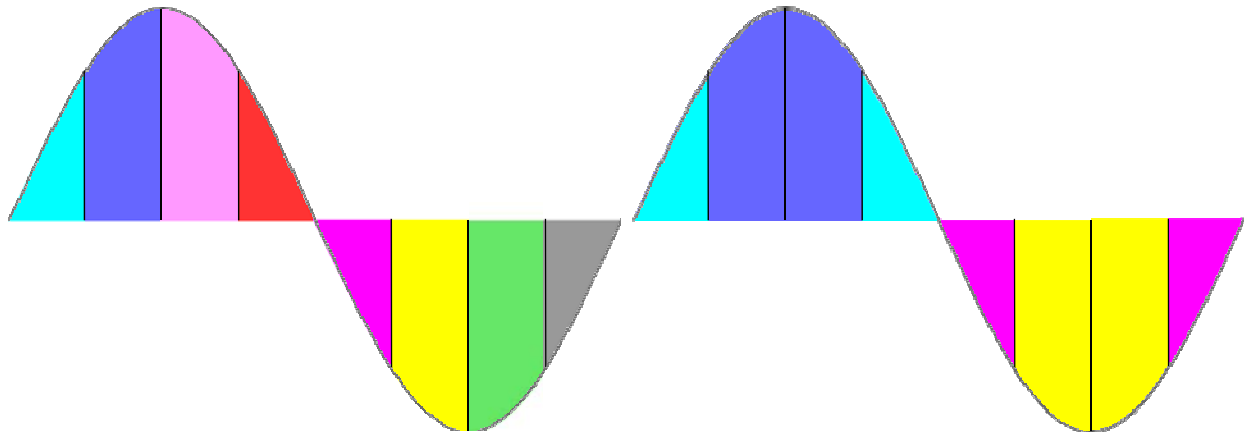
(a) Original data set of the full AC operation

(b) Quadrants 1 and 3 are mirrored to quadrants 2 and 4, respectively
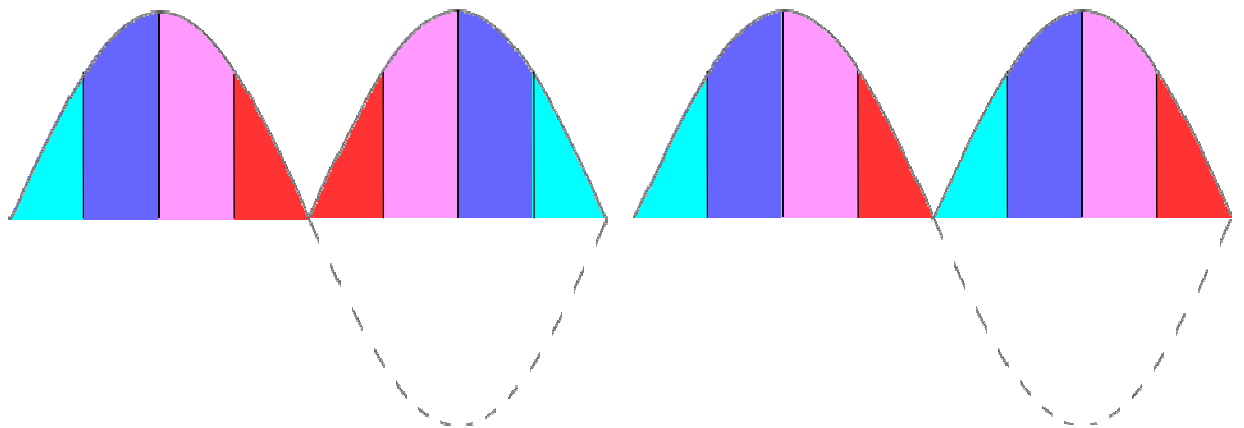
(c) First half is mirrored about the middle to produce the second half.

(d) First half is copied to the second half.

Fig. 4.23: An illustration of three types of symmetry examined for the single-phase system. The different colors are only present to visually see the type of symmetry involved. Accompanying equations are in (4-2).

$$
\begin{cases}
\text{Period}\left(\frac{P}{4}+1 \rightarrow \frac{P}{2}\right) = \text{Period}\left(\frac{P}{4} \rightarrow 1\right) \\
\text{Period}\left(\frac{3P}{4}+1 \rightarrow P\right) = \text{Period}\left(\frac{P}{2} \rightarrow \frac{3P}{4}\right)
\end{cases} \quad \text{(b)}
$$

$$
\text{Period}\left(\frac{P}{2}+1 \rightarrow P\right) = \text{Period}\left(\frac{P}{2} \rightarrow 1\right) \quad \text{(c)}
$$

$$
\text{Period}\left(\frac{P}{2}+1 \rightarrow P\right) = \text{Period}\left(1 \rightarrow \frac{P}{2}\right) \quad \text{(d)}
$$

(4-2)

An important aspect in conducting the symmetry operations is to preserve the period's orientation to each other. That is, if the commutation is left aligned then the approximated symmetric data should also be left aligned. Furthermore, any ringing in a period should be reproduced in the same fashion on the symmetric side from the original side. As (4-2) describes, entire periods are copied from one location to another (in reverse order for mirroring), but the beginning and end of each period should remain the beginning and end and not flipped around. This is illustrated in Fig. 4.24, where the correct way to mirror a dataset is proved in (a) and an incorrect method is shown in (b). The correct method preserves each individual period, but mirrors the order of the periods. However, the incorrect method in Fig. 4.24b mirrors the entire dataset. This will cause a drastic error and is physically incorrect to the operation approximated. Using Fig. 4.24b will cause inaccuracies of the turn-on and turn-off instances, phase differences of the periods, and any ringing will be drastically wrong. That is, it will cause normally damped ringing to increase and occur in the wrong orientation to the adjacent period.

(a) Correct way to perform the mirroring operation.

(b) Incorrect way to mirror the data.

Fig. 4.24: Illustration of two mirroring option; the periods must be mirrored (a) as opposed to the full string of data (b). This mimics the proper switching events

(a) Center aligned   **(b) Edge aligned**

Fig. 4.25: Results from mirroring quadrants 1 and 3 to quadrants 2 and 4, respectively, Fig. 4.23b.

(a) Center aligned   **(b) Edge aligned**

Fig. 4.26: Results from mirroring the first half about the middle to produce the second half, Fig. 4.23c.

(a) Center aligned   **(b) Edge aligned**

Fig. 4.27: Results from copying the first half to produce the second half, Fig. 4.23d.

4.2.3.2 Three-phase

To further explore the possibilities with symmetry a three-phase system is also investigated. Additionally, this shows the ability to use the terminal model for a three-phase system for the first time. The three-phase system is an inverter with a DC input and three-phase AC output. The schematic in Fig. 4.28 is the simulated model. In the simulation all switches are detailed models of actual components and additional parasitics are approximated for all passive elements as well as interconnections to mimic an actual inverter.

Fig. 4.28: Schematic of the three-phase inverter simulated to investigate symmetry. Each switch and diode are models of actual components, and additional parasitics were included throughout the model to provide closer results to an actual inverter.

Two types of symmetry are investigated for three-phase systems in addition to the symmetry used in the previous section. The three-phase operating region is divided into 6 and 12 equally spaced divisions. The symmetry used will be similar to that of the single-phase case using both copy and mirror type functions. Due to the nature of the three-phases, the 1st, 3rd, and 5th of 6 total divisions are the same if the system is balanced with identical components; likewise the 2nd, 4th, and 6th divisions are the same. Therefore, copying the 1st and 2nd $1/6^{th}$ portions of the operating point to their respective division an accurate representation of the system is maintained due to symmetry. This method is illustrated in Fig. 4.29a. A second method involves dividing the operating space into 12 divisions and mirroring the 1st $1/12^{th}$ division to the 2nd division, and then the 3rd to the 4th and so on until the 11th is mirrored to the 12th. This is shown in Fig. 4.29b.

Both methods showed nearly ideal results. Finally, a combination of the two approaches is performed. The data is mirrored to predict the first 3rd of the operating region (dark mirror lines in Fig. 4.29b) then copying the rest as in Fig. 4.29a to reproduce the entire operating region. This only requires knowledge of 1/6th of the operating region to predict the entire line cycle. The terminal model solution using both methods of symmetry is compared to no symmetry in Fig. 4.30 and proves to be very accurate.

(a) Copying 1st 1/6th portion to the 3rd and 5th 1/6th divisions and copying the 2nd portion to the 4th and 6th

(b) Mirroring each of the odd 1/12th divisions to the next even division, ie. 1st 1/12th is mirrored about the pink line to the 2nd 1/12th division
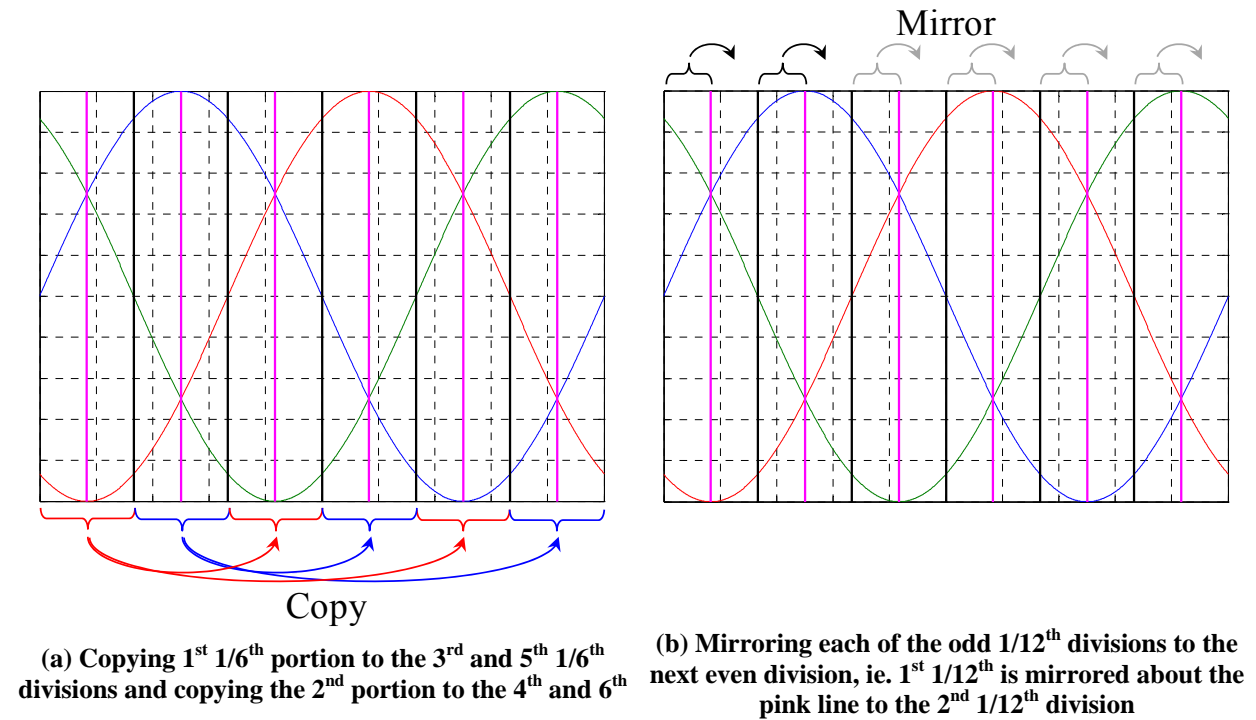
Fig. 4.29: An additional two types of symmetry examined for the three-phase system. The three-phase sine waves are present to see the symmetry at 1/6th (black) and 1/12th (pink) divisions.

(a) Equivalent current source

(b) Equivalent terminal impedance
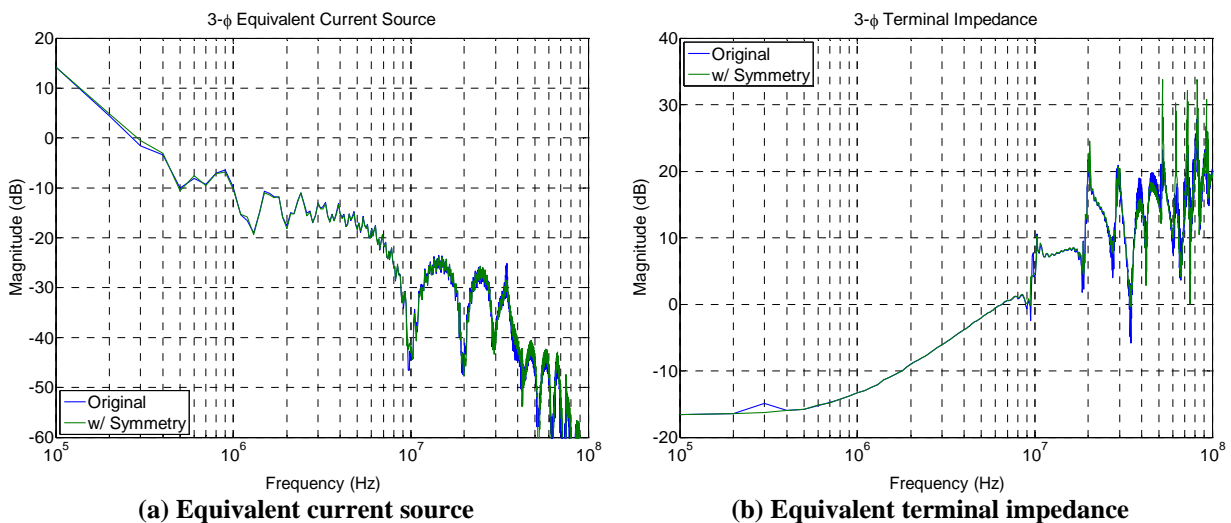
Fig. 4.30: Calculated terminal solution comparing the full three-phase data to that using symmetry. Both symmetry options in Fig. 4.29 were used; hence, only 1/6th of the AC line cycle is used to predict the rest.

5 CONCLUSION

5.1 SUMMARY

The verification of a boost converter, phase-leg module, and cascaded networks shows great promise for the modeling procedure and methodology. The procedure shows excellent agreement for all EMI frequencies. The improvement over previous methods is largely due to the systematic characterization and requirements of the modeling parameters and the well calibrated measurement fixture. Defining the bounds on the source and shunt impedances (or attenuation between different measurements) was critical in finding a general solution with high accuracy and has not been completed in prior publications. Furthermore, the measurement procedures identified many errors that can occur in the modeling process. Solutions to minimize these errors were presented and accurate results at frequencies an order of magnitude higher over previous work were demonstrated.

The overall time to create the model, once the measurements are taken, is relatively short compared to a full time-domain model. The modeled converter can then be used under many conditions (for example, different values for Z_{Source}) very quickly as long as the operating point remains constant. With a complete model realized— noise impedance and sources—interactions between systems and filters are studied and allow for a filter design and EMI prediction. Finally, an accurate model for a system under AC operation without greatly increasing the complexity of modeling procedure is defined. The objectives of this study are achieved and the major accomplishments and contributions are:

1) The accuracy of the model was improved compared to previous studies to go up to and beyond the EMI conducted frequency range – the boost converter is accurate up to 50 MHz.

2) Two- and three-terminal systems are modeled for various power electronic applications; four-terminal modeling was outlined for future work.

3) The model can identify a "black box" system of any size much faster than a complete detailed model.

4) Cascading two terminal systems together was used to examine the interaction and noise characteristics at the system-level. The interactions assisted in predicting the filtered noise and design of an EMI filter.

5) The modeling procedure was demonstrated for AC inverters. Additional data reduction techniques were explored to reduce the computations and measurements required.

6) Accuracy and limitations of the model are defined to ensure accurate modeling results.

5.2 FUTURE WORK

The work presented here provides a basis for the modeling procedure. Much progress has been made to model EMI quicker and more accurately. However there is still more that needs to be done; for example, a full sensitivity analysis as demonstrated in Section 3.1.1.2. The terminal modeling approach is still at the beginning stages, however, the ground work is well established and in place to build and expand the applications of the modeling procedure. Some of the immediate areas of interest that can directly follow this work are outlined below.

5.2.1 Increased Range of Accuracy

The frequency range of interest in this work was for typical EMI frequency and even beyond, that is, 100 kHz up to as high as 100 MHz. Although 100 MHz was difficult to achieve in measurements, if the appropriate equipment is used and the signal-to-noise ratio is significant enough, the results are attainable. It was never the focus of this work to look below the 100 kHz mark, since many standards start at 150 kHz. However, some sensitive standards start as low as 10 kHz and have a switching frequency on this order as well, especially for higher power converters. Modifying the process to accommodate the lower frequencies needs to be done. Maintaining the low frequency operating point while satisfying the parameters needed for accurate modeling results may be difficult. For example, the measurement fixture has an inductive impedance below 100 kHz. When a large source impedance is needed it will be difficult to increase without adding a larger inductor; however, when too much inductance is used other issues may occur, such as stability at the input of the system, or parallel capacitance of the inductor limiting the upper end of the frequencies of interest. Care would need to be taken when designing the source impedance and measurement fixture for lower frequencies. Two procedures may need to be implemented for low and high frequency model characterization.

5.2.2 AC Operation

The AC operation was investigated; however, measurement verification is still needed. The theory and simulations covered in this work for the AC operating conditions was only for systems with a DC input and AC load. A system with an AC input also needs to be examined in order to determine if the same procedures can be used. Furthermore, only center or edge aligned sinusoidal PWM systems were explored. Many more switching schemes are available, such as hysteresis, space vector modulations, harmonic control, etc. that can be explored. An approach that can generally reduce the data required regardless of the commutation scheme would be advantageous.

5.2.3 Four Terminal

The four-terminal model can be used to represent a three-phase input with a common ground, or as seen below, an unterminated model. However, as mentioned in Section 2.4 potential roadblocks in this terminal modeling approach increase as the number of terminals increase. For example, the lack of significance in some parameters is a serious one that would need to be solved before proceeding further with the four-terminal model. This issue will only worsen as the number of terminals increases. These parameters that are insignificant do not necessarily need to be involved in the modeling process, however, in the general case it may not be possible to know which parameter should be excluded. Additionally, an impedance may be insignificant at some frequencies but not others, which makes it increasingly difficult to exclude certain parameters at only certain frequencies. Finding a particular method to systematically justify the appropriate modeling conditions is needed for the four-terminal system as well as a general approach for n-terminal systems.

5.2.4 Unterminated Model

An unterminated, or an unloaded, circuit could also be investigated for a more general model. This can potentially be completed by increasing the number of terminals in the system. For example, a four-terminal system might represent a converter with a common negative terminal, positive input and output and then a ground, illustrated in Fig. 5.1. A challenge would be how to attenuate the output terminals distinctly from attenuating the input terminals. If it is a controlled converter with constant current, power, or voltage, a shunt impedance may not be appropriate in

all cases. Furthermore, care would need to be taken in defining the operating point of validity for the switching stage.

One further extension of this could be a phase-leg module, or even a full three-phase switching bridge. A single phase-leg would require a four-terminal model, however a full three-phase module might need as many as six terminals (2 input, 3 output, and a common path). The main challenge, in addition to the additional terminals is how to model the phase-leg without the large inductor (or current source) at the output. It may have similar issues as the switched impedance case if an element is not present that will cause the switched impedance to appear more like a switched source. Another option could be to model the phase-leg as a three-terminal model, and define the operating point of validity as a function of the output current and do not model it as an unterminated system.
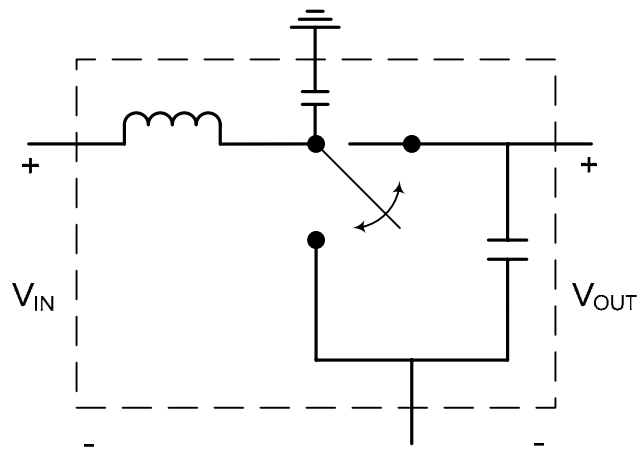
Fig. 5.1: Example an unterminated boost converter represented as a four-terminal model.

APPENDIX A FUNCTIONS USED

FAST FOURIER TRANSFORM (FFT)

Various factors need to be considered for accurate FFT results. First, an adequately large sampling frequency needs to be used; in other words, a small enough time step in the time data is needed. The Nyquist criterion states that to avoid aliasing, the maximum frequency attainable is half the sampling frequency of the time domain data [70], as shown in (A-1). Although this is the limit to achieve real data, the results at frequencies close to the Nyquist frequency can have large errors [71]. For this reason, the sampling frequency is chosen to be 10 times the maximum frequency desired. In this paper the maximum frequency investigated is 100 MHz; therefore, the sampling frequency is $\geq$1 GHz.

$$f_{max} = \frac{1}{2 \cdot t_s} = \frac{1}{2} f_s \qquad\qquad \text{(A-1)}$$

Another consideration for creating a model is the frequency resolution of the transformed data set. The finer the frequency step, f_{step}, the more accurate the frequencies of interest can be determined. Since the range of frequency is quite large (100 kHz – 100 MHz), it will become too computationally intensive if the frequency step is too small. Therefore, a frequency step needs to adequately large (for example $\geq$ 1 kHz). The frequency step is determined by the total time, T_{total}, used in the FFT calculation. Equation (A-2) defines the frequency step and total time relationship.

$$f_{step} = \frac{1}{T_{total}} \qquad\qquad \text{(A-2)}$$

An additional factor to take into account is to have the number of periods be an integer. This may affect the total time of the data used, and likewise the frequency step. In fact, if one period is used then f_{step} will be equal to the switching frequency of the system and the FFT will create an envelope of the frequency spectrum. As more periods are used the noise floor of the FFT may be reduced by an 'averaging' of all periods during the FFT calculations. When the number of periods used in the FFT is not an integer, leakage occurs. A result of leakage is that the noise floor is increased drastically; likewise the signal-to-noise ratio is derogated. Leakage can be reduced with certain windowing techniques. For simulated data or when one period is measured, a rectangular window works best, since it is trivial to produce a periodic data set. For measured

data, however, a more complex windowing such as a Hanning window [70] might be needed when many periods are captured.

A final concern is the bit resolution of the time domain data. If there are not a significant number of bits for the input to the FFT calculation, the noise floor will increase, again, hurting the signal-to-noise ratio. Time-domain simulation data, in general, is capable of providing a large enough bit resolution for a superior signal-to-noise ratio. Measurements, however, may not be able to provide enough significant bits, and the data could be lost in the noise; this is also referred to as quantization error.

The FFT calculation has inherent error as well. Through the nature of reducing integrals to finite summations, the error will increase as the frequency approaches the Nyquist frequency. For the parameters used in this paper ($f_s = 1\ GHz$ and $T_{total} = 1\ ms$) the inherent error of the FFT function is illustrated in Fig. A.1 [71].
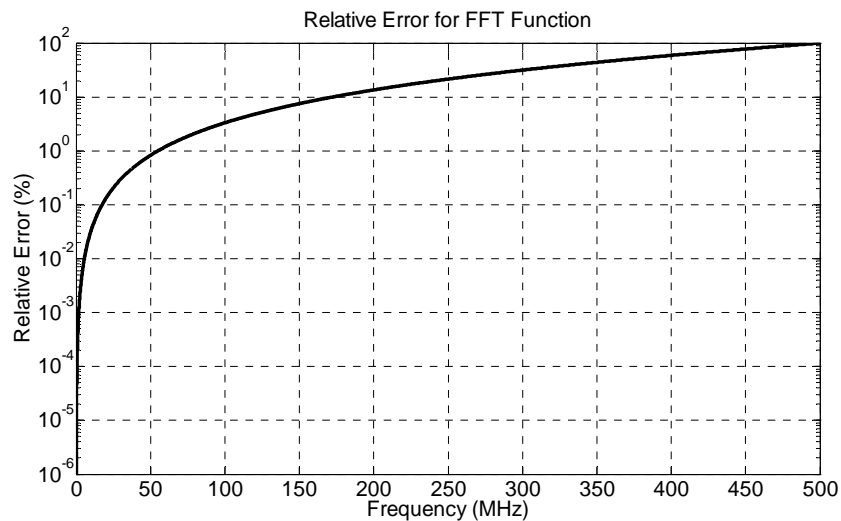
Fig. A.1: Inherent relative error in the FFT function [71].

LEAST SQUARES

TABLE III outlines three different functions available. With the use of *lsqnonlin* many if not all attenuation schemes can be used, and the minimum least square error (L2 norm) for all equations will determine the solution of the 5 unknown parameters. For most examples in this study five total sets of equations were used: nominal, the attenuation example shown in Fig. 2.8 and all three possibilities with one shunt impedance.

The FFT produces complex numbers that define magnitude and phase of the time-domain waveform at various frequency points. Using *lsqnonlin* with complex numbers directly is not advised. The least square approximation calculates the first and second gradient to assist in the iterative process, since the gradient of a complex number is not well defined each equation in the system is divided into two equations: one defining the real and another the imaginary components. From the 5 sets of measurements, 10 complex equations are obtained, creating 20 equations that *lsqnonlin* solves simultaneously.

In order to solve an iterative process an initial condition is needed. Since the solution from three conditions is typically close, it is an easy and accurate starting point for the *lsqnonlin* function to use. In general, it was found that the three best conditions to use are the nominal case, shunt impedance between positive and ground, and then a shunt impedance between negative and ground. The convergence rate and error of *lsqnonlin* are user controlled, as expected the smaller the error the longer the time needed to solve the system.

The inherent characteristics of a power converter has a fundamental switching frequency from which the noise is produced, only the fundamental and every harmonic of the fundamental (up to 100 MHz) is needed. All the other frequency data between the harmonics are practically zero and can be ignored. Once the fundamental frequency is obtain, either by inspection or a search routine, the complex value of the terminal voltages can be found for each harmonic of the fundamental. With a 400 kHz switching frequency, for example, there are only 250 points of interest in the desired frequency range; allowing the system to be solved in minutes.

TABLE III.
DIFFERENT FUNCTIONS IN MATLAB FOR SOLVING SYSTEMS OF EQUATIONS.

	Backslash, /	*fsolve*	*lsqnonlin*
Linear	✓	✓	✓
Non-linear		✓	✓
Well defined	✓	✓	✓
Over determined	✓		✓

APPENDIX B MODEL CODE (MATLAB M-FILES)

INPUT DATA AND CREATE FFT

```
Data=dlmread('filename.txt',',',1,0);
Datasize=length(Data(:,1));
Total_time=Data(Datasize,1)-Data(1,1);
%%%%%%%%%%%%%%%%%%%%%%%%%%%%%%%%%%%%%%%%%%%%%%%%%%%%%%%%%%%%%%%%%%%%%%%%%%%%
% Defines the frequency array based on the time domain sampling data

f_sample=(Datasize-1)/(Total_time);
f=transpose((0:f_sample/Datasize:f_sample));
f(Datasize+1)=[];


%%%%%%%%%%%%%%%%%%%%%%%%%%%%%%%%%%%%%%%%%%%%%%%%%%%%%%%%%%%%%%%%%%%%%%%%%%%%
% Perform an FFT to the data set

% w=1; % Rectangular windowing
w=(0.53836-0.46164*cos(2*pi*Data(:,1)/(Data(Datasize,1)-Data(1,1))))/0.54;
   %Hamming Window

% Only one condition is shown
Vpg(:,1)=fft(Data(:,2).*w,Datasize)/Datasize;%+1e-8;
Vng(:,1)=fft(Data(:,3).*w,Datasize)/Datasize;%+1e-8;
```

ENVELOPE OF FFT

```
%%%%%%%%%%%%%%%%%%%%%%%%%%%%%%%%%%%%%%%%%%%%%%%%%%%%%%%%%%%%%%%%%%%%%%%%%%%%
% Create the envelope of each frequency response data (knowing the fundamental
   frequency)

fundamental_freq=100e3;
FFT_step_freq=round(f(2));
envelope_step_freq=fundamental_freq/FFT_step_freq; % Step every harmonic of
   the fundamental frequency, with points spaced by FFT function
envelope_end_freq=100e6/FFT_step_freq+1; %End at 100 MHz

fnew(1,1)=f(1);
Vpgnew(1,:)=Vpg(1,:);
Vngnew(1,:)=Vng(1,:);

peak_window=floor(envelope_step_freq/2);
count=2;
for            i=harmonics*envelope_step_freq+1:harmonics*envelope_step_freq
   :envelope_end_freq
    fnew(count,1)=f(i);
    Vpgnew(count,:)=max(Vpg(i-peak_window:i+peak_window,:));
    Vngnew(count,:)=max(Vng(i-peak_window:i+peak_window,:));
    count=count+1;
end
```

SOLVING SOLUTION

```
% Nominal condition - Vpgnew(:,1) & Vngnew(:,1), uses both equations
% Attenuated across P & G - Vpgnew(:,3) & Vngnew(:,3), uses both equations
% Attenuated across N & G - Vpgnew(:,4) & Vngnew(:,4), uses only one of the
   equations that define the system, negative loop (N-G)
% Used as an initial condition for the solution


Zpgnew=-(-Vngnew(:,4).*Vpgnew(:,1).^2+Vpgnew(:,1).^2.*Vngnew(:,3)-
   Vngnew(:,1).*Vpgnew(:,3).*Vpgnew(:,1)-Vngnew(:,3).*Vpgnew(:,3).*
   Vpgnew(:,1)+Vpgnew(:,4).*Vngnew(:,1).*Vpgnew(:,1)+2.*Vngnew(:,4).*Vpgnew(:,
   3).*Vpgnew(:,1)-Vpgnew(:,1).*Vngnew(:,3).*Vpgnew(:,4)-Vpgnew(:,3).^2.*
   Vngnew(:,4)+Vpgnew(:,4).*Vngnew(:,3).*Vpgnew(:,3)+Vpgnew(:,3).^2.*Vngnew(:,
   1)-Vngnew(:,1).*Vpgnew(:,3).*Vpgnew(:,4)).*          Zshuntn_2new(:,1).*
   Zlisnpnew(:,1).*Zshuntp_1new(:,1)./(Zshuntn_2new(:,1).*Zshuntp_1new(:,1).*V
   pgnew(:,1).^2.*Vngnew(:,3)-Vpgnew(:,1).^2.*Zshuntn_2new(:,1).*
   Zshuntp_1new(:,1).*Vngnew(:,4)-Vpgnew(:,1).*Zlisnpnew(:,1).*Z
   shuntp_1new(:,1).*Vngnew(:,3).*Vngnew(:,4)+2.*Vpgnew(:,1).*
   Zshuntn_2new(:,1).*Zshuntp_1new(:,1).*Vngnew(:,4).*Vpgnew(:,3)-
   Zshuntn_2new(:,1).*          Zshuntp_1new(:,1).*Vngnew(:,3).*Vpgnew(:,1).*
   Vngnew(:,3)-Zshuntn_2new(:,1).*Zshuntp_1new(:,1).*Vpgnew(:,3).*
   Vpgnew(:,1).*Vngnew(:,1)+Vpgnew(:,1).*Zlisnpnew(:,1).*Zshuntp_1new(:,1).*
   Vngnew(:,1).*Vngnew(:,4)+Vpgnew(:,1).*Vngnew(:,4).*Zshuntn_2new(:,1).*Zlisn
   pnew(:,1).*Vpgnew(:,3)-Zshuntn_2new(:,1).*Zlisnpnew(:,1).*Vpgnew(:,3).*
   Vpgnew(:,1).*Vngnew(:,3)+Vpgnew(:,1).*Zshuntn_2new(:,1).*Zshuntp_1new(:,1).
   *Vpgnew(:,4).*Vngnew(:,1)-Vpgnew(:,1).*Zshuntn_2new(:,1).*
   Zshuntp_1new(:,1).*Vpgnew(:,4).*Vngnew(:,3)+Vpgnew(:,4).*
   Zshuntn_2new(:,1).*Zlisnpnew(:,1).*Vpgnew(:,3).*Vngnew(:,3)-Vpgnew(:,4).*
   Zshuntn_2new(:,1).*Zlisnpnew(:,1).*Vngnew(:,1).*Vpgnew(:,3)+
   Zshuntp_1new(:,1).*Vngnew(:,3).*Zlisnpnew(:,1).*Vngnew(:,4).*Vpgnew(:,3)+
   2.*Zlisnpnew(:,1).*Zshuntp_1new(:,1).*Vngnew(:,3).*Vngnew(:,1).*Vngnew(:,4)
   -Zlisnpnew(:,1).*Zshuntp_1new(:,1).*Vngnew(:,1).*Vngnew(:,4).*Vpgnew(:,3)+
   Zshuntn_2new(:,1).*Zshuntp_1new(:,1).*Vpgnew(:,3).*Vpgnew(:,4).*Vngnew(:,3)
   -Zshuntn_2new(:,1).*Zshuntp_1new(:,1).*Vpgnew(:,3).*Vpgnew(:,4).*
   Vngnew(:,1)-Zshuntn_2new(:,1).*Zlisnpnew(:,1).*Vpgnew(:,3).^2.*Vngnew(:,4)-
   Zlisnpnew(:,1).*Zshuntp_1new(:,1).*Vngnew(:,3).^2.*Vngnew(:,4)-
   Zshuntn_2new(:,1).*Zshuntp_1new(:,1).*Vpgnew(:,3).^2.*Vngnew(:,4)-
   Zlisnpnew(:,1).*Zshuntp_1new(:,1).*Vngnew(:,1).^2.*Vngnew(:,4)+
   Zshuntn_2new(:,1).*Zlisnpnew(:,1).*Vpgnew(:,3).^2.*Vngnew(:,1)+
   Zshuntn_2new(:,1).*Zshuntp_1new(:,1).*Vpgnew(:,3).^2.*Vngnew(:,1));
```

```
Zngnew=Zshuntn_2new(:,1).*Zlisnnnew(:,1).*(Vpgnew(:,1).*Vngnew(:,3)+Vpgnew(:,4
   ).*Vngnew(:,1)-Vpgnew(:,4).*Vngnew(:,3)-Vngnew(:,1).*Vpgnew(:,3)-
   Vngnew(:,4).*Vpgnew(:,1)+Vngnew(:,4).*Vpgnew(:,3))./(-Zshuntn_2new(:,1).*
   Vngnew(:,1).*Vpgnew(:,4)+Zshuntn_2new(:,1).*Vpgnew(:,4).*Vngnew(:,3)+Zshunt
   n_2new(:,1).*Vngnew(:,1).*Vpgnew(:,3)+Vngnew(:,4).*Zlisnnnew(:,1).*Vpgnew(:
   ,1)-Vngnew(:,4).*Zlisnnnew(:,1).*Vngnew(:,1)-Vngnew(:,4).*Zlisnnnew(:,1).*
   Vpgnew(:,3)+Vngnew(:,4).*Zlisnnnew(:,1).*Vngnew(:,3)+Vngnew(:,4).*
   Zshuntn_2new(:,1).*Vpgnew(:,1)-Vngnew(:,4).*Zshuntn_2new(:,1).*Vpgnew(:,3)-
   Zshuntn_2new(:,1).*Vpgnew(:,1).*Vngnew(:,3));

Zpnnew=Zshuntn_2new(:,1).*(Vpgnew(:,1).*Vngnew(:,3)+Vpgnew(:,4).*Vngnew(:,1)-
   Vpgnew(:,4).*Vngnew(:,3)-Vngnew(:,1).*Vpgnew(:,3)-Vngnew(:,4).*Vpgnew(:,1)+
   Vngnew(:,4).*Vpgnew(:,3))./(-Vngnew(:,3)+Vngnew(:,1))./Vngnew(:,4);


Ipgnew=-1./Zshuntn_2new(:,1).*(-
   Zshuntn_2new(:,1).*Vpgnew(:,1).^2.*Vpgnew(:,3).*Vngnew(:,3)+
   Zshuntn_2new(:,1).*Vpgnew(:,1).^2.*Vngnew(:,4).*Vpgnew(:,3)-Vpgnew(:,1).*
   Zshuntp_1new(:,1).*Vngnew(:,3).^2.*Vngnew(:,4)+Vpgnew(:,1).*
   Zshuntp_1new(:,1).*Vngnew(:,3).*Vngnew(:,1).*Vngnew(:,4)+Zshuntn_2new(:,1).
   *Vpgnew(:,1).*Vpgnew(:,3).*Vpgnew(:,4).*Vngnew(:,3)-Zshuntn_2new(:,1).*
   Vpgnew(:,1).*Vpgnew(:,3).*Vpgnew(:,4).*Vngnew(:,1)+Zshuntn_2new(:,1).*
   Vpgnew(:,1).*Vpgnew(:,3).^2.*Vngnew(:,1)-Zshuntn_2new(:,1).*Vpgnew(:,1).*
   Vpgnew(:,3).^2.*Vngnew(:,4)+Vngnew(:,1).*Zshuntp_1new(:,1).*Vngnew(:,3).*
   Vngnew(:,4).*Vpgnew(:,3)-Zshuntp_1new(:,1).*Vpgnew(:,3).*     Vngnew(:,4).*
   Vngnew(:,1).^2)./(Vpgnew(:,1).*Vngnew(:,3)+Vpgnew(:,4).*Vngnew(:,1)-
   Vpgnew(:,4).*Vngnew(:,3)-Vngnew(:,1).*Vpgnew(:,3)-Vngnew(:,4).*Vpgnew(:,1)+
   Vngnew(:,4).* Vpgnew(:,3))./Zshuntp_1new(:,1)./(Vpgnew(:,1)-Vpgnew(:,3));

Ingnew=-1./Zshuntn_2new(:,1).*Vngnew(:,4).*(-Vngnew(:,1).*Vpgnew(:,3)+
   Vpgnew(:,1).*Vngnew(:,3))./(Vpgnew(:,1).*Vngnew(:,3)+Vpgnew(:,4).*
   Vngnew(:,1)-Vpgnew(:,4).*Vngnew(:,3)-Vngnew(:,1).*Vpgnew(:,3)-
   Vngnew(:,4).*Vpgnew(:,1)+ Vngnew(:,4).*Vpgnew(:,3));
```

LEAST SQUARES

```
tempsolution=zeros(5,length(fnew)-1);


for i=2:length(fnew)
    [xtemp,resnorm,residual,exitflag,output] =
        lsqnonlin(@myfun_r_i_dif_Zlisn,[real(Zpgnew(i))          imag(Zpgnew(i))
        real(Zngnew(i))    imag(Zngnew(i))    real(Zpnnew(i))    imag(Zpnnew(i))
        real(Ipgnew(i))    imag(Ipgnew(i))    real(Ingnew(i))    imag(Ingnew(i))],
        [],[],optimset('MaxFunEvals',5000,'TolFun',1e-10,'TolX',1e-10,
        'MaxIter',5000),real(Vpgnew(i,:)),imag(Vpgnew(i,:)),real(Vngnew(i,:))
        ,imag(Vngnew(i,:)),real(Zlisnpnew(i,:)),imag(Zlisnpnew(i,:)),real(Zli
        snnnew(i,:)),imag(Zlisnnnew(i,:)),real(Zshuntxnew(i,1)),imag(Zshuntxn
        ew(i,1)),real(Zshuntp_1new(i,1)),imag(Zshuntp_1new(i,1)),real(Zshuntn
        _1new(i,1)),imag(Zshuntn_1new(i,1)),real(Zshuntp_2new(i,1)),imag(Zshu
        ntp_2new(i,1)),real(Zshuntn_2new(i,1)),imag(Zshuntn_2new(i,1)));
    tempsolution(:,i-1)=[complex(xtemp(1),xtemp(2))
                        complex(xtemp(3),xtemp(4))
                        complex(xtemp(5),xtemp(6))
                        complex(xtemp(7),xtemp(8))
                        complex(xtemp(9),xtemp(10))];
    Freq_pts_left=length(fnew)-i
end
%%%%%%%%%%%%%%%%%%%%%%%%%%%%%%%%%%%%%%%%%%%%%%%%%%%%%%%%%%%%%%%%%%
function   F   =   myfun(x,Vpg_r,Vpg_i,Vng_r,Vng_i,Zlisnp_r,Zlisnp_i,Zlisnn_r,
   Zlisnn_i,Zshuntp_1_r,Zshuntp_1_i,Zshuntn_1_r,Zshuntn_1_i,Zshuntp_2_r,
   Zshuntp_2_i,Zshuntn_2_r,Zshuntn_2_i)


% The function 'F' is equal to the equations of the nodal equations of each
   nominal and attenuated condition.  Additionally, the real and imaginary
   portion of each equation is separated.  The equations are not shown here
   due to their complexity.
```

Z-PARAMETER FILTER MATRIX

```
R=50;

A13=dlmread(A13.txt','\t',[15 0 415 1]);
A13(:,3)=dlmread(A13.txt','\t',[429 1 829 1]);
Z11=dlmread(Z11.txt','\t',[21 0 421 1]);
Z11(:,3)=dlmread(Z11.txt','\t',[428 1 828 1]);
Z44=dlmread(Z44.txt','\t',[21 0 421 1]);
Z44(:,3)=dlmread(Z44.txt','\t',[428 1 828 1]);

Z11_CM=dlmread(Z11_CM.txt','\t',[21 0 421 1]);
Z11_CM(:,3)=dlmread(Z11_CM.txt','\t',[428 1 828 1]);
Z22_CM=dlmread(Z22_CM.txt','\t',[21 0 421 1]);
Z22_CM(:,3)=dlmread(Z22_CM.txt','\t',[428 1 828 1]);
IG_CM=dlmread(IG_CM.txt','\t',[15 0 415 1]);
IG_CM(:,3)=dlmread(IG_CM.txt','\t',[429 1 829 1]);

Z11_DM=dlmread(Z_IN.txt','\t',[21 0 421 1]);
Z11_DM(:,3)=dlmread(Z_IN.txt','\t',[428 1 828 1]);
Z22_DM=dlmread(Z_OUT.txt','\t',[21 0 421 1]);
Z22_DM(:,3)=dlmread(Z_OUT.txt','\t',[428 1 828 1]);
IG_DM=dlmread(IG_DM.txt','\t',[15 0 415 1]);
IG_DM(:,3)=dlmread(IG_DM.txt','\t',[429 1 829 1]);

Freq_ind=find(1e3<=Z11(:,1) & Z11(:,1)<=1e8);
Frequency=Z11(Freq_ind,1);

Z_IN=1./vec2complex(Z_IN(Freq_ind,2),Z_IN(Freq_ind,3));
Z_OUT=1./vec2complex(Z_OUT(Freq_ind,2),Z_OUT(Freq_ind,3));
Z_CM=2*vec2complex(Z_CM(Freq_ind,2),Z_CM(Freq_ind,3));
Z_DM=2*vec2complex(Z_DM(Freq_ind,2),Z_DM(Freq_ind,3));

Z11_CM=vec2complex(Z11_CM(Freq_ind,2),Z11_CM(Freq_ind,3)*pi/180);
Z22_CM=vec2complex(Z22_CM(Freq_ind,2),Z22_CM(Freq_ind,3)*pi/180);
IG_CM=vec2complex(10.^(IG_CM(Freq_ind,2)/20),IG_CM(Freq_ind,3)*pi/180);
IG_CM_low=find(real(IG_CM)<=0); IG_CM_up=find(real(IG_CM)>0);
Z12_CM(IG_CM_low)=-R./IG_CM(IG_CM_low)-sqrt((R./IG_CM(IG_CM_low)).^2+R.^2+R.*
    (Z11_CM(IG_CM_low)+Z22_CM(IG_CM_low))+Z11_CM(IG_CM_low).*Z22_CM(IG_CM_low));
Z12_CM(IG_CM_up)=-R./IG_CM(IG_CM_up)+sqrt((R./IG_CM(IG_CM_up)).^2+R.^2+R.*
    (Z11_CM(IG_CM_up)+Z22_CM(IG_CM_up))+Z11_CM(IG_CM_up).*Z22_CM(IG_CM_up));
Z12_CM=transpose(Z12_CM);
```

```
Z11_DM=vec2complex(Z11_DM(Freq_ind,2),Z11_DM(Freq_ind,3)*pi/180);
Z22_DM=vec2complex(Z22_DM(Freq_ind,2),Z22_DM(Freq_ind,3)*pi/180);
IG_DM=vec2complex(10.^(IG_DM(Freq_ind,2)/20),IG_DM(Freq_ind,3)*pi/180);
IG_DM_low=find(real(IG_DM)<=0); IG_DM_up=find(real(IG_DM)>0);
Z12_DM(IG_DM_low)=-R./IG_DM(IG_DM_low)-sqrt((R./IG_DM(IG_DM_low)).^2+R.^2+R.*
   (Z11_DM(IG_DM_low)+Z22_DM(IG_DM_low))+Z11_DM(IG_DM_low).*Z22_DM(IG_DM_low));
Z12_DM(IG_DM_up)=-R./IG_DM(IG_DM_up)+sqrt((R./IG_DM(IG_DM_up)).^2+R.^2+R.*
   (Z11_DM(IG_DM_up)+Z22_DM(IG_DM_up))+Z11_DM(IG_DM_up).*Z22_DM(IG_DM_up));
Z12_DM=transpose(Z12_DM);

A13=vec2complex(10.^(A13(Freq_ind,2)/20),A13(Freq_ind,3)*pi/180);
A13_low=find(real(A13)<=0); A13_up=find(real(A13)>0);
Z11=vec2complex(Z11(Freq_ind,2),Z11(Freq_ind,3)*pi/180);
Z44=vec2complex(Z44(Freq_ind,2),Z44(Freq_ind,3)*pi/180);

Z22=(2.*sqrt(Z11_DM).*(Z11-Z11_CM).^1.5+Z11.^2+Z11.*(Z11_DM-Z11_CM)-Z11_CM.*
   Z11_DM)./(Z11-Z11_CM);
Z33_low=find(imag(Z22_DM)<=0); Z33_up=find(imag(Z22_DM)>0);
Z33(Z33_low)=2.*sqrt(Z22_CM(Z33_low)-Z44(Z33_low)).*sqrt(-Z22_DM(Z33_low))+
   Z22_DM(Z33_low)+Z44(Z33_low);
Z33(Z33_up)=-2.*sqrt(Z22_CM(Z33_up)-Z44(Z33_up)).*sqrt(-Z22_DM(Z33_up))+
   Z22_DM(Z33_up)+Z44(Z33_up);
Z33=transpose(Z33);

Z13(A13_low)=-Ro./A13(A13_low)-sqrt((Ro./A13(A13_low)).^2+Ro.*Ri+
   Ro.*Z11(A13_low)+Ri.*Z33(A13_low)+Z11(A13_low).*Z33(A13_low));
Z13(A13_up)=-Ro./A13(A13_up)+sqrt((Ro./A13(A13_up)).^2+Ro.*Ri+
   Ro.*Z11(A13_up)+Ri.*Z33(A13_up)+Z11(A13_up).*Z33(A13_up));
Z13=transpose(Z13);

Z12=sqrt(Z11_DM).*sqrt(Z11-Z11_CM)+Z11;
Z34(Z33_low)=sqrt(Z22_CM(Z33_low)-Z44(Z33_low)).*sqrt(-Z22_DM(Z33_low))+
   Z44(Z33_low);
Z34(Z33_up)=-sqrt(Z22_CM(Z33_up)-Z44(Z33_up)).*sqrt(-Z22_DM(Z33_up))+
   Z44(Z33_up);
Z34=transpose(Z34);
Z14=(Z12_CM.*(Z33-2.*Z34+Z44)+Z13.*(Z34-Z44))./(Z33-Z34);
Z24=(Z12_CM.*(Z33-2.*Z34+Z44)+(Z12_DM-Z13+Z14).*(Z44-Z34))./(Z33-2*Z34+Z44);
Z23=(Z12_CM.*(Z33-2.*Z34+Z44)+(Z12_DM-Z13+Z14).*(Z34-Z33))./(Z33-2*Z34+Z44);
```

PARTITIONING AND MODIFICATIONS FOR AC OPERATIONS

```
function Data=Time_partition(partitions,Nominal,APN,duty,commutation,modify)
%Time_partition(partitions,Datasize,Nominal,APN,duty,commutation, modify)
%
% duty is a duty cycle vector for the data used
%     Use duty=1 to automatically solve for the duty cycle vector
%
% Center aligned...commutation=1
% Edge aligned...commutation=0
%
% no data manipulation...modify=0
% alpha manipulation...modify=1
% beta manipulation...modify=2
if commutation~=1 & modify~=0
    display('ERROR:  Modification  are  only  valid  for  center  aligned
  commutations')
    Data=pi;
    return
end
if duty==1
    duty=zeros(1,1666);
    for i=0:1665
        X=find(Nominal(1+5000*i:5000*(i+1)-2500)==
            max(Nominal(1+5000*i:5000*(i+1)-2500)));
        Y=find(Nominal(1+5000*i+2500:5000*(i+1))==
            max(Nominal(1+5000*i+2500:5000*(i+1))));
        duty(i+1)=(Y+2500-X)*2e-9/10e-6;
    end
end

Datasize=length(Nominal(:,1));
off_fact=0;
switch partitions
    case 8
        Data=zeros(Datasize,2);
        for j=105:208:1561;     %8 partitions linearly divided
            if j==105
                for i=j-104:j+104
                    dif=floor((duty(i)-duty(j))*10e-6/(2*2e-9));
                    if modify==0
                        Data(5000*(i-1)+1:5000*i,1)=Nominal(5000*(j-1)+1+
                            commutation* 1388:5000*j,:);
```

```
                Data(5000*(i-1)+1:5000*i,2)=APN(5000*(j-1)+1+
                        commutation* 1388:5000*j,:);
        elseif modify==1
                Data(5000*(i-1)+1:5000*i-2500-dif,1)=Nominal(5000*(j-
                        1)+1+dif:5000*j-2500,:);
                Data(5000*(i-1)+1+2500+dif:5000*i,1)=Nominal(5000*(j-
                        1)+1+2500:5000*j-dif,:);
                Data(5000*(i-1)+1:5000*i-2500-dif,2)=APN(5000*(j-
                        1)+1+dif:5000*j-2500,:);
                Data(5000*(i-1)+1+2500+dif:5000*i,2)=APN(5000*(j-
                        1)+1+2500:5000*j-dif,:);
        elseif modify==2
                Data(5000*(i-1)+1:5000*i-dif,1)=Nominal(5000*(j-
                        1)+1+dif:5000*j,:);
                Data(5000*i-dif+1:5000*i,1)=Nominal(5000*(j-
                        1)+1:5000*(j-1)+dif,:);
                Data(5000*(i-1)+1:5000*i-dif,2)=APN(5000*(j-
                        1)+1+dif:5000*j,:);
                Data(5000*i-dif+1:5000*i,2)=
                        APN(5000*(j-1)+1:5000*(j-1)+dif,:);
        end
    end
elseif j==1561
    for i=j-103:j+105
        dif=floor((duty(i)-duty(j))*10e-6/(2*2e-9));
        if modify==0
                Data(5000*(i-1)+1:5000*i,1)=Nominal(5000*(j-
                        1)+1:5000*j,:);
                Data(5000*(i-1)+1:5000*i,2)=
                        APN(5000*(j-1)+1:5000*j,:);
        elseif modify==1
                Data(5000*(i-1)+1:5000*i-2500-dif,1)=Nominal(5000*(j-
                        1)+1+dif:5000*j-2500,:);
                Data(5000*(i-1)+1+2500+dif:5000*i,1)=Nominal(5000*(j-
                        1)+1+2500:5000*j-dif,:);
                Data(5000*(i-1)+1:5000*i-2500-dif,2)=APN(5000*(j-
                        1)+1+dif:5000*j-2500,:);
                Data(5000*(i-1)+1+2500+dif:5000*i,2)=APN(5000*(j-
                        1)+1+2500:5000*j-dif,:);
        elseif modify==2
                Data(5000*(i-1)+1:5000*i-dif,1)=Nominal(5000*(j-
                        1)+1+dif:5000*j,:);
```

117

```
                            Data(5000*i-dif+1:5000*i,1)=Nominal(5000*(j-
                                    1)+1:5000*(j-1)+dif,:);
                            Data(5000*(i-1)+1:5000*i-dif,2)=APN(5000*(j-
                                    1)+1+dif:5000*j,:);
                            Data(5000*i-dif+1:5000*i,2)=
                                    APN(5000*(j-1)+1:5000*(j-1)+dif,:);
                    end
              end
          else
              for i=j-103:j+104
                  dif=floor((duty(i)-duty(j))*10e-6/(2*2e-9));
                  if modify==0
                      Data(5000*(i-1)+1:5000*i,1)=Nominal(5000*(j-
                              1)+1:5000*j,:);
                      Data(5000*(i-1)+1:5000*i,2)=
                              APN(5000*(j-1)+1:5000*j,:);
                  elseif modify==1
                      Data(5000*(i-1)+1:5000*i-2500-dif,1)=Nominal(5000*(j-
                              1)+1+dif:5000*j-2500,:);
                      Data(5000*(i-1)+1+2500+dif:5000*i,1)=Nominal(5000*(j-
                              1)+1+2500:5000*j-dif,:);
                      Data(5000*(i-1)+1:5000*i-2500-dif,2)=APN(5000*(j-
                              1)+1+dif:5000*j-2500,:);
                      Data(5000*(i-1)+1+2500+dif:5000*i,2)=APN(5000*(j-
                              1)+1+2500:5000*j-dif,:);
                  elseif modify==2
                      Data(5000*(i-1)+1:5000*i-dif,1)=Nominal(5000*(j-
                              1)+1+dif:5000*j,:);
                      Data(5000*i-dif+1:5000*i,1)=Nominal(5000*(j-
                              1)+1:5000*(j-1)+dif,:);
                      Data(5000*(i-1)+1:5000*i-dif,2)=APN(5000*(j-
                              1)+1+dif:5000*j,:);
                      Data(5000*i-dif+1:5000*i,2)=
                              APN(5000*(j-1)+1:5000*(j-1)+dif,:);
                  end
              end
          end
      end
  case 16
      Data=zeros(Datasize,2);
      for j=53:104:1613;        %16 partitions linearly divided
          if j==53
              for i=j-52:j+52
```

```
                dif=floor((duty(i)-duty(j))*10e-6/(2*2e-9));
                if modify==0
                    Data(5000*(i-1)+1:5000*i,1)=Nominal(5000*(j-
                            1)+1:5000*j,:);
                    Data(5000*(i-1)+1:5000*i,2)=
                            APN(5000*(j-1)+1:5000*j,:);
                elseif modify==1
                    Data(5000*(i-1)+1:5000*i-2500-dif,1)=Nominal(5000*(j-
                            1)+1+dif:5000*j-2500,:);
                    Data(5000*(i-1)+1+2500+dif:5000*i,1)=Nominal(5000*(j-
                            1)+1+2500:5000*j-dif,:);
                    Data(5000*(i-1)+1:5000*i-2500-dif,2)=APN(5000*(j-
                            1)+1+dif:5000*j-2500,:);
                    Data(5000*(i-1)+1+2500+dif:5000*i,2)=APN(5000*(j-
                            1)+1+2500:5000*j-dif,:);
                elseif modify==2
                    Data(5000*(i-1)+1:5000*i-dif,1)=Nominal(5000*(j-
                            1)+1+dif:5000*j,:);
                    Data(5000*i-dif+1:5000*i,1)=Nominal(5000*(j-
                            1)+1:5000*(j-1)+dif,:);
                    Data(5000*(i-1)+1:5000*i-dif,2)=APN(5000*(j-
                            1)+1+dif:5000*j,:);
                    Data(5000*i-dif+1:5000*i,2)=
                            APN(5000*(j-1)+1:5000*(j-1)+dif,:);
                end
            end
        elseif j==1613
            for i=j-51:j+53
                dif=floor((duty(i)-duty(j))*10e-6/(2*2e-9));
                if modify==0
                    Data(5000*(i-1)+1:5000*i,1)=Nominal(5000*(j-
                            1)+1:5000*j,:);
                    Data(5000*(i-1)+1:5000*i,2)=APN(5000*(j-
                            1)+1:5000*j,:);
                elseif modify==1
                    Data(5000*(i-1)+1:5000*i-2500-dif,1)=Nominal(5000*(j-
                            1)+1+dif:5000*j-2500,:);
                    Data(5000*(i-1)+1+2500+dif:5000*i,1)=Nominal(5000*(j-
                            1)+1+2500:5000*j-dif,:);
                    Data(5000*(i-1)+1:5000*i-2500-dif,2)=APN(5000*(j-
                            1)+1+dif:5000*j-2500,:);
                    Data(5000*(i-1)+1+2500+dif:5000*i,2)=APN(5000*(j-
                            1)+1+2500:5000*j-dif,:);
```

```
            elseif modify==2
                Data(5000*(i-1)+1:5000*i-dif,1)=Nominal(5000*(j-
                        1)+1+dif:5000*j,:);
                Data(5000*i-dif+1:5000*i,1)=Nominal(5000*(j-
                        1)+1:5000*(j-1)+dif,:);
                Data(5000*(i-1)+1:5000*i-dif,2)=APN(5000*(j-
                        1)+1+dif:5000*j,:);
                Data(5000*i-dif+1:5000*i,2)=
                        APN(5000*(j-1)+1:5000*(j-1)+dif,:);
            end
        end
    else
        for i=j-51:j+52
            dif=floor((duty(i)-duty(j))*10e-6/(2*2e-9));
            if modify==0
                Data(5000*(i-1)+1:5000*i,1)=Nominal(5000*(j-
                        1)+1:5000*j,:);
                Data(5000*(i-1)+1:5000*i,2)=
                        APN(5000*(j-1)+1:5000*j,:);
            elseif modify==1
                Data(5000*(i-1)+1:5000*i-2500-dif,1)=Nominal(5000*(j-
                        1)+1+dif:5000*j-2500,:);
                Data(5000*(i-1)+1+2500+dif:5000*i,1)=Nominal(5000*(j-
                        1)+1+2500:5000*j-dif,:);
                Data(5000*(i-1)+1:5000*i-2500-dif,2)=APN(5000*(j-
                        1)+1+dif:5000*j-2500,:);
                Data(5000*(i-1)+1+2500+dif:5000*i,2)=APN(5000*(j-
                        1)+1+2500:5000*j-dif,:);
            elseif modify==2
                Data(5000*(i-1)+1:5000*i-dif,1)=Nominal(5000*(j-
                        1)+1+dif:5000*j,:);
                Data(5000*i-dif+1:5000*i,1)=Nominal(5000*(j-
                        1)+1:5000*(j-1)+dif,:);
                Data(5000*(i-1)+1:5000*i-dif,2)=APN(5000*(j-
                        1)+1+dif:5000*j,:);
                Data(5000*i-dif+1:5000*i,2)=
                        APN(5000*(j-1)+1:5000*(j-1)+dif,:);
            end
        end
    end
    end
    end
end
```

SYMMETRY FOR AC OPERATION

```
function Nominal_sym = Time_symmetry(Nominal,phases,sym)

% Time_symmetry(Data,phases,sym)
% First half copied to second half...sym=1
% First half mirrored to second half...sym=2
% 1st and 3rd quadrant mirrored to 2nd and 4th quandrant, respectively...sym=3

Nominal_sym=Nominal;
if phases==1
    if sym==1
        Nominal_sym(4165001:8330000)=Nominal(1:4165000);

    elseif sym==2
        for i=1:5000:5000*833
            Nominal_sym(5000*833+i:5000*833+i+4999)=
                    Nominal_sym(5000*833+2-5000-i:5000*833+1-i);
        end

    elseif sym==3
        for i=1:5000:5000*416
            Nominal_sym(5000*416+i:5000*416+i+4999)=
                    Nominal_sym(5000*416+2-5000-i:5000*416+1-i);
        end
        for i=5000*833+1:5000:5000*1249
            Nominal_sym(5000*1249+i:5000*1249+i+4999)=
                    Nominal_sym(5000*1249+2-5000-i:5000*1249+1-i);
        end
    end
end
```

REFERENCES

[1]   H. W. Ott, *Noise Reduction Techniques In Electronic Systems*, 2 ed. New York, NY: John Wiley & Sons, 1988.

[2]   R. Redl, "Power Electronics and Electromagnetic Compatibility," presented at the Power Electronics Specialists Conference, IEEE 27th Annual (PESC), Baveno, Italy, 1996.

[3]   International Special Committee on Radio Interference, "Information technology equipment – Radio disturbance characteristics – Limits and methods of measurement (CISPR 22)," 5 ed: International Electrotechinical Commission, 2005.

[4]   V. P. Kodali, *Engineering Electromagnetic Compatibility: Principles, Measurements, Technologies, and Computer Models*, 2 ed.: Wiley-IEEE Press, 2001.

[5]   US Department of Defense, "Requirement for the Control of Electromagnetic Interference Characteristics of Subsystems and Equipment," in *Military Standard 461E*, ed, 1999.

[6]   C. R. Paul and K. B. Hardin, "Diagnosis and Reduction of Conducted Noise Emissions," *Electromagnetic Compatibility, IEEE Transaction on,* vol. 30, pp. 553-560, November 1988.

[7]   M. C. Caponet, *et al.*, "EMI Filters Design for Power Electronics," presented at the Power Electronics Specialists Conference, IEEE 33rd Annual (PESC), Cairns, Qld., Australia, 2002.

[8]   Q. Zhaoming, *et al.*, "Status of electromagnetic compatibility research in power electronics," presented at the Power Electronics and Motion Control Conference Proceedings, The 3rd International (PIEMC), Beiging, China, 2000.

[9]   V. Vlatkovic, *et al.*, "Input Filter Design for Power Factor Correction Circuits," *Power Electronics, IEEE Transactions on,* vol. 11, pp. 199-205, 1996.

[10]   M. J. Nave, *Power Line Filter Design for Switch-Mode Power Supply*. New York: Van Nostrand Reinhild, 1991.

[11]   L. Ferraris and C.-Y. Wu, "EMI Shielding-Common Problems and Containment Strategies," presented at the Electromagnetic Compatibility Proceeding, IEEE International Symposium on (EMC), Beijing, China, 1997.

[12]   W. Xin, *et al.*, "A Study of Common Mode Noise in Switching Power Supply from a Current Balancing Viewpoint," presented at the Power Electronics and Drive Systems, IEEE International Conference on (PEDS), Hong Kong, 1999.

[13]   T. Broom and I. W. Hofsajer, "Some Origins and Mitigation of Conducted Common Mode EMI in Switching Converters," presented at the Africon Conference in Africa, George, South Africa, 2002.

[14]   D. Cochrane, *et al.*, "Passive Cancellation of Common-Mode Noise in Power Electronic Circuits," *Power Electronics, IEEE Transactions on,* vol. 18, pp. 756-763, 2003.

[15]   D. H. Liu, *et al.*, "A Systematic Approach to Analyze EMI in Control Circuit of Power Electronic Equipment," presented at the 16th Annual IEEE Applied Power Electronics Conference and Exposition (APEC), Anaheim, CA, 2001.

[16]   L. Rossetto, *et al.*, "Conducted EMI Issues in a Boost PFC Design," presented at the Telecommunications Energy Conference, 12th International (INTELEC), San Francisco, CA, 1998.

[17]   W. Zhang, *et al.*, "Conducted EMI Analysis of a Boost PFC Circuit," presented at the Applied Power Electronics Conference and Exposition, IEEE 12th Annual (APEC), Atlanta, GA, 1997.

[18]   K. N. Sakthivel, *et al.*, "Significance of critical components placement to control EMI in power supplies: A case study," presented at the International Conference on Electromagnetic Interference and Compatibility, Proceedings of the, 1999.

[19]   J. Z. Chen, *et al.*, "Electrical and Thermal Layout Design Considerations for Integrated Power Electronics Modules," presented at the Industry Applications Conference, IEEE 37th Annual (IAS), Pittsburgh, PA, 2002.

[20]   J.-L. Schanen, *et al.*, "Layout optimization to reduce EMI of a switched mode power supply," presented at the Power Electronics Specialists Conference, IEEE 33rd Annual (PESC), Cairns, Qld., Australia, 2002.

[21]   A. R. Hefner, Jr., "An Improved Understanding for the Transient Operation of the Power Insulated Gate Bipolar Transistor (IGBT)," *Power Electronics, IEEE Transactions on,* vol. 5, pp. 459-468, 1990.

[22]   H. Zhu, *et al.*, "Modeling-Based Examination of Conducted EMI Emissions from Hard- and Soft-Switching PWM Inverters," *Industry Applications, IEEE Transactions on,* vol. 37, pp. 1383-1393, 2001.

[23]   J.-S. Lai, *et al.*, "EMI Characterization and Simulation with Parasitic Models for a Low-Voltage High-Current AC Motor Drive," *Industry Applications, IEEE Transactions on,* vol. 40, pp. 178-185, 2004.

[24]   A. C. Baisden, *et al.*, "High Frequency Modeling of a Converter with an RF-EMI Filter," presented at the Industry Applications Conference, IEEE 41st Annual (IAS), Tampa, FL, 2006.

[25]   J. A. Ferreira, *Electromagnetic Modeling of Power Electronic Converters*. Boston: Kluwer, 1989.

[26]   J. A. Ferreira and S. J. Marais, "A New Approach to Model Component Parasitics," presented at the Industry Applications Conference, IEEE 30th Annual (IAS), Orlando, FL, 1995.

[27]   L. Zhao and J. D. van Wyk, "Electromagnetic modeling of an integrated RF EMI Filter," presented at the Industry Applications Conference, IEEE 38th Annual (IAS), Salt Lake City, UT, 2003.

[28]   R. Chen, *et al.*, "Integrated Transmission Line EMI Filter," presented at the International Conference on Integrated Power Electronic Systems (CIPS), Naples, Italy, 2006.

[29]   M. Kchikack, *et al.*, "Modeling and Simulation for Conducted Common-Mode Current in Switching Circuits," presented at the Electromagnetic Compatibility Proceeding, IEEE International Symposium on (EMC), Montreal, Que., Canada, 2001.

[30]   M. N. Gitau, "Modeling Conducted EMI Noise Generation and Propagation in Boost Converters," presented at the International Symposium on Industrial Electronics, IEEE (ISIE), Cholula, Puebla, Mexico, 2000.

[31]   H. M. Schlicke and H. Weidmann, "Compatible EMI Filters," *Electromagnetic Compatibility, IEEE Transaction on,* vol. 10, p. 223, 1968.

[32]   R. D. Middlebrook, "Input Filter Consideration in Design and Application of Switching Regulators," presented at the Industry Applications Conference, IEEE 14th Annual (IAS), 1979.

[33]   L. M. Schneider, "Noise Source Equivalent Circuit Model of Off-line Converters and its Use in Input Filter Design," in *International Conference on Power System Technology (POWERCON)*, 1982.

[34]   M. T. Zhang*, et al.*, "Characterization and analysis of electromagnetic interference in a high frequency AC distributed power system," presented at the Power Electronics Specialists Conference, 1996. PESC '96 Record., 27th Annual IEEE, 1996.

[35]   B. Revol*, et al.*, "EMI study of a three phase inverter-fed motor drives," presented at the Industry Applications Conference, 2004. 39th IAS Annual Meeting. Conference Record of the 2004 IEEE, 2004.

[36]   D. Zhang*, et al.*, "Measurement of noise source impedance of off-line converters," *Power Electronics, IEEE Transactions on,* vol. 15, pp. 820-825, 2000.

[37]   Q. Liu*, et al.*, "Modular-Terminal-Behavioral (MTB) Model for Characterizing Switching Module Conducted EMI Generation in Converter Systems," *Power Electronics, IEEE Transactions on,* vol. 21, pp. 1804-1814, 2006.

[38]   H. Chen*, et al.*, "Modeling and measurement of the impedance of common mode noise source of switching converters," presented at the Applied Power Electronics Conference and Exposition, 2006. APEC '06. Twenty-First Annual IEEE, 2006.

[39]   M. J. Nave, "The effect of duty cycle on SMPS common mode emissions: theory and experiment," in *Electromagnetic Compatibility, 1989. IEEE 1989 National Symposium on*, 1989, pp. 211-216.

[40]   Y.-K. Lo and T.-H. Song, "On approximating the frequency responses of the common-mode electromagnetic interference noise source," in *Power Electronics and Drive Systems, 2003. PEDS 2003. The Fifth International Conference on*, 2003, pp. 1320-1322 Vol.2.

[41]   X. Huang*, et al.*, "Three-phase inverter differential mode EMI modeling and prediction in frequency domain," in *Industry Applications Conference, 2003. 38th IAS Annual Meeting. Conference Record of the*, 2003, pp. 2048-2055 vol.3.

[42]   K. Y. See and J. Deng, "Measurement of noise source impedance of SMPS using a two probes approach," *Power Electronics, IEEE Transactions on,* vol. 19, pp. 862-868, 2004.

[43]   J. Meng*, et al.*, "Noise Source Lumped Circuit Modeling and Identification for Power Converters," *Industrial Electronics, IEEE Transactions on,* vol. 53, pp. 1853-1861, 2006.

[44]   L. Ran*, et al.*, "Conducted electromagnetic emissions in induction motor drive systems. I. Time domain analysis and identification of dominant modes," *Power Electronics, IEEE Transactions on,* vol. 13, pp. 757-767, 1998.

[45]   C. Chen, "Novel EMC debugging methodologies for high-power converters," in *Electromagnetic Compatibility, 2000. IEEE International Symposium on*, 2000, pp. 385-390 vol.1.

[46]   P. R. Mugur*, et al.*, "Power electronic converter EMC analysis through state variable approach techniques," *Electromagnetic Compatibility, IEEE Transactions on,* vol. 43, pp. 229-238, 2001.

[47]   E. Gubia*, et al.*, "Frequency domain model of conducted EMI in electrical drives," *Power Electronics Letters, IEEE,* vol. 3, pp. 45-49, 2005.

[48]   S. Brehaut*, et al.*, "A conducted EMI model for an industrial power supply full bridge," in *Power Electronics Specialists Conference, 2004. PESC 04. 2004 IEEE 35th Annual*, 2004, pp. 3227-3231 Vol.4.

[49]   H. Akagi and T. Shimizu, "Attenuation of Conducted EMI Emissions From an Inverter-Driven Motor," *Power Electronics, IEEE Transactions on,* vol. 23, pp. 282-290, 2008.

[50]   Q. Liu*, et al.*, "Frequency-domain EMI noise emission characterization of switching power modules in converter systems," presented at the Applied Power Electronics Conference and Exposition, IEEE 20th Annual (APEC), 2005.

[51]   Q. Liu*, et al.*, "Conducted EMI Noise Prediction and Characterization for Multi-phase-leg Converters Based on Modular-Terminal-Behavioral (MTB) Equivalent EMI Noise Source Model," presented at the Power Electronics Specialists Conference, IEEE 37th Annual (PESC), 2006.

[52]   Q. Liu, "Modular Approach for Characterizing and Modeling Conducted EMI Emissions in Power Converters," Ph.D, Electrical and Computer Engineering, Virginia Polytechnic Institute and State University, Blacksburg, Virginia, 2005.

[53]   Q. Liu*, et al.*, "Conducted-EMI Prediction for AC Converter Systems Using an Equivalent Modular-Terminal-Behavioral (MTB) Source Model," *Industry Applications, IEEE Transactions on,* vol. 43, pp. 1360-1370, 2007.

[54]   H. F. Mayer, "Ueber das Ersatzschema der Verstärkerröhre," *Telegraphen- und Fernsprech-technik,* vol. 15, pp. 335-337, 1926.

[55]   S. Abdelkader*, et al.*, "A Norton Equivalent Model for Nonlinear Loads," presented at the Power Engineering, Large Engineering Systems Conference on (LESCOPE), 2001.

[56]   E. Thunberg and L. Soder, "A Norton Approach to Distribution Network Modeling for Harmonic Studies," *Power Delivery, IEEE Transactions on,* vol. 14, pp. 272-277, 1999.

[57]   W. Xu*, et al.*, "A Multiphase Harmonic Load Flow Solution Technique," *Power Systems, IEEE Transactions on,* vol. 6, pp. 174-182, 1991.

[58]   G. Efthivoulidis, "Linear Switched-Capacitor Circuit Theorems," presented at the Circuits and Systems, IEEE International Symposium on (ISCAS), 2006.

[59]   M. Fauri, "Harmonic Modelling of Non-Linear Load by means of Crossed Frequency Admittance Matrix," *Power Systems, IEEE Transactions on,* vol. 12, pp. 1632-1638, 1997.

[60]   B. M. Grafov, "Langevin Dual Equation for Nonlinear Multiports," *Electrochemistry, Russian Journal of,* vol. 42, pp. 476-479, 2006.

[61]   M. Reformat*, et al.*, "Non-linear Load Modeling for Simulations in Time Domain," presented at the Harmonics And Quality of Power, 8th International Conference on, 1998.

[62]   D. C. Mikulecky, "A Network Thermodynamic Two-Port Element to Represent the Coupled Flow of Salt and Current: Improved Alternative for the Equivalent Circuit," *Biophysical Journal,* vol. 25, pp. 323-340, 1979.

[63]   W. F. Pickard, "Nonlinear equivalent circuits for membranes," *Mathematical Biology, Journal of,* vol. 21, pp. 11-23, 1984.

[64]   M. Hosoya, "The Simplest Equivalent Circuit of a Multi-Terminal Network," *Bulletin of the College of Science, University of the Ryukus,* pp. 1-10, 2000.

[65]   "MATLAB/Simulink," 7.6 ed. Natick, MA: MathWorks, 2008.

[66]   "Simplorer," 7 ed. Pittsburgh, PA: Ansoft Corporation, 2007.

[67]   V. K. Madisetti and D. B. Williams, Eds., *The Digital Signal Processing Handbook.* Boca Raton, FL: CRC Press, 1998.

[68]   E. Hertz, "Thermal and EMI Modeling and Analysis of a Boost PFC Circuit Designed Using a Genetic-based Optimization Algorithm," MS, Electrical Engineering, Virginia Tech, Blacksburg, VA, 2001.

[69]   D. Zhang, *et al.*, "A new method to characterize EMI filters," in *Applied Power Electronics Conference and Exposition, Thirteenth Annual, APEC '98*, 1998, pp. 929-933 vol.2.

[70]   E. O. Brigham, *The Fast Fourier Transform.* Englewood Cliffs, NJ: Prentice Hall, 1974.

[71]   R. I. Becker and N. Morrison, "The Errors in FFT Estimation of the Fourier Transform," *Signal Processing, IEEE Transactions on,* vol. 44, pp. 2073-2077, 1996.